Task 2 Report – Close Minor Research Gaps
USE OF FIBER-REINFORCED POLYMER COMPOSITES
FOR BRIDGE REPAIRS IN MONTANA

Prepared By:

Emtiaz Ahmed

Graduate Research Assistant,

Kirsten Matteson, PhD

Associate Professor,

and

Michael Berry, PhD

Professor

Civil Engineering Department

College of Engineering

Montana State University – Bozeman

Disclaimer Statement:

This document is disseminated under the sponsorship of the Montana Department of Transportation (MDT) and the United States Department of Transportation (USDOT) in the interest of information exchange. The State of Montana and the United States assume no liability for the use or misuse of its contents.

The contents of this document reflect the views of the authors, who are solely responsible for the facts and accuracy of the data presented herein. The contents do not necessarily reflect the views or official policies of MDT or the USDOT.

The State of Montana and the United States do not endorse products of manufacturers.

This document does not constitute a standard, specification, policy or regulation.

Alternative Format Statement:

Alternative accessible formats of this document will be provided on request. Persons who need an alternative format should contact the Office of Civil Rights, Department of Transportation, 2701 Prospect Avenue, PO Box 201001, Helena, MT 59620. Telephone 406-444-5416 or Montana Relay Service at 711.

TABLE OF CONTENTS

LIST OF FIGURES

LIST OF TABLES

1. INTRODUCTION

The focus of this research is to investigate the potential of using Fiber Reinforced Polymer (FRP) composites to repair deteriorating members on bridges in Montana. This includes identifying the most promising applications of FRP technology for use in the state and filling in any minor research gaps that may inhibit their use. Ultimately, this project will culminate in an implementation project that uses the most relevant technology in an actual bridge project in Montana.

The specific tasks associated with this research are as follows:

> Task 0 – Project Management
>
> Task 1 – Literature Review and Identification of Pursued Application
>
> Intermediate Technical Panel Meeting Task
>
> Task 2 – Close Minor Research Gaps
>
> Task 3 – Implementation
>
> Task 4 – Monitoring Bridge Performance
>
> Task 5 – Analysis of Results and Reporting

This report documents the work completed as part of Task 2 – Close Minor Research Gaps. Following discussions with the MDT technical panel, it was determined that the primary focus of Task 2 should be on the repair and strengthening of timber bridge girders using pultruded FRP materials. Therefore, Task 2 involved the structural testing of salvaged timber girders from around the state that were strengthened/repaired with FRP materials. Specifically, this task report covers the material properties of FRP, the specific repair and strengthening processes, the experimental design, and test results from this research. It concludes with a comprehensive discussion of test results.

2. BACKGROUND

The use of FRP as a construction and repair material for bridges in the United States began in the early 1970s [1]. The Federal Highway Administration (FHWA) and the National Science Foundation (NSF) increased funding for research on FRP materials for infrastructure applications in the late 1980s after observing the growing acceptance of advanced composite materials in various fields (e.g., aerospace and sporting goods industries) [2]. Since then, increased research and development have led to the introduction of FRP materials being used in pedestrian and vehicular bridges.

Timber bridges represent a significant portion of the transportation infrastructure in the United States. In Montana alone, there are over 400 timber bridges [3]. Many of them were constructed several decades ago using older design codes. Over time, they have become increasingly vulnerable to environmental degradation, biological decay, and load-induced damage. As a result, there is a need for effective and efficient repair methodologies. The use of FRP in this context offers a promising solution for extending the service life of these bridges. FRP offers significant potential as a corrosion-resistant repair material, and the application processes require less installation time compared to some traditional building materials, resulting in minimal road closures. Furthermore, some research suggests that a bridge can remain functional

during the repair process, as traffic loading does not affect the strength of the FRP bond [4, 5]. As a result of this initial research and the known benefits of this material, several state departments of transportation (DOTs) have started investigating the use of FRPs as a bridge repair method.

The current project aims to investigate the efficacy of various FRP strengthening/repair techniques and identify potential suitable methods for use in Montana. The ultimate goal of this project is to apply the chosen application and methodology on a bridge project in the state (Task 3) and monitor its performance (Task 4). The research is a necessary step to fully understand and capitalize on the benefits of using FRP for repairing/strengthening and to subsequently increase the performance and durability of Montana bridges.

Specifically, this report presents the findings from an experimental program in which a total of 22 timber beams (recovered from existing bridges in Montana) were strengthened/repaired with varying configurations of FRP components. Undamaged control beams were tested, giving a baseline of performance. The control beams were compared to tests on undamaged beams strengthened with FRP. Additionally, the now-damaged control beams were repaired with FRP and tested again under the same loading conditions, providing a direct comparison of the performance of the undamaged beam before testing to the performance of the same beam after repair. The following sections discuss details of the FRP materials, the timber beams, and the experimental design. The results from these tests are then presented and discussed. The report concludes with a summary of results and conclusions.

3. TIMBER BEAMS, FRP MATERIALS, AND REPAIR/STRENGTHENING TECHNIQUES

This section provides a brief overview of the timber beams used in the study, including their origin, properties, and condition prior to testing. It also outlines the observed damage, the repair techniques adopted, and the FRP installation procedures implemented as part of this investigation.

The timber beams for this investigation were originally salvaged from bridges across the state and were collected from the MDT storage yard in Lewistown, MT. The beams include two common sizes historically used in Montana bridges, 6"x18"x20' and 8"x18"x26'. The beams (examples shown in Figure 1) are Douglas-fir/Larch (dense No. 1) with allowable bending and shear stresses of 1.55 ksi and 0.085 ksi, from Table 13.5.1A, AASHTO [6], respectively, though some of the beams have lower values because of existing defects. The actual dimensions of the beams and pre-existing (before testing) cracks or splits are documented in Appendix B.

(a) Beam stack prior to testing
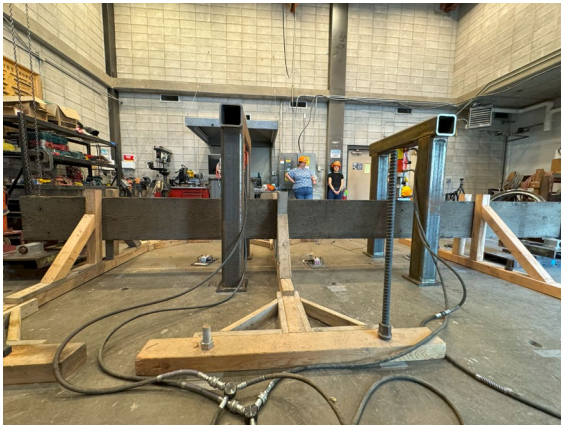
(b) 6"x18"x20' beam
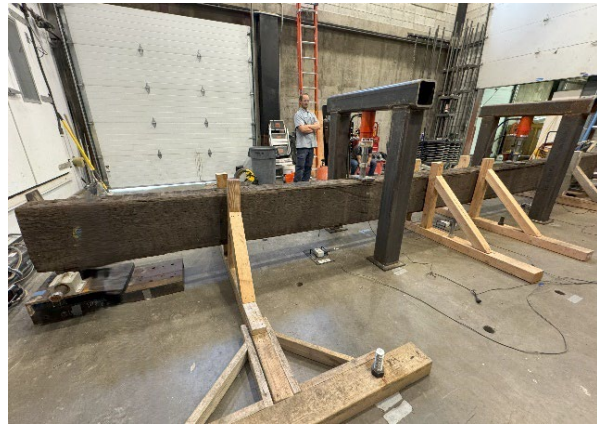
(c) 8"x18"x26' beam

Figure 1: Example Timber Beams

3.1 Timber Beam Damage

This subsection provides an overview of the natural imperfections observed in the timber beams prior to testing, as well as the various failure modes documented during the experimental program.

Timber beams often have natural imperfections that can impact their performance. These imperfections, such as knots, checks, waning, and grain deviations, are not classified as damage. However, if they are significant enough, they can contribute to premature failure. Figure 2 shows a couple of examples of natural imperfections.

| (a) Checks | (b) Knots |

Figure 2: Examples of checks and knots

Timber beams have been observed to exhibit several failure mechanisms in the field and in this research, including tension cracking, shear splitting, compression cracking, and bearing failures. These failure mechanisms are discussed below. However, while all of these mechanisms were observed in this research, this study focused primarily on tension cracking and shear splitting as they are the most common and structurally significant damage types observed in the field.

Tension cracks are commonly formed due to flexure-induced stresses on the tension face of the beam, and extend at an angle through the member, generally along the grain of the wood (as shown in Figure 3). They often begin near mid-span (where tension stresses are greatest) and initiate at imperfections such as knots or checks, or at the site of impact or handling damage.

Figure 3: Example of a tension crack failure

Shear splitting (as observed in Figure 4), result from horizontal shear stresses induced from loading. They run parallel to the top and bottom faces and initiate near the ends of the beam where the shear forces are the greatest. Like in tension failures, these failures often initiate at imperfections in the beam.

Figure 4: Example of a shear split failure

Another failure mechanism of timber beams is longitudinal (parallel to the grain) crushing of the wood in compression zones (as observed in Figure 5). In the beams in this research this occurred at the top mid-span of the beam where the positive moments were the highest.

Figure 5: Example of a compression crushing/cracking failure

Bearing failure (crushing of the wood perpendicular to the grain) is another form of damage that can occur in timber beams. In the beams tested in this research this failure mechanism was observed under the applied loads (Figure 6-a) and at the supports (Figure 6-b).

(a) At load-bearing block   (b) At the reaction-bearing plate

Figure 6: Examples of bearing failure.

3.2 FRP Materials and Fasteners

Multiple FRP materials were selected to repair/strengthen the timber beams. This section discusses the FRP materials used in this research, including the Glass FRP channels, the Carbon/Glass hybrid FRP strengthening strips, and the fasteners. An example of the FRP materials attached to a timber beam are shown in Figure 7 and the following subsections discuss each composite in detail.

Figure 7: Example timber beam with FRP materials attached

3.2.1   GFRP Channels

The glass FRP channels (Figure 8) used in this study are the EXTREN Series 525, manufactured by Strongwell [7]. This series offers a combination of high strength, durability, and enhanced fire resistance. The channels are made with a general-purpose polyester resin that provides excellent corrosion resistance, making them suitable for various structural applications, especially in harsh environmental conditions. The resin is formulated with UV inhibitors and flame-retardant additives to enhance performance. The EXTREN Series 525 channels have a standard slate gray color.

The manufacturer-specified longitudinal tensile strength and elastic modulus of the FRP channels are 30 ksi and 2500 ksi, respectively. However, coupon testing conducted as part of this study revealed higher values. The control channel coupon exhibited a tensile strength of 53.2 ksi and an elastic modulus of 4090 ksi, representing 177% and 164% of the tabulated values, respectively. Moreover, the channel coupons extracted from full-scale tested beams (mid-span and end-region) retained high mechanical performance, with tensile strengths exceeding 150% of the tabulated values and elastic modulus values remaining above 120%. These results indicate strong durability and performance retention of the GFRP channels after beam application. Detailed procedures and results of the coupon testing are provided in Appendix E .

Figure 8: Example FRP Channels

3.2.2   SAFSTRIP

The FRP strengthening strip (SAFSTRIP®, see Appendix D for material properties and manufacturer information), manufactured by Strongwell [7], is a pultruded composite strip designed to enhance the strength of an existing structural member when mechanically fastened to the structure. This strip is 4" wide and 1/8" thick and is typically shipped in rolls up to 100' long (Figure 9). The FRP strip is a carbon/glass hybrid and is comprised of carbon tows sandwiched between layers of fiberglass mats and rovings, bonded together by a highly corrosion-resistant vinyl ester resin. The inclusion of carbon fibers increases the stiffness of the strip, while the glass mat provides the necessary bearing strength.

The manufacturer-specified tensile strength and longitudinal elastic modulus of the strip are 92.90 ksi and 9020 ksi, respectively. Coupon testing showed that the control strip specimens had higher measured properties, with tensile strengths of up to 133.7 ksi (107–109% of the tabulated value) and elastic moduli up to 9822 ksi (109%). The tested coupons removed from full-scale beams also performed well, maintaining

tensile strengths and stiffness within ±10% of the design values. These results suggest minimal degradation and confirm the reliability of the FRP strip in structural strengthening applications. Additional details on the coupon testing procedure and results are provided in Appendix E.

Figure 9: Safstrip sample in rolled/shipped condition

3.2.3   Fasteners

RSS-GRK screws (Figure 10-a) were used as the fasteners in this study to attach the channels and strips to the timber beams. These screws feature a washer head design that effectively addresses potential bearing issues. For the channels, 5/16"x3-1/8" screws were used, while 1/4"x3-1/2" screws were selected for the strips. These fasteners were chosen for their specified high shear capacities of 982 lb and 754 lb, respectively. In addition, #12x6-3/8" R4-GRK screws (Figure 10-b) were used to close the cracks before attaching the channels and strips to the repaired beams.

(a) RSS-GRK screws for attaching FRP to timber beams

(b) R4-GRK screws for repairing crack beams prior to FRP installation

Figure 10: Fasteners used in repair/strengthening

3.3 Repair/strengthening techniques

As stated above, the focus of this research was primarily on strengthening/repairing beams to avoid/repair tension cracking and shear splitting mechanisms. This section outlines the FRP repair and strengthening techniques used in this study. A total of four configurations were tested under either flexure- or shear-controlled loading schemes. Specifically, these techniques included (1) a combination of FRP channels and strips to improve the performance of flexure-controlled beams, (2) FRP strips used alone for flexure-controlled beams, (3) FRP channels used alone for shear-controlled beams, and (4) and FRP channels used in specific locations to repair existing splits in flexure-controlled beams.

To align with dimensions in the field on actual bridges and thereby simplify future implementation, the strips were 23.5' in length for the 25' span beams and 17.5' for the 19' span beams. The shortened strip ensures conservative test results, in case blocking or other obstacles exist on a physical bridge, hindering the strip from spanning the entire beam. Similarly, the channel lengths were 24', 18', and 8' for the 25', 19', and 9' span beams, respectively. Each technique is discussed in detail in the following sub-sections.

3.3.1   FRP Channels and Strip for Flexure-Controlled Beams

This technique was used to strengthen undamaged beams and repair beams with tension cracks and shear splits, to be tested in a flexure-controlled manner. This technique was used for both beam sizes used in this study, and consisted of two GFRP channels screwed to the faces of the beam (either at the bottom or top) and a GFRP/CFRP strip screwed to the tension face (bottom) of the beam. Note that the location of the channels was at times dependent on existing damage within the beam. That is, the channels were installed on the bottom of the beam to repair tension cracks, while they were installed in the middle to repair shear splits. Schematics of this repair/strengthening technique are shown in Figure 11 and Figure 12, while actual beams with this technique employed are shown in Figure 13.

(a) Cross-section   (b) Elevation
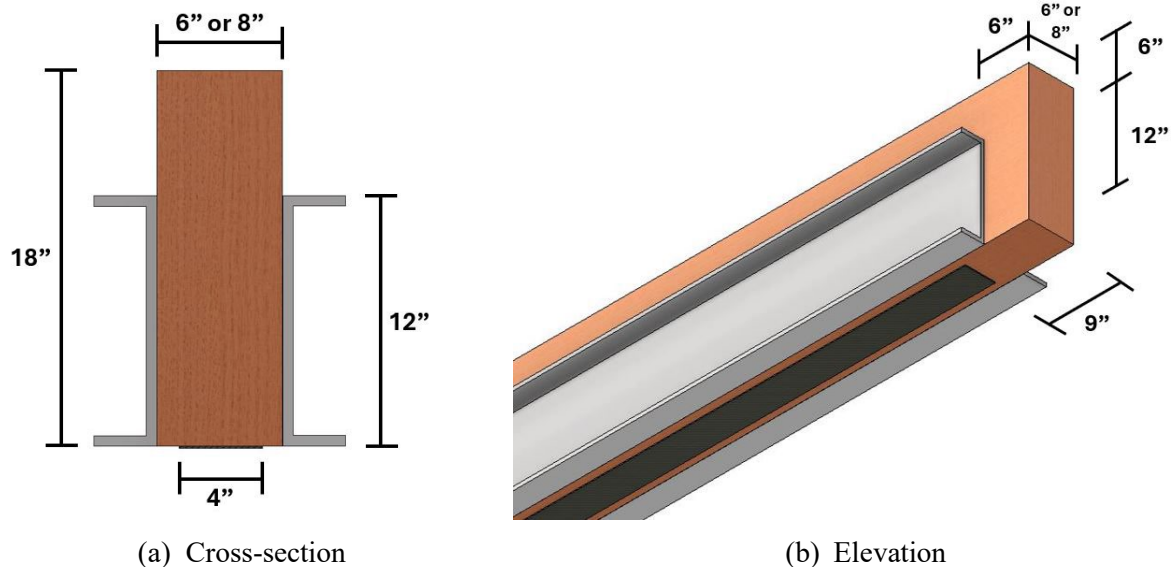
Figure 11: Schematic of FRP channels and strip repair technique (bottom channel)

(a) Cross-section
(b) Elevation
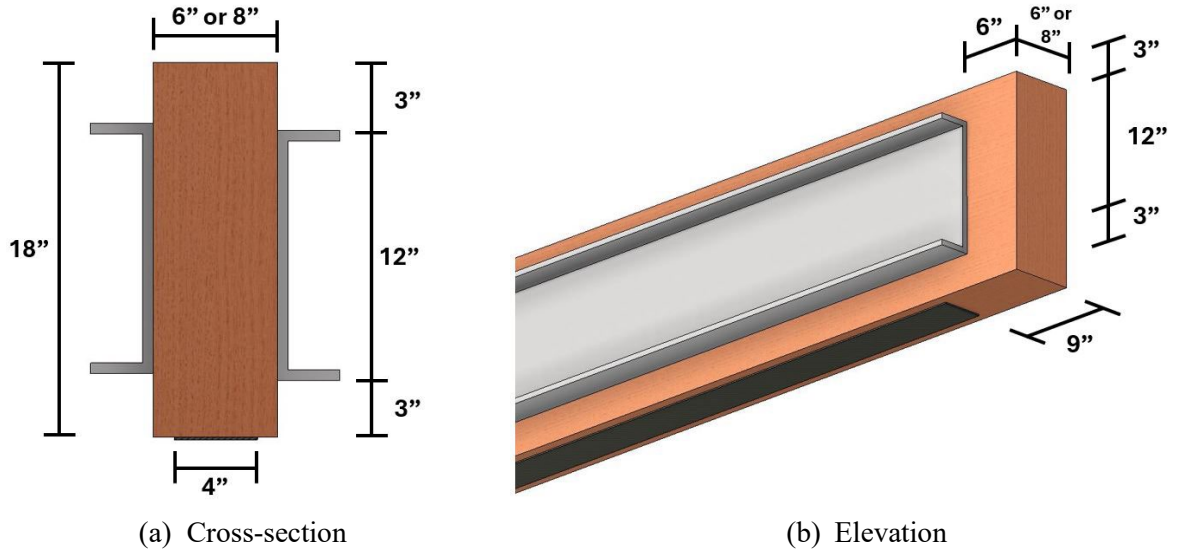
Figure 12: Schematic of FRP channels and strip repair technique (middle channel)

(a) Beam on its side with strip on bottom and channels on bottom edge
(b) Beam in testing position with channels in the mid-height of the beam
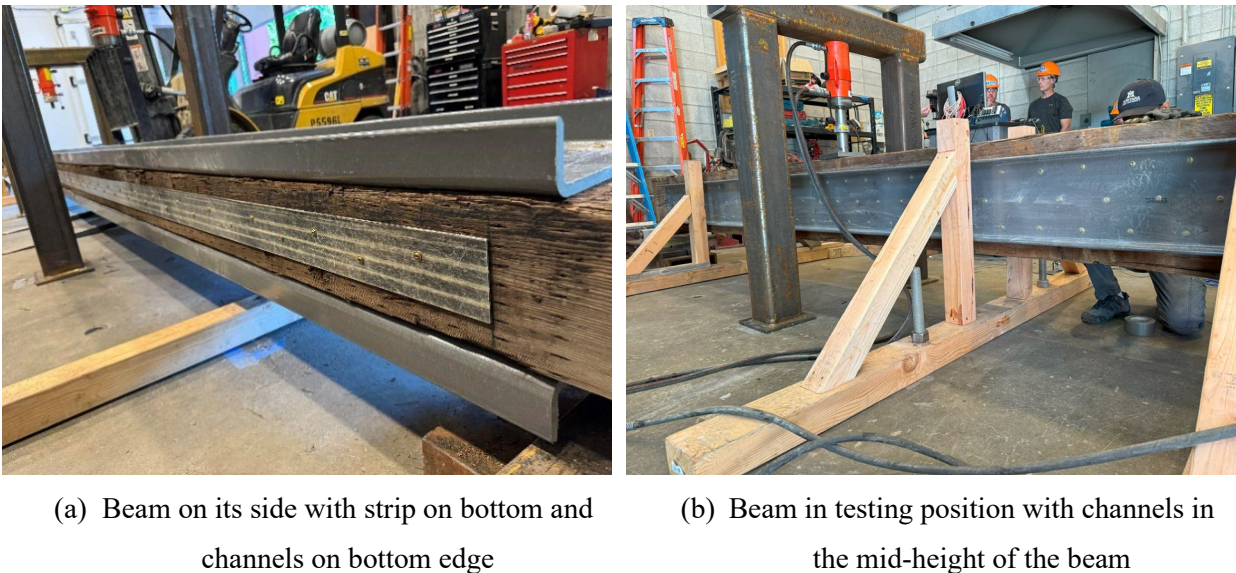
Figure 13: FRP channels and strip repair technique on test beams

3.3.2   *FRP Strips for Flexure-Controlled Beams*

With this technique, on beams to be tested in flexure, FRP strips were used without channels to strengthen undamaged beams and repair beams with tension cracks. Strips were screwed to the sides and bottoms of the beams, as shown in Figure 14-Figure 16. On each side, either one or two strips were included depending on the severity and location of tension cracks.

(a) Cross-section

(b) Isometric
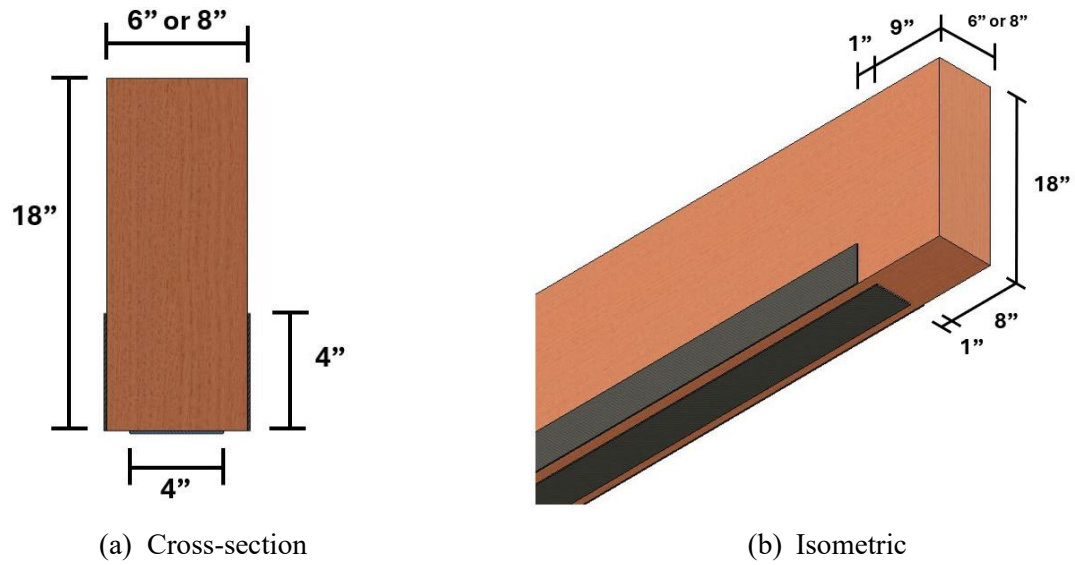
Figure 14: Schematic of FRP strips for flexure-controlled beams – one strip per side

(a) Cross-section

(b) Isometric
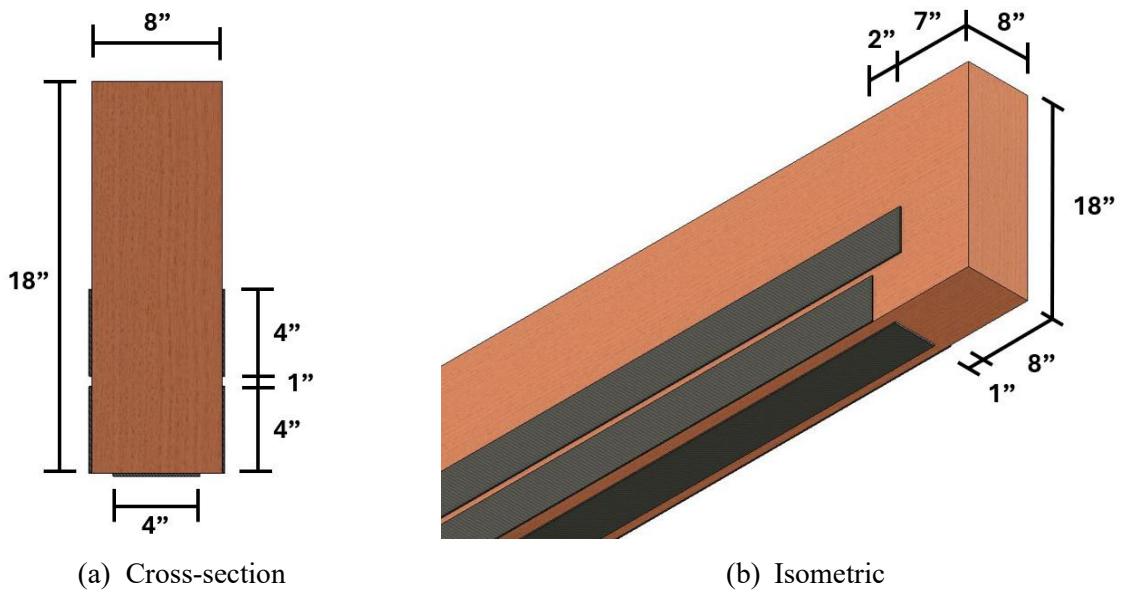
Figure 15: Schematic of FRP strips for flexure-controlled beams – two strips per side

(a) Beam on its side with one strip per side   (b) Beam on its side with two strips per side
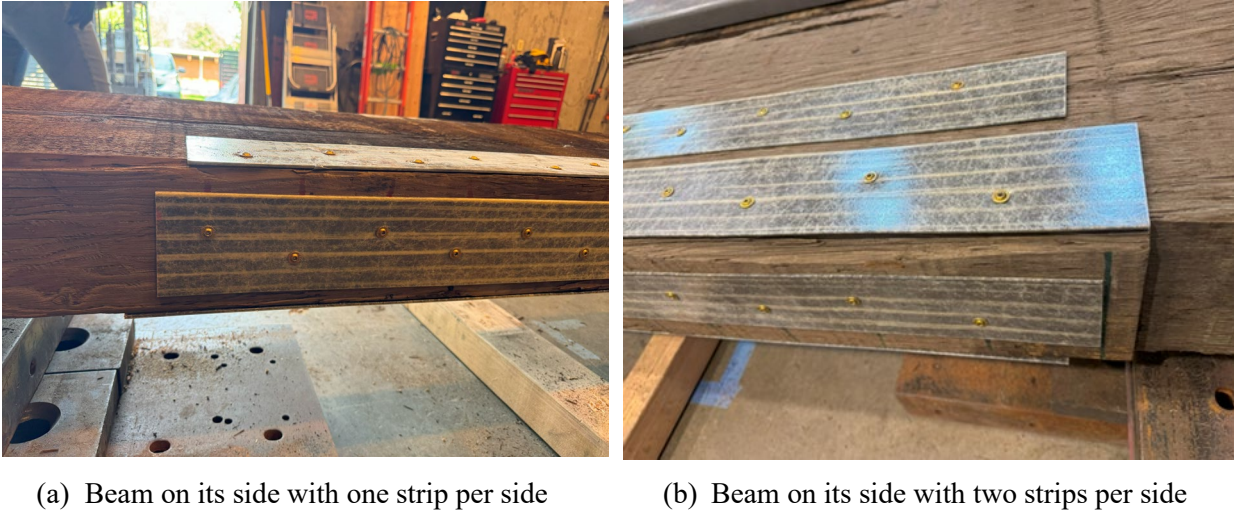
Figure 16: FRP strip technique applied to test beams

3.3.3 FRP Channels for Shear-Controlled Beams

This technique was used to strengthen undamaged beams and repair shear-split beams to be tested in shear. This technique consisted of GFRP channels screwed to the sides of the beams (in the middle), as shown in Figure 17 and Figure 18.
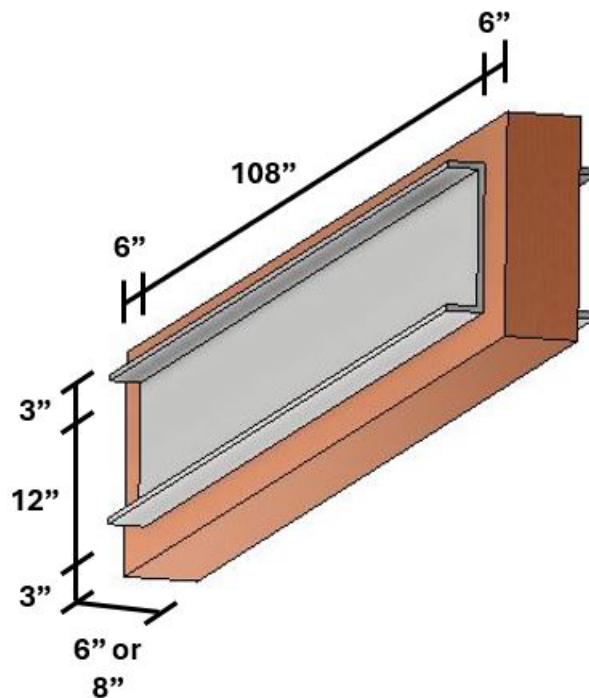
Figure 17: Schematic of FRP channels for shear-controlled beams

Figure 18: FRP channel technique applied to test beam

3.3.4   FRP Channels in Specific Locations to Repair Splits in Flexure-Controlled Beams

In some cases, the test beams had localized shear-splits near their ends, and FRP channels were used at these specific locations to repair this damage. After repair, these specimens were tested in flexure. This technique consisted of either 3' or 6' channels attached to the sides of the beams (in the middle), as shown in Figure 19 and Figure 20. Two different lengths were used to evaluate the effect that this parameter has on the performance.

(a) 3' channels
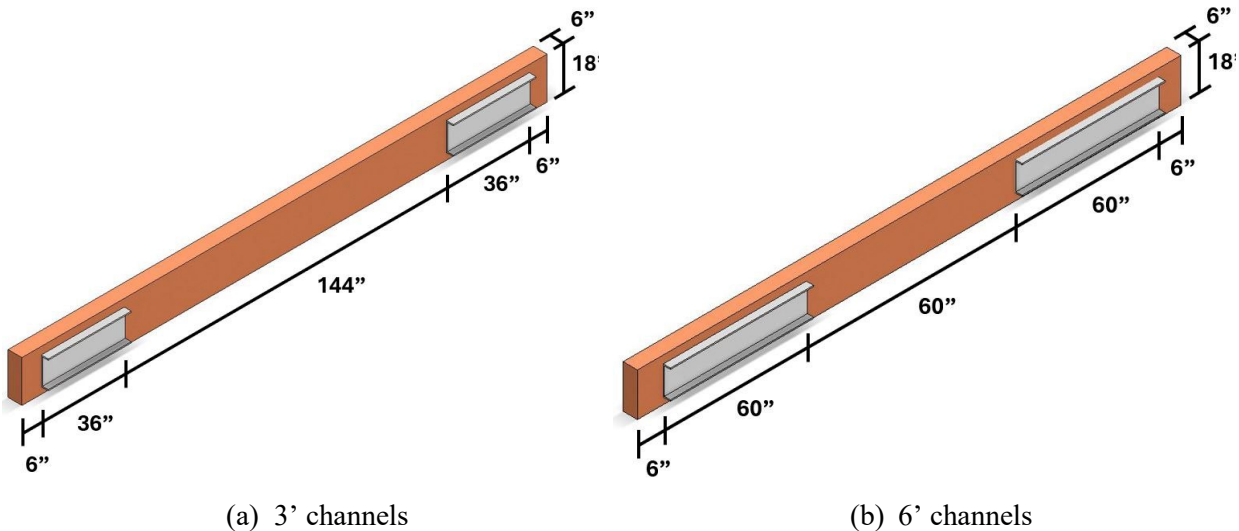
(b) 6' channels

Figure 19: Schematics of localized split repairs with channels

(a) 3' channels   (b) 6' channels

Figure 20: Localized split repair technique applied to test beams

3.3.5   Example Repairs

As mentioned previously, the focus of this research was on quantifying the efficacy of the above-mentioned techniques at strengthening undamaged beams and repairing damaged beams. To do this, several undamaged control beams were tested without employing the methods discussed above, giving a baseline of performance. The results from these tests were then compared to the results of tests on undamaged beams strengthened with these techniques. Additionally, the now-damaged control beams were then repaired with one of these techniques, and tested again under the same loading conditions, providing a direct comparison of the performance of the undamaged beam before testing to the performance of the same beam after repair. In some cases, the repair was quite extensive, as shown below.

Figure 21 shows a flexure-controlled beam that failed due to a large tension crack that was repaired with the FRP channel and strip method discussed above. Figure 22 shows another beam that failed due to a tension crack that was repaired with FRP strips alone. Figure 23 shows a shear-controlled beam that failed due to a shear split and repaired with FRP channels. Finally, Figure 24 shows a beam that had an existing shear split, that was repaired with FRP channels and a strip.

(a) After initial failure, before repair   (b) After repair, before re-testing

Figure 21: An example of a tension-crack repair with FRP channels and strips
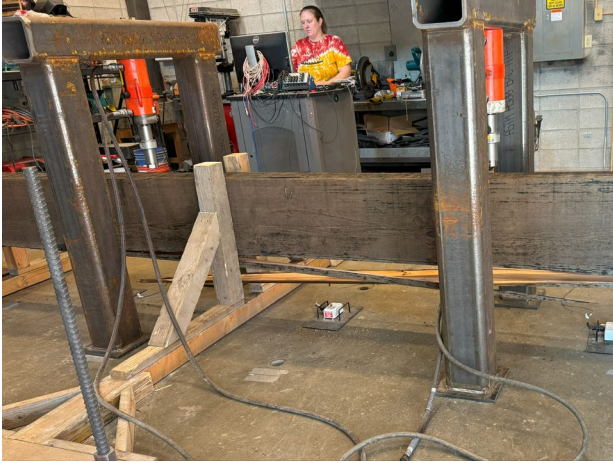
(a) After initial failure, before repair
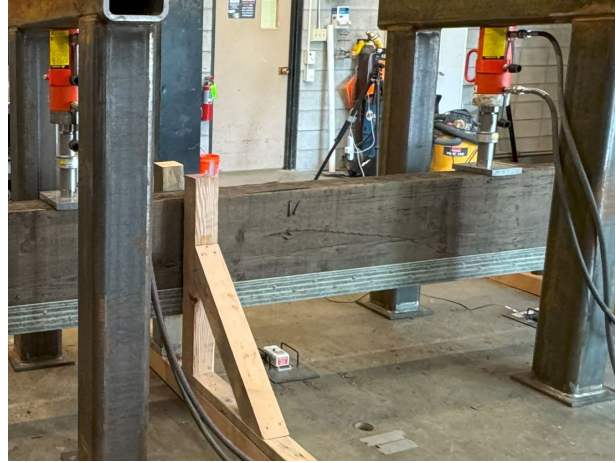
(b) After repair, before re-testing

Figure 22: An example of a tension-crack repair with FRP strips alone

(a) After initial failure, before repair

(b) After repair, before re-testing

Figure 23: An example of the shear-split repair with FRP channels

(a) Existing split, before repair   (b) After repair, before testing

Figure 24: An example of an existing shear-split repair with channels and strip

4. FRP INSTALLATION

Implementing the repairing/strengthening techniques discussed in the previous chapter involved several steps, including cutting the FRP strips and channels to length, predrilling the FRP section, preparing the timber beam surface for application (including closing the existing crack when applicable), and finally attaching the FRP materials to the timber beam with fasteners.

4.1 Cutting the FRP

The FRP strips were supplied from the manufacturer in 100' rolls, while the FRP channels were shipped in 24' lengths. The channels were cut to length using a reciprocating saw with a metal cutting blade (Figure 25-a). The strips were cut with a standard miter saw with a metal blade (Figure 25-b).

<table>
<tr><td>(a) Channel</td><td>(b) Strip</td></tr>
</table>

Figure 25: Cutting the FRP material

4.2 Pre-drilling

Strongwell recommends predrilling sections thicker than 5/16", and therefore the channels and strips in this research were predrilled prior to installation. Details on the screw count calculations and screw pattern schematics are provided in Appendix C (C.2). The channels and strips were drilled (Figure 26) with a standard impact drill with 5/16" and 1/4" Milwaukee titanium twist metal drill bits, respectively.

<table>
<tr><td>(a) Channel</td><td>(b) Strip</td></tr>
</table>

Figure 26: Pre-drilling the FRP

4.3 Surface preparation for repairs

The surface of each beam to be repaired/strengthened with the FRP methods discussed previously was first cleaned off with a broom. When applicable, existing or induced damage was repaired prior to installation. Specifically, beams with existing or induced flexure-cracks were turned upside down and secured with ratchet straps (Figure 27). The tension cracks were then closed using #12 x 6-3/8" R4-GRK screws. There was no specific screw pattern for closing the cracks, as the crack formation was different for each beam. However, care was given to avoid overlapping screws between FRP strip screws and repair screws (Figure 28). In contrast, no additional fasteners (beyond those required for the channels) were needed for the beams with existing or induced shear splits, as these beams would return to the undamaged configuration after the load was removed (shown in Figure 29).
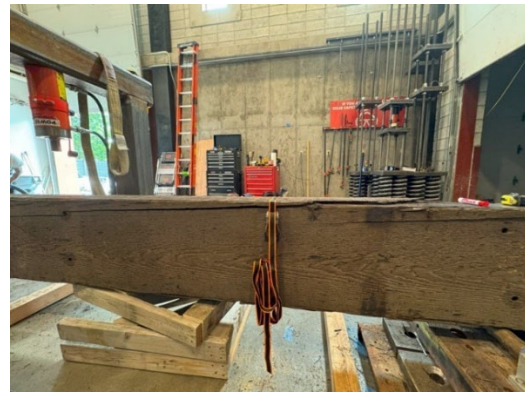
(a) Before   (b) After

Figure 27: Using ratchet straps to close any existing cracks
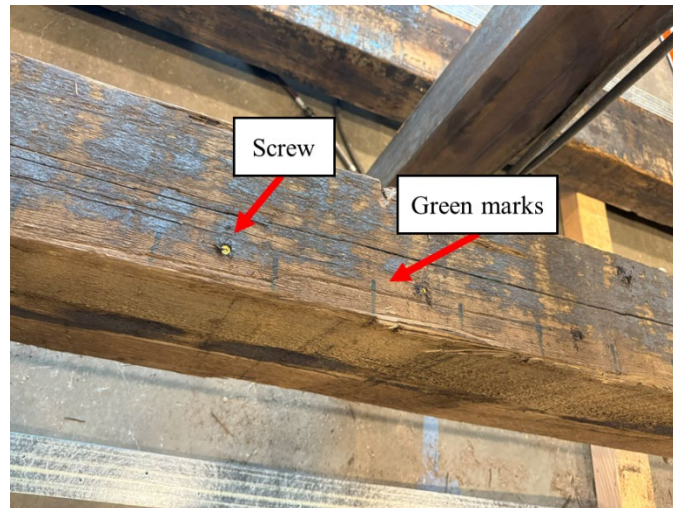
Figure 28: Marking the strip screw pattern (green marks in the photograph) and closing the crack

| (a) At maximum load | (b) After load removal |
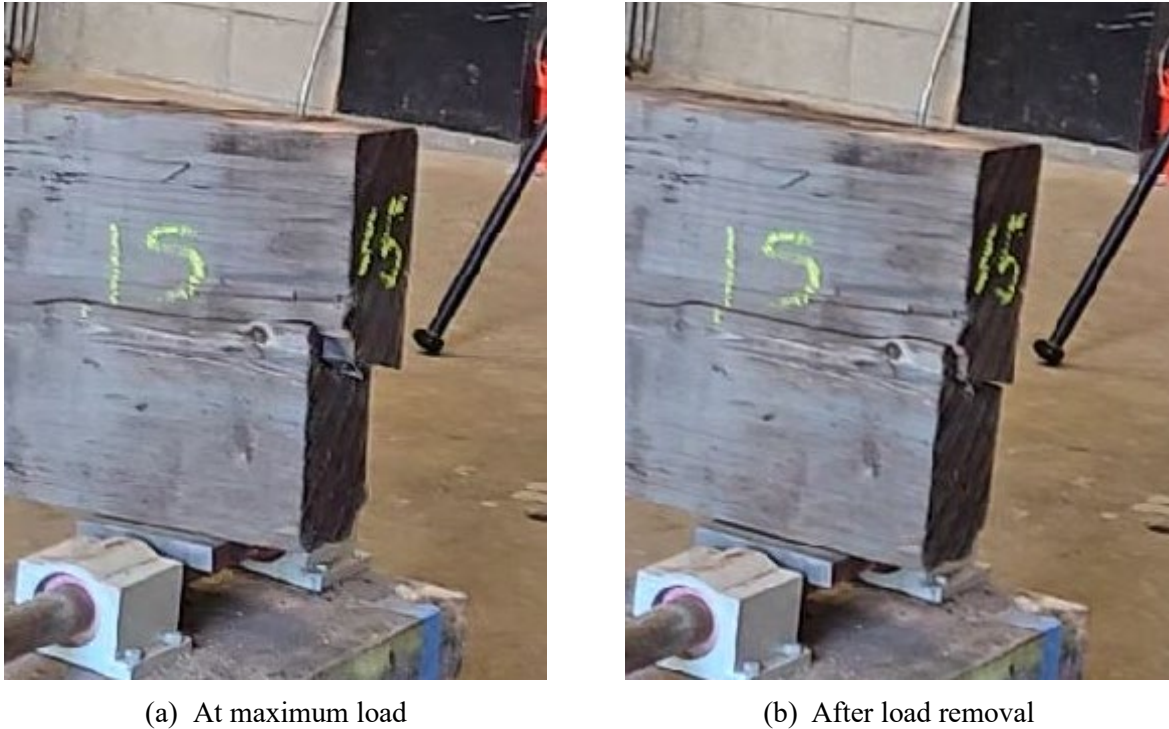
Figure 29: An example of a split closing after load removal

4.4 <u>Attaching the FRP to the beam</u>

The channels and strips were attached to the beams with 5/16"x3-1/8" and 1/4"x3-1/2" RSS-GRK screws, respectively.

The FRP strips were secured to the beams using 1/4"x3-1/2" RSS-GRK screws, starting in the center of the beam and working towards the ends, while ensuring the strip remained aligned with the beam and taught (Figure 30). Similarly, the channels were attached to the beams with 5/16"x3-1/8" RSS-GRK screws, Ratchet straps were occasionally used to align the channels with the beams, especially when the beams were not perfectly straight. The channel installation process involved securing one end of the channel with a few screws first, then aligning the channel with the beam (Figure 31-a), securing the opposite end, and then completing the screwing along the length (Figure 31-b). When used to repair shear splits, care was given to position the FRP to span across the splits.

Figure 30: Attaching strip to the beam
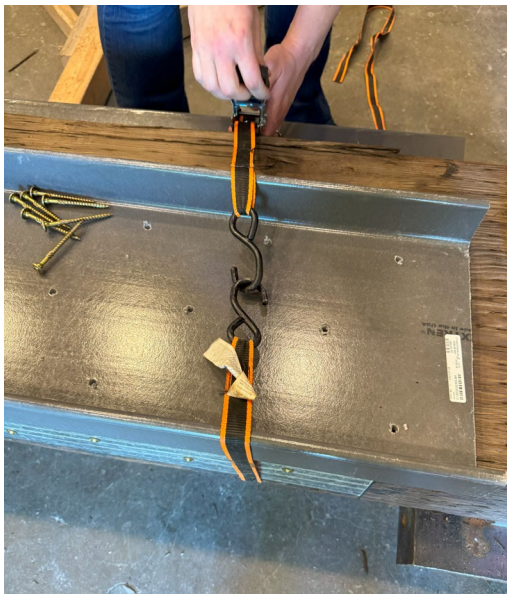
(a) Aligning the channel with the beam

(b) Screwing along the length

Figure 31: Attaching channel to the beam.

5. EXPERIMENTAL DESIGN

This chapter outlines the experimental design and testing protocols used to evaluate the performance of FRP repair and strengthening techniques on salvaged Douglas-fir/Larch timber bridge girders. The focus was to replicate field conditions while capturing consistent and comparable results that could guide future repair and strengthening applications in Montana.

In general, to quantify the efficacy of the FRP techniques proposed in this research (Chapter 3), several undamaged control beams were tested without employing these methods, providing a baseline of

performance. The now-damaged control beams were then repaired with one of these techniques, and tested again under the same loading conditions, providing a direct comparison of the performance of the undamaged beam before testing to the performance of the same beam after repair. Additionally, the results from these tests were then compared to the results of tests on undamaged beams strengthened with these techniques.

5.1 Test Matrix

Two standard sizes of Douglas-fir/Larch (dense No. 1) beams were tested in this study: 6"x18"x20' and 8"x18"x26'. For each size group, the test matrix included three undamaged/unstrengthened control beams (two tested in flexure and one in shear), two flexure crack-repair beams (previously tested controls that were repaired), one shear split-repair beam (a previously tested control repaired after splitting), and three strengthened beams (undamaged beams reinforced with FRP). In addition, three 6"×18" beams and one 8"×18" beam with pre-existing splits (salvaged from bridges) were repaired and tested. An overview of all beam cases and repairing/strengthening schemes are presented in Table 1.

Throughout this report, each beam is identified by an acronym that encodes its key attributes. The first number in the acronym indicates the beam's nominal size (6 for a 6″×18″ beam, or 8 for an 8″×18″ beam). The letters following the number denote the test setup: Sh for a shear test or Fl for a flexure test. If the acronym includes a number in parentheses immediately after (for example, 6-Fl(1)), that number identifies a specific control beam (e.g., "(1)" or "(2)" for the first or second control in that group). The final letters of the acronym indicate the repair or strengthening method, if applicable: CR for a crack-repair beam, SR for a split-repair beam, or St for a strengthened beam. Any additional parentheses at the end specify the repair/strengthening scheme used: (C-S) for a combination of FRP channels and a strip, (S) for FRP strips only, (C) for FRP channels only, (C3) for 3′-long channels on the beam ends, and (C6) for 6′-long channels on the beam ends. In Table 1, the second column lists the original beam numbers (as marked on the beams before delivery to MSU); an "(R)" following the number indicates a beam that was previously tested as a control and then repaired for a subsequent test.

Table 1: Test beam details

Acronym	Original #	Nominal cross-section	Test setup	Span length	Type	Repairing/Strengthening
6-Sh(1)	16		**Sh**ear	9'	Control	None
6-Fl(1)	22		**Fl**exure	19'		None
6-Fl(2)	15		**Fl**exure	19'		None
6-Fl(1)-CR(C-S)	22 (R)		**Fl**exure	19'	Control - **C**rack **R**epair	**C**hannels on the sides - **S**trip on the bottom
6-Fl(2)-CR(S)	15 (R)		**Fl**exure	19'		**S**trips on the sides and bottom
6-Sh(1)-SR(C)	16 (R)		**Sh**ear	9'	Control – **S**plit **R**epair	**C**hannels on the sides
6-Fl-SR(C-S)	17	**6"** x 18"	**Fl**exure	19'	**S**plit **R**epair	**C**hannels on the sides - **S**trip on the bottom
6-Fl-SR(C3)	21		**Fl**exure	19'		**C**hannels (**3** ft) on each ends of the sides
6-Fl-SR(C6)	23		**Fl**exure	19'		**C**hannels (**6** ft) on each ends of the sides
6-Sh-St(C)	13		**Sh**ear	9'	**St**rengthened	**C**hannels on the sides
6-Fl-St(C-S)	24		**Fl**exure	19'		**C**hannels on the sides - **S**trip on the bottom
6-Fl-St(S)	20		**Fl**exure	19'		**S**trips on the sides and bottom
8-Sh(1)	9		**Sh**ear	9'	Control	None
8-Fl(1)	7		**Fl**exure	25'		None
8-Fl(2)	5		**Fl**exure	25'		None
8-Fl(1)-CR(C-S)	7 (R)		**Fl**exure	25'	Control - **C**rack **R**epair	**C**hannels on the sides - **S**trip on the bottom
8-Fl(2)-CR(S)	5 (R)		**Fl**exure	25'		**S**trips on the sides and bottom
8-Sh(1)-SR(C)	9 (R)	**8"** x 18"	**Sh**ear	9'	Control – **S**plit **R**epair	**C**hannels on the sides
8-Fl-SR(C-S)	12		**Fl**exure	25'	**S**plit **R**epair	**C**hannels on the sides - **S**trip on the bottom
8-Sh-St(C)	1		**Sh**ear	9'	**St**rengthened	**C**hannels on the sides
8-Fl-St(C-S)	11		**Fl**exure	25'		**C**hannels on the sides - **S**trip on the bottom
8-Fl-St(S)	8		**Fl**exure	25'		**S**trips on the sides and bottom

5.2 Test setup and instrumentation

All the beams in this investigation were tested in 4-point bending, following ASTM D198 − 22a [8], which includes both flexure and shear setups. The flexure test setup was designed to induce a flexural (bending) failure at mid-span (high moment region), whereas the shear test setup was intended to cause a shear failure at the beam ends (high shear region). Figure 32 illustrates the load configuration diagrams (free-body, shear, and moment) for the four-point bending tests.
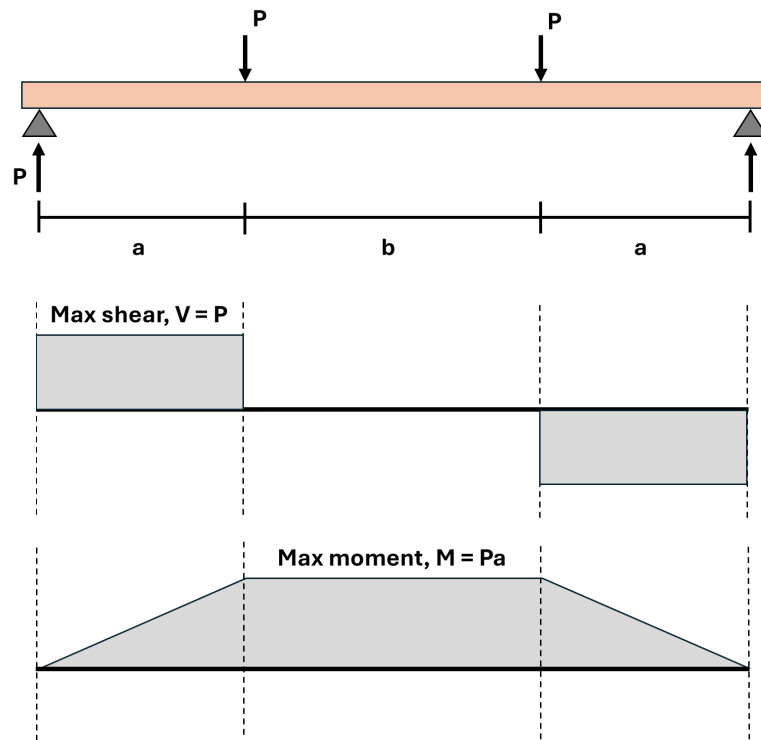
Figure 32: General 4-point bending test setup

The flexure and shear setups were geometrically similar, differing primarily in the distances between supports and loading points (dimensions "a" and "b" in Figure 32). The flexure-controlled beams had longer spans with greater moment demands, while the shear-controlled beams were shorter with increased shear demand relative to moment demand. Schematic diagrams of the flexure and shear test configurations for both beam sizes are shown in Figure 33 and Figure 34, respectively, with all key dimensions labeled.

(a) 19' span (6"x18"x20') beam   (b) 25' span (8"x18"x26') beam
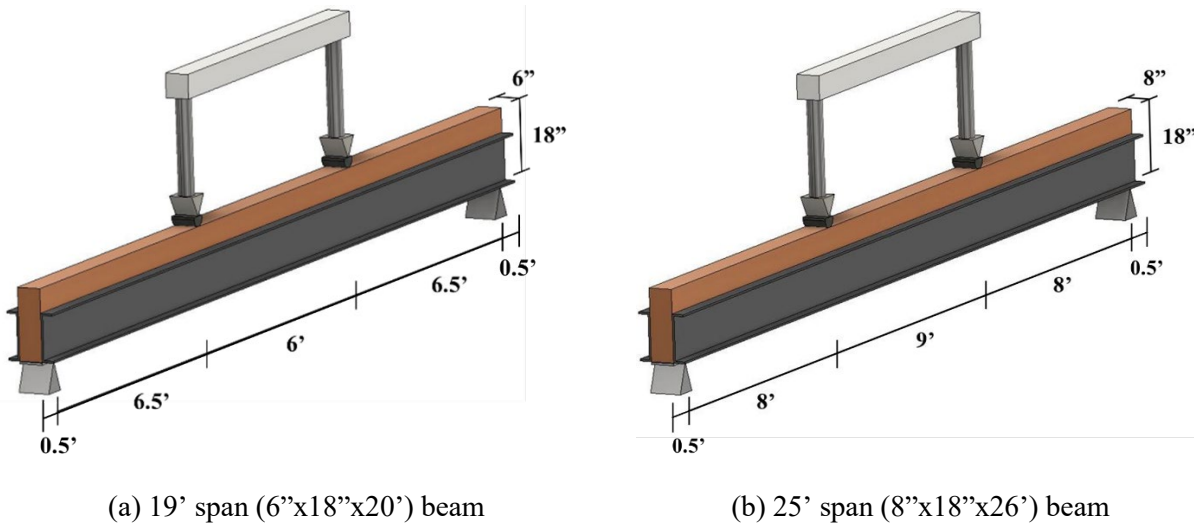
Figure 33: Flexure-controlled test setup
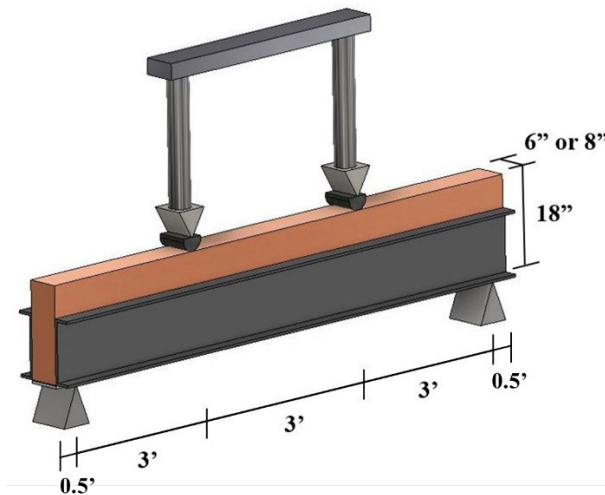
Figure 34: Shear-controlled test setup (for both 6"x18" and 8"x18")

In the setups, the loads were applied with two power-team 110 kip hydraulic actuators on the same hydraulic line, which resulted in equal loads on each actuator. Steel bearing plates (6"x8"x1") were included between the supports and the beams. Similarly, steel bearing plates were also included (6"x8"x1") between the actuators and the tops of the beam specimens. It should be noted that in accordance with the ASTM specifications, the plates between the actuators and the top of the beam had a radius of curvature of 4' on the loading surface of the block (Figure 35). Lateral bracings were provided at intermediate locations along the beam length to address any out-of-plane lateral instability and to prevent lateral torsional buckling.

Figure 35: Bearing plate with curvature

The specimens were tested until failure while recording the applied load and resultant deflections. The load was recorded with load cells attached to the ends of the actuators, and string potentiometers were used to record deflections at three points (midspan and quarter spans). Additionally, photographs were taken throughout testing and two GoPros were used to record videos of each test. Actual beam configurations in the lab are shown in Figure 36 - Figure 38.

Figure 36: Flexure test setup for 19' span beam
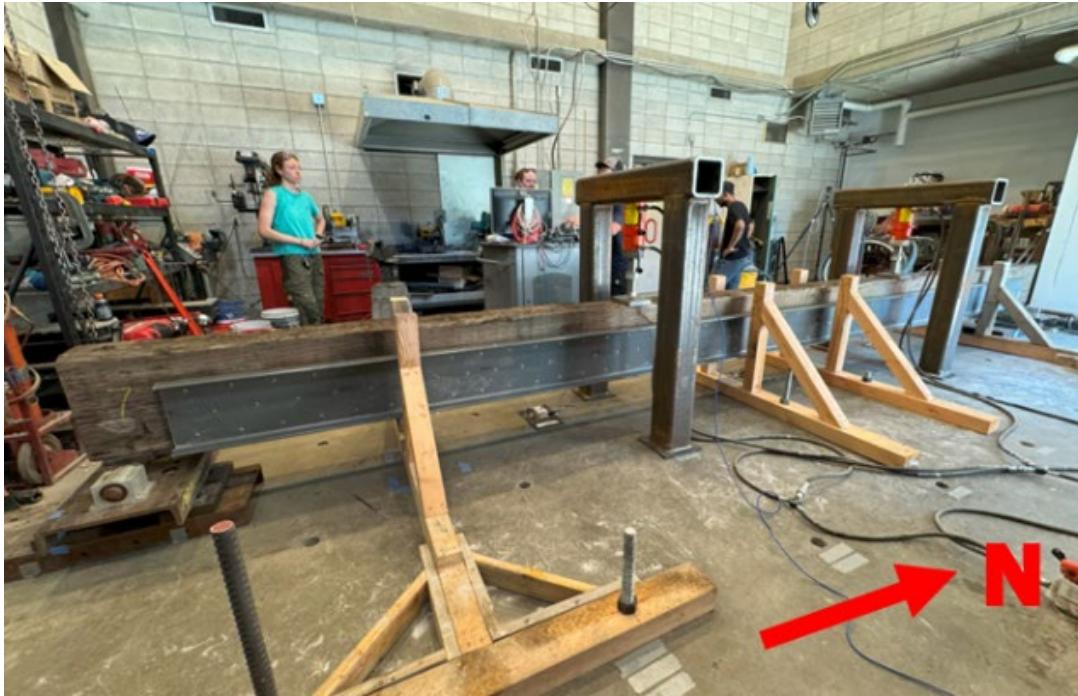
Figure 37: Flexure test setup for 25' span beam
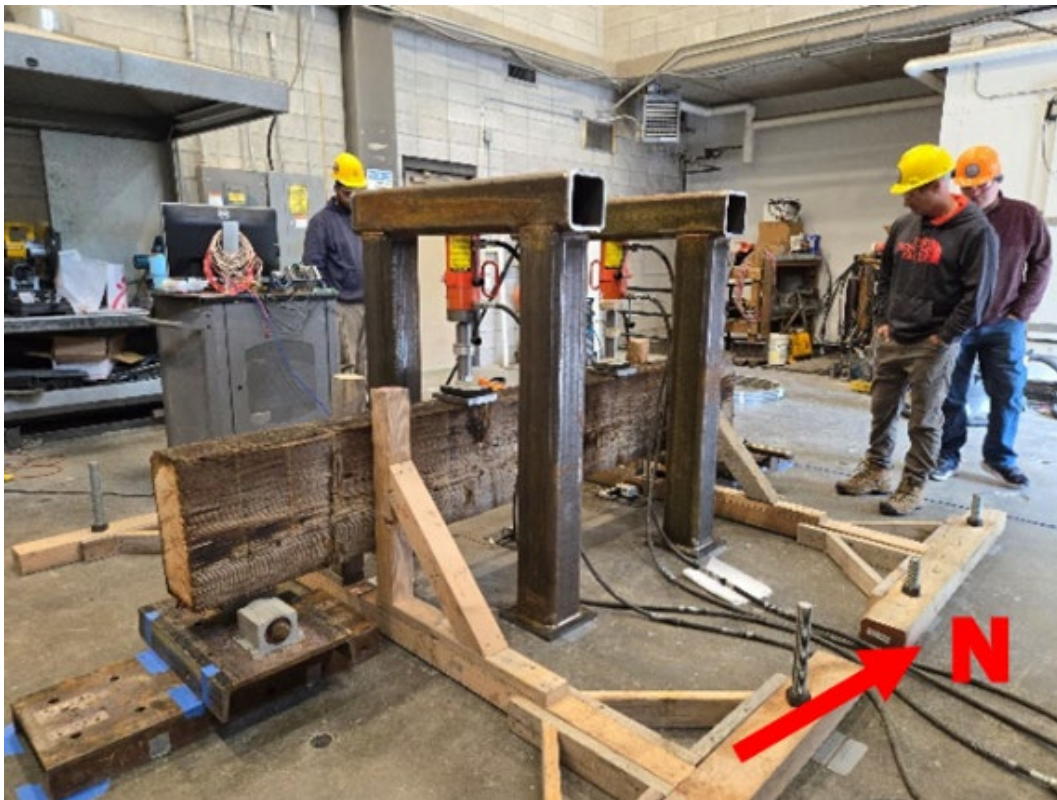
Figure 38: Shear test setup

6. TEST RESULTS

As discussed in the previous chapter, a total of twenty-two timber beams were tested in this research. These consisted of twelve 6"×18" beams and ten 8"×18" beams, encompassing various categories: control beams (tested under either flexure or shear), crack-repair beams (previously tested as controls and then repaired), split-repair beams (some initially tested as controls and others with existing splits prior to testing), and strengthened beams (which were undamaged prior to applying FRP reinforcement).

Results from this test series are summarized for the 6"x18" beams and 8"x18" beams in Table 2 and Table 3, respectively. The full detailed test summaries for each beam, along with the complete load–deflection plots and damage discussion, are provided in Appendix A. Common behavioral trends observed in these results are as follows.

- In general, beam size had no discernible influence on qualitative behavior or repair effectiveness, aside from the expected higher absolute capacity of the larger 8" sections.

- For the flexure-controlled beams, all control beams failed by fiber tension cracking near the center of the beams, with cracks often initiating at an imperfection. The repaired and strengthened beams increased ultimate capacity and postponed cracking. In most cases the FRP shifted the ultimate failure to either compressive crushing/cracking at the top of the beam, or in some cases the tests were terminated prior to failure due to instability/misalignment issues or actuator stroke limits.

- For the shear-controlled beams, the controls failed abruptly when horizontal splits formed at the supports, again often initiating at imperfections. The side-channel split repairs restored/increased the shear capacity of the beams, and in several cases, redirected the governing failure to crushing of the timber from bearing at the supports and/or loading points.

- Both crack- and split-repair schemes reliably restored the original strength, while preventive strengthening added 15–25% extra capacity. The combined flexure crack-repair and strengthening method, which includes FRP channels and strips (C-S) was more effective than the FRP strips alone (S).

The following sections of this chapter discuss these findings in more detail, with comprehensive data and analysis for each beam provided to support these summary observations.

Table 2: Summary results of 6"x18" beams

Beam Acronym	Creaking			First crack/split			Bearing failure			Crushing on top			Ultimate load		Ultimate failure/End of the test
	Load* (kips)	Deflection (inch)	Location	Load (kips)	Deflection (inch)	Location	Load (kips)	Deflection (inch)	Location	Load (kips)	Deflection (inch)	Location	Load (kips)	Deflection (inch)	
6-Sh(1)	**	**	**	**	**	**	21.3	0.50"	Load bearing blocks	**	**	**	27.0	0.89"	Shear splitting on the left end of the beam through a knot
6-Fl(1)	17.0	1.80"	Near South lateral bracing	20.0	2.00"	Crack near D1	**	**	**	**	**	**	22.4	2.53"	Tension crack
6-Fl(2)	16.5	1.66"	**	**	**	**	**	**	**	**	**	**	19.4	1.96"	Tension crack
6-Fl(1)-CR(C-S)	13.8	1.34"	South end	16.2	1.60"	**	**	**	**	28.7	3.69"	North load block	29.1	3.98"	Stopped loading because blocks weren't centered
6-Fl(2)-CR(S)	15.0	1.43"	**	21.0	2.02"	Split on the North end	**	**	**	**	**	**	21.0	2.02"	Reached stroke limit
6-Sh(1)-SR(C)	**	**	**	**	**	**	30.0	1.69"	Load bearing blocks	**	**	**	30.1	1.69"	The north end leaned due to bearing failure
6-Fl-SR(C-S)	9.0	0.89"	at the ends	10.5	1.00"	Split on the south end	**	**	**	28.0	3.51"	Middle	30.9	4.27"	Slight eccentricity on the load cell
6-Fl-SR(C3)	Started immediately with the testing			4.0	0.58"	Crack at mid-span	**	**	**	**	**	**	9.9	2.16"	Mid-span shot off middle string potentiometer
6-Fl-SR(C6)	12.5	1.20"	**	12.5	1.20"	Compression crack near the top, close to the north load cell	**	**	**	16.2	1.56"	Near South load cell	21.7	2.77"	Tension crack
6-Sh-St(C)	30.4	0.96"	**	30.4	0.96"	Split on the south end	30.5	0.97"	Load bearing blocks	**	**	**	33.2	1.10"	Eccentricity started on the north load cell
6-Fl-St(C-S)	9.0	0.72"	**	25.8	2.05"	Crack at mid-span	29.1	2.77"	North Load bearing block	**	**	**	29.1	2.77"	Bearing failure at the north load-bearing block
6-Fl-St(S)	13.0	1.17"	Midspan	22.2	2.10"	Cracking under strip on the east	24.0	2.50"	North Load bearing block	**	**	**	25.4	2.81"	Shear split at the south end

* The load is from one actuator ("P" in Figure 32).

Table 3: Summary results of 8"x18" beams

Beam Acronym	Creaking			First crack/split			Bearing failure			Crushing on top			Ultimate load		Ultimate failure/End of the test
	Load* (kips)	Deflection (inch)	Location	Load (kips)	Deflection (inch)	Location	Load (kips)	Deflection (inch)	Location	Load (kips)	Deflection (inch)	Location	Load (kips)	Deflection (inch)	
8-Sh(1)	**	**	**	**	**	**	25.0	0.45"	Load bearing blocks	**	**	**	37.9	0.98"	Shear split at the end
8-Fl(1)	3.0	0.48"	**	16.5	2.37"	Tension crack at mid-span	**	**	**	**	**	**	22.0	3.28"	Tension crack
8-Fl(2)	10.5	1.66"	Midspan	11.8	1.93"	Shear split at the north end	**	**	**	**	**	**	12.0	2.56"	Tension crack at the bottom mid-span
8-Fl(1)-CR(C-S)	10.4	1.53"	**	30.3	4.28"	Compression in the middle	**	**	**	31.7	4.64"	Near South load cell	33.1	5.28"	Reached stroke limit
8-Fl(2)-CR(S)	13.0	2.30"	Midspan	20.0	3.79"	Crack at the top middle through a knot	**	**	**	**	**	**	23.6	5.08"	Failed in compression through a knot at the top middle
8-Sh(1)-SR(C)	**	**	**	**	**	**	26.0	0.76"	North Load bearing block	**	**	**	42.3	1.58"	Shear failure on the south end, propagated from the bearing failure
8-Fl-SR(C-S)	11.8	1.41"	**	16.7	1.99"	Bottom middle	**	**	**	22.9	2.86"	Top middle	24.8	5.22"	Reached stroke limit
8-Sh-St(C)	35.0	0.65"	**	**	**	**	43.0	0.87"	Reaction bearing plates at the supports	**	**	**	56.3	1.45"	Shear split on the north end
8-Fl-St(C-S)	16.0	1.86"	**	21.5	2.47"	**	**	**	**	28.5	3.52"	Top middle	31.9	5.32"	Reached stroke limit
8-Fl-St(S)	14.0	1.68"	Throughout the beam	22.7	2.81"	**	25.0	4.46"	North load block	**	**	**	28.8	3.76"	Tension crack propagating mid-span and compression failure at the north load block

* The load is from one actuator ("P" in Figure 32).

6.1 Flexure test-setup beam results

This section discusses the performance of beams tested in the flexure test setup, including control, crack-repair, split-repair, and strengthened beams, using various repairing and strengthening techniques for 6"x18" and 8"x18" beams.

6.1.1   Control vs crack-repair and strengthened beams with FRP channels and strip

Figure 39 and Figure 40 show the three tested configurations of 6"×18" and 8"x18" timber beams, respectively: control, crack repair with C-S, and strengthened with C-S. The control beam displays the damage from testing. The repair beam is the same beam retrofitted with C-S combination, while the strengthened beam is an intact beam reinforced with C-S combination.
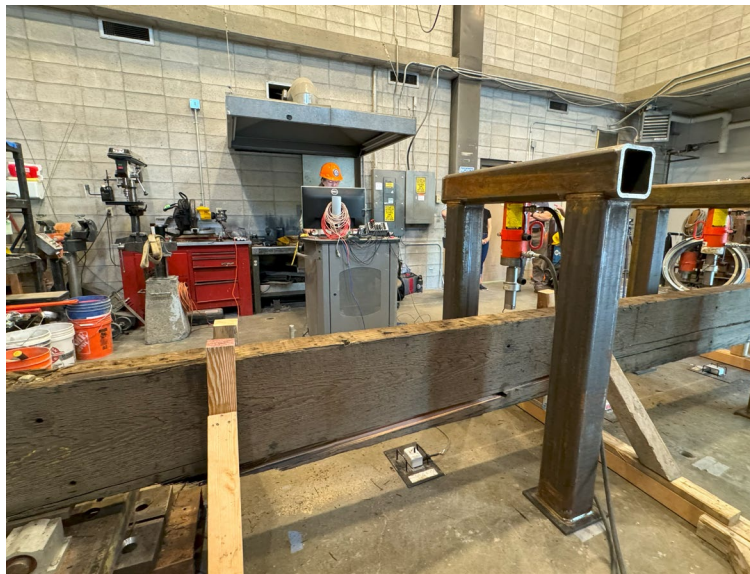
(a) Control – 6-Fl(1)
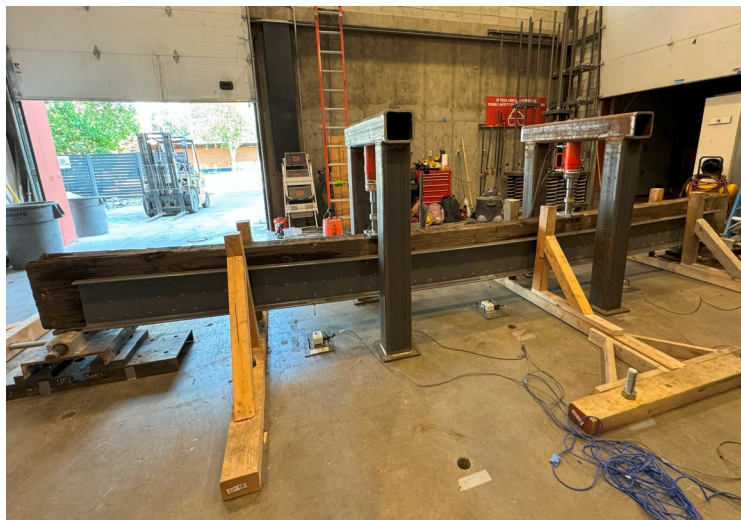
(b) Crack repair - 6-Fl(1)-CR(C-S)

(a) Strengthened - 6-Fl-St(C-S)

Figure 39: Control, crack-repair and strengthened 6"x18" beams with C-S combination

(a) Control - 8-Fl(1)

(b) Crack repair - 8-Fl(1)-CR(C-S)
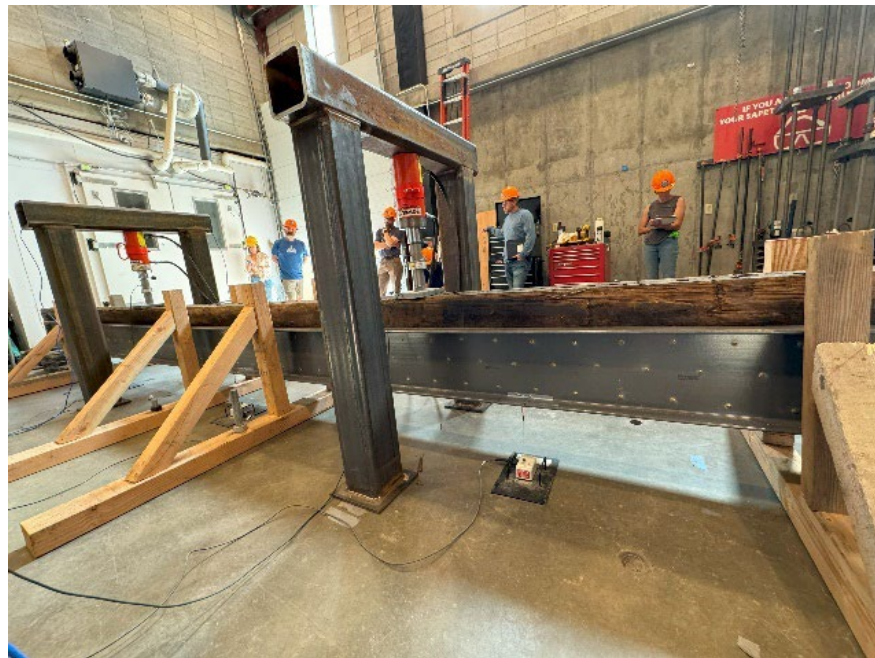
(c) Strengthened - 8-Fl-St(C-S)

Figure 40: Control, crack-repair and strengthened 8"x18" beams with C-S combination

Figure 41-a compares the 6"×18" beam results, a control beam (6-Fl(1)), a crack-repair beam with FRP channels and strips (6-Fl(1)-CR(C-S)), and a strengthened beam with FRP channels and strips (6-Fl-St(C-S)). As can be observed in this plot, the control beam reached an ultimate moment of 145.6 kip-ft at a mid-span deflection of 2.53", failing abruptly due to a tension crack. The crack-repair beam – which was the

previously tested control beam retrofitted with side channels and a bottom strip – achieved a higher moment capacity of 189.2 kip-ft with nearly the same initial stiffness as the control. This beam eventually failed by crushing of the wood under the north load block. The strengthened beam, which had the same FRP configuration applied to an undamaged specimen attained an ultimate moment of 189.15 kip-ft and exhibited the greatest stiffness among the three, finally failing by a bearing failure at the north load point. This demonstrates that adding the channel-and-strip reinforcement significantly increased the capacity over the unreinforced baseline.

Figure 41-b shows the analogous comparison for the 8"×18" beams. The unreinforced control beam (8-Fl(1)) carried an ultimate moment of 176.0 kip-ft at a deflection of 3.28″ before failing due to a mid-span tension crack. The crack-repair beam (8-Fl(1)-CR(C-S)), which had side channels and a strip added after its initial test, reached a higher ultimate moment of 264.0 kip-ft at 5.28″ deflection. The strengthened beam (8-Fl-St(C-S)), with similar FRP enhancements applied from the start, achieved an ultimate moment of 255.2 kip-ft at 5.32″. Both the repaired and strengthened 8" beams sustained greater loads and larger deformations than the control. The crack-repair beam's initial stiffness was similar to the control's, whereas the strengthened beam was noticeably stiffer. In terms of ultimate capacity, both FRP-enhanced beams significantly outperformed the control.

These results indicate that the FRP channel-and-strip reinforcement is highly effective: the repair technique successfully restored (and even increased) the beams' load capacities, and the strengthening approach appreciably enhanced stiffness and strength beyond the original values.

(a) 6"x18" beam data   (b) 8"x18" beam data
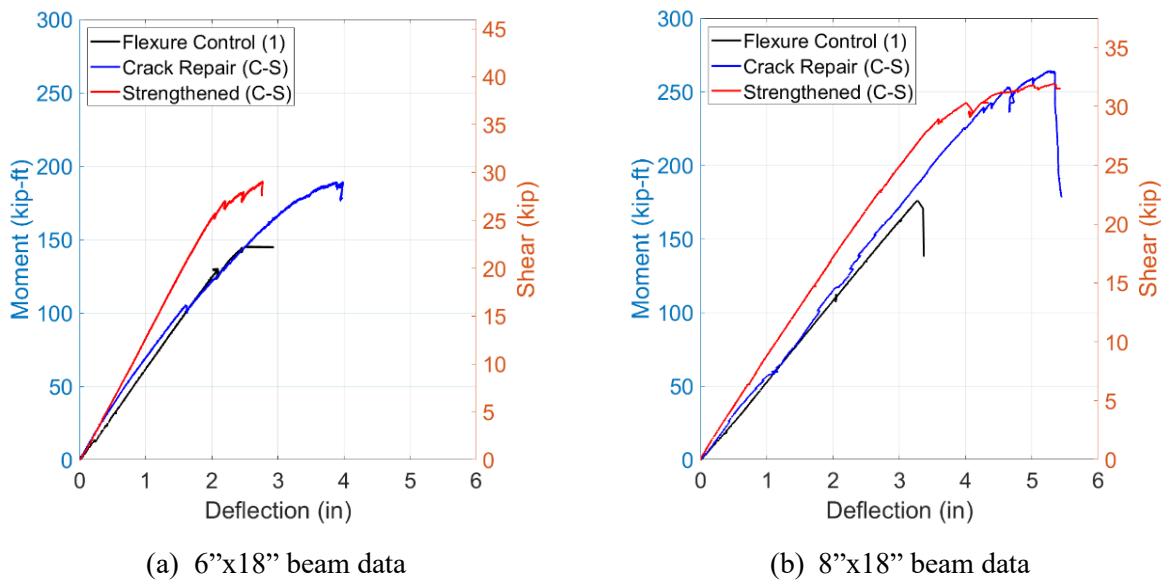
Figure 41: Comparison of control vs crack repair and strengthened beams with channels and strip

6.1.2   *Control vs crack-repair and strengthened beams with FRP strips*

Figure 42 and Figure 43 show the three tested configurations of 6"×18" and 8"x18" timber beams, respectively: control, crack repair with strip only, and strengthened with strip only. The control beam displays the damage from testing. The repair beam is the same beam retrofitted with strip only, while the strengthened beam is an intact beam reinforced with strip only.

(a) Control - 6-Fl(2)
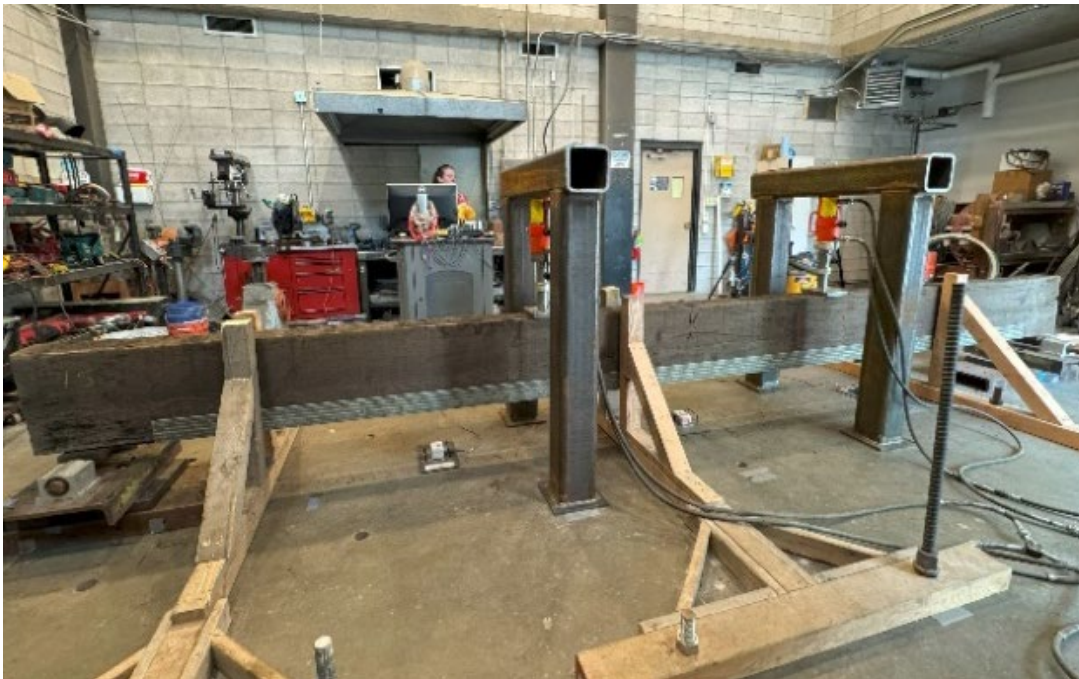
(b) Crack repair - 6-Fl(2)-CR(S)
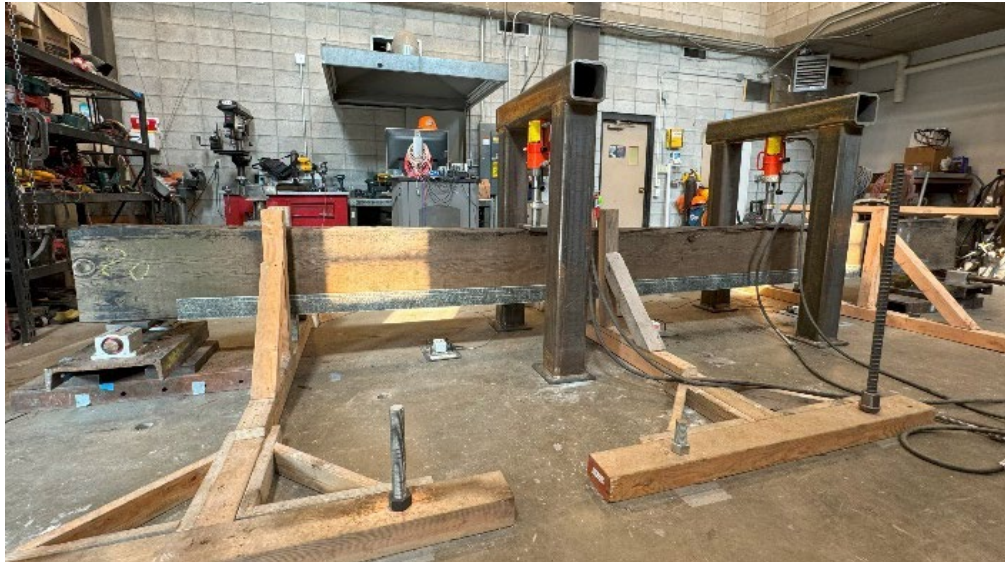
(c) Strengthened - 6-Fl-St(S)

Figure 42: Control, crack-repair and strengthened 6"x18" beams with strip only
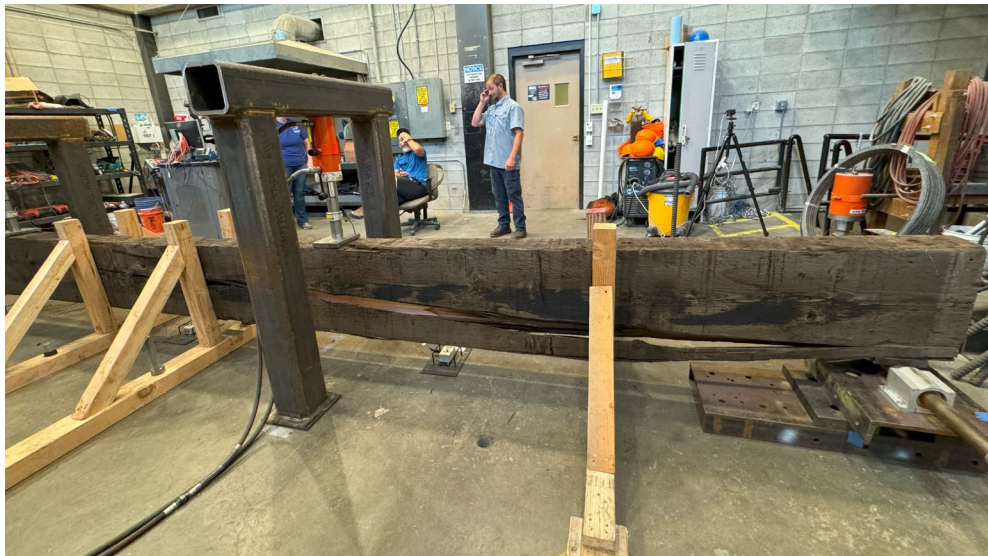
(a) Control - 8-Fl(2)

(b) Crack repair - 8-Fl(2)-CR(S)

(c) Strengthened - 8-Fl-St(S)

Figure 43: Control, crack-repair and strengthened 8"x18" beams with strip only

Figure 44-a compares the moment-deflection curves for the 6"x18" control beam (6-Fl(2)), the crack-repair beam with only FRP strips (6-Fl(2)-CR(S)), and the strengthened beam with only FRP strips (6-Fl-St(S)). The control beam exhibited a brittle failure, reaching an ultimate moment of 126.1 kip-ft before suddenly fracturing at a deflection of 1.96". The crack-repair beam, which was the same beam repaired by screwing FRP strips to its sides and bottom, initially mirrored the control's response and successfully restored the beam's original strength. However, a sharp drop in its curve occurred when a split opened at about 136.5 kip-ft and 2.02″ deflection. The strengthened beam, reinforced with strips on an undamaged beam, achieved a higher ultimate moment of 165.1 kip-ft and avoided the sudden post-peak drop observed in the repaired beam. All three 6″ beams displayed very similar initial stiffness.

Figure 44-b shows the moment-deflection curves for the 8″×18″ beams: control (8-Fl(2)), crack-repair with strips (8-Fl(2)-CR(S)), and strengthened with strips (8-Fl-St(S)). The control beam suddenly failed due to cracking at the mid-span, achieving an ultimate moment of approximately 96.0 kip-ft at a deflection of 2.50". The crack-repair beam, which had been heavily damaged in its initial test and then mended with FRP strips, demonstrated greatly improved performance: it reached roughly 188.0 kip-ft and sustained larger deflections than the control before failure. The strengthened beam, despite exhibiting some moderate pre-test checking along its length, carried the highest moment—nearly 232 kip-ft—and far outperformed the others. The strengthened beam's ability to maintain moment capacity illustrates the effectiveness of the strip reinforcement, providing enhanced structural resilience and delaying catastrophic failure. The initial stiffness of the crack-repair beam closely matched that of the control beam, while the stiffness of the strengthened beam surpassed the other two beams.

The comparison of the moment-deflection curves for both sets of beams highlights the significant benefits of either crack repair or strengthening using the FRP strip reinforcement. The control beams in each set displayed typical brittle failure with sudden fracture. The crack repair restored and even improved the beams' original strength, but a sudden drop in the moment-deflection graph was still observed due to the splitting of the 6"x18" beam. In contrast, the strengthened beams demonstrated superior performance, carrying the highest moments and maintaining structural integrity even after initial signs of damage. This indicates that FRP strip reinforcement enhances moment capacity and improves the beams' overall stiffness and resilience, effectively delaying catastrophic failure.

(a) 6"x18" beam data   (b) 8"x18" beam data
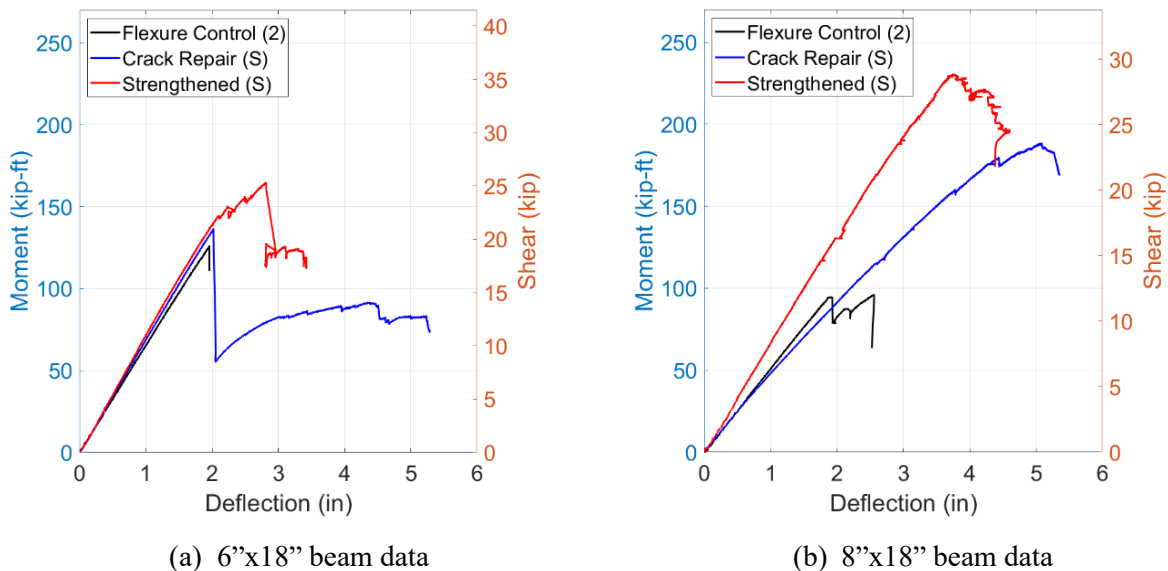
Figure 44: Comparison of control vs crack repair and strengthened beams with strips

6.1.3   Control vs split-repair flexure beams

Several beams in the flexure test series have preexisting splits near their ends. This section demonstrates the effectiveness of several repair methods at repairing these splits. Figure 45 show the three split repair configurations for 6"×18", respectively: split repair with channel and strip combination, split repair with 6' channel, and split repair with 3' channel. The 8"×18" split repair beam with channel and strip combination is shown in Figure 46.

(a) Split repair – 6-Fl-SR(C-S)

(b) Split repair - 6-Fl-SR(C6)

(c) Split repair - 6-Fl-SR(C3)

Figure 45: 6"x18" split repair beams tested in flexure setup

Figure 46: 8"x18" split repair beam with C-S tested in flexure setup - 8-Fl-SR(C-S)

Figure 47-a presents moment-deflection curves comparing two control beams and three different split-repair strategies for 6"×18" beams. Among the repaired beams, the one retrofitted with full-length side channels plus a bottom strip (6-Fl-SR(C-S)) was the most effective, reaching an ultimate moment of 200.9 kip-ft at a deflection of 4.27". This is a significant improvement compared to the control beams, where the first control beam (6-Fl(1)) reached 145.6 kip-ft and the second control beam (6-Fl(2)) reached 126.1 kip-ft. Additionally, the fully repaired beam demonstrates similar stiffness as the control beams, while maintaining its stiffness and continuing to carry higher moments surpassing the control ultimate capacities.

The beam repaired with 6' channels on each end (blue line) achieved an ultimate moment of 141.1 kip-ft at a deflection of 2.77", which is closer to the performance of the control beams but significantly lower than the robust repair with full-length channels and strip. The repair method with 3' channels on the ends (green line) was least effective, with this beam reaching a moment of only 64.4 kip-ft at a deflection of 2.16". This method offered minimal improvement compared to the second control beam and fell short compared to the other repair methods, suggesting that 3' of the channel sections is insufficient to fully repair an existing split and restore shear capacity. The analysis shows that the split repair method using side channels combined with a strip is the most effective, providing the highest moment capacity, but a minimum of 6' channels for a split repair can result in capacities comparable to undamaged beams.

The performance of the 8″×18″ beams with split repairs is shown in Figure 47-b. The beam repaired with side channels and a strip (8-Fl-SR(C-S)) attained an ultimate moment of 198.4 kip-ft, substantially higher than the two control beams (8-Fl(1) at 176.0 kip-ft, and 8-Fl(2) at 96.0 kip-ft). It is noteworthy that the two 8″ control beams had a large disparity in strength, likely due to pre-existing defects (such as severe checks and wane in the weaker beam) and the inherent variability in timber, such as knots, cracks, and variations in growth patterns in the timber. The repaired beam not only recovered the capacity lost due to the split but actually exceeded the stronger control's capacity, and it also exhibited higher stiffness than both controls (unlike the 6″ case, where the repaired beam's stiffness was on par with the controls). The load-deflection response of the repaired beam featured multiple smaller peaks, indicating a progressive failure with stages of damage rather than one sudden break. Overall, the split-repair technique with full-length channels and a strip significantly improved the structural performance of the 8″ beam, making it much more resilient under load than either control beam.

Overall, the split repair method using side channels combined with a strip significantly enhanced the structural performance of both the 6"x18" and 8"x18" beams, making it the most effective repair technique among those tested. This method increased the ultimate moment capacity and maintained or improved the stiffness compared to the control beams. In the short channels repair method, the 6' channel successfully repaired the split, achieving a moment capacity comparable to the control beam, whereas the 3' channel proved insufficient for effective repair. Overall, this comprehensive repair approach significantly improves the moment capacity, demonstrating the importance of robust reinforcement strategies in structural repair. Figure 45 and Figure 46 show the 6"x18" and 8"x18" split repair beams tested in flexure setup, respectively.

(a) 6"x18" beam data

(b) 8"x18" beam data
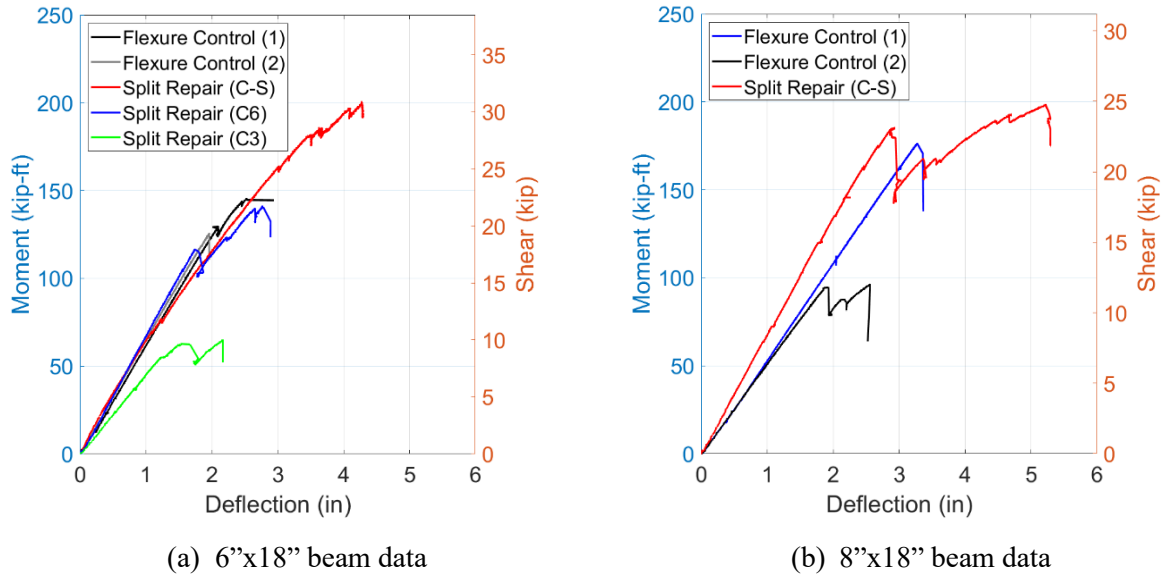
Figure 47: Comparison of control vs split repair beams

6.2 Shear test-setup beam results

This section discusses the performance of beams tested in the shear setup, including control beams and those that were split-repaired or strengthened with side channels along the entire length of the beam, for both 6"×18" and 8"×18" members. Figure 48 and Figure 49 show the three tested configurations of 6"×18" and 8"x18" timber beams, respectively: control, split repair with channel, and strengthened with channel. The control beam displays the damage from testing. The repair beam is the same beam retrofitted with channel, while the strengthened beam is an intact beam reinforced with channel.

(a) Control – 6-Sh(1)

(b) Split repair – 6-Sh(1)-SR(C)

(c) Strengthened - 6-Sh-St(C)

Figure 48: Control, split repair and strengthened 6"x18" beams with channel only
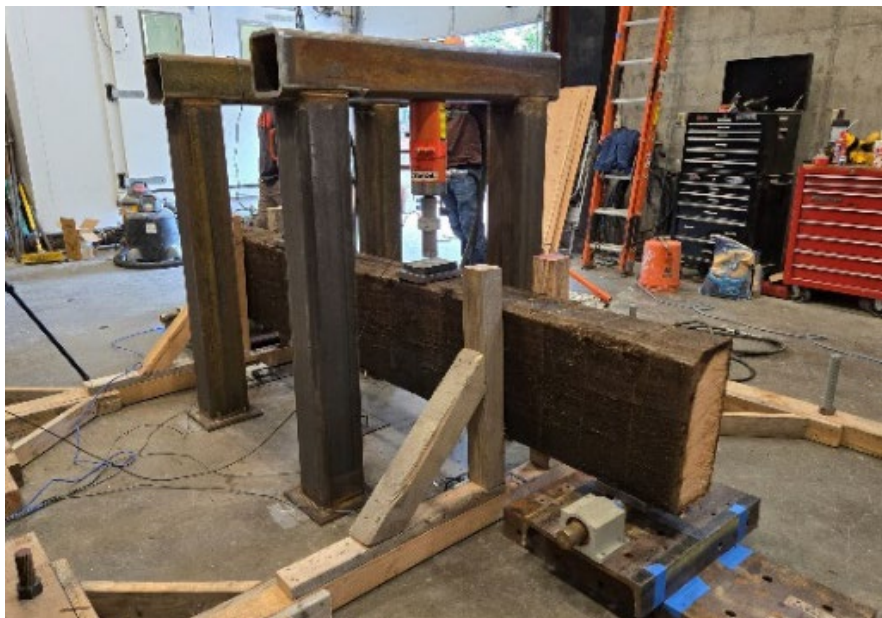
(a) Control – 8-Sh(1)

(b) Split repair – 8-Sh(1)-SR(C)

(c) Strengthened - 8-Sh-St(C)

Figure 49: Control, split repair and strengthened 6"x18" beams with channel only

Figure 50-a compares the shear-deflection curves of the three 6"x18" beams tested in this configuration: the control beam (6-Sh(1)), the split-repair (6-Sh(1)-SR(C)), and the strengthened beam (6-Sh-St(C)). The control beam reached an ultimate shear of 27.0 kips with a mid-span deflection of 0.89" before failing abruptly due to the formation of a horizontal split near the supports of the beam. In contrast, the split-repair beam, which had its end split repaired by attaching full-length FRP channels to the sides, demonstrated a more gradual load increase and ultimately bore a higher shear of 30.1 kips at a deflection of about 1.69". The

strengthened beam exhibits the best performance, achieving the highest ultimate shear of 33.2 kips at a mid-span deflection of 1.1".

Figure 50-b shows the shear-deflection graphs of the three 8"x18" beams tested in this configuration: control beam (8-Sh(1)), split-repair beam (8-Sh(1)-SR(C)), and strengthened beam (8-Sh-St(C)). The control beam exhibited an ultimate shear of 37.9 kips at a mid-span deflection of 0.98" before failing due to a split at its end. In contrast, the split-repair beam (same original control beam repaired with channels on its sides) had an increased shear capacity, reaching 42.3 kips at a mid-span deflection of 1.58". The most significant improvement is seen in the strengthened beam, which achieved a peak shear of 56.3 kips due to the strengthening channels and initially undamaged state of the beam.

(a) 6"x18" beam data   (b) 8"x18" beam data
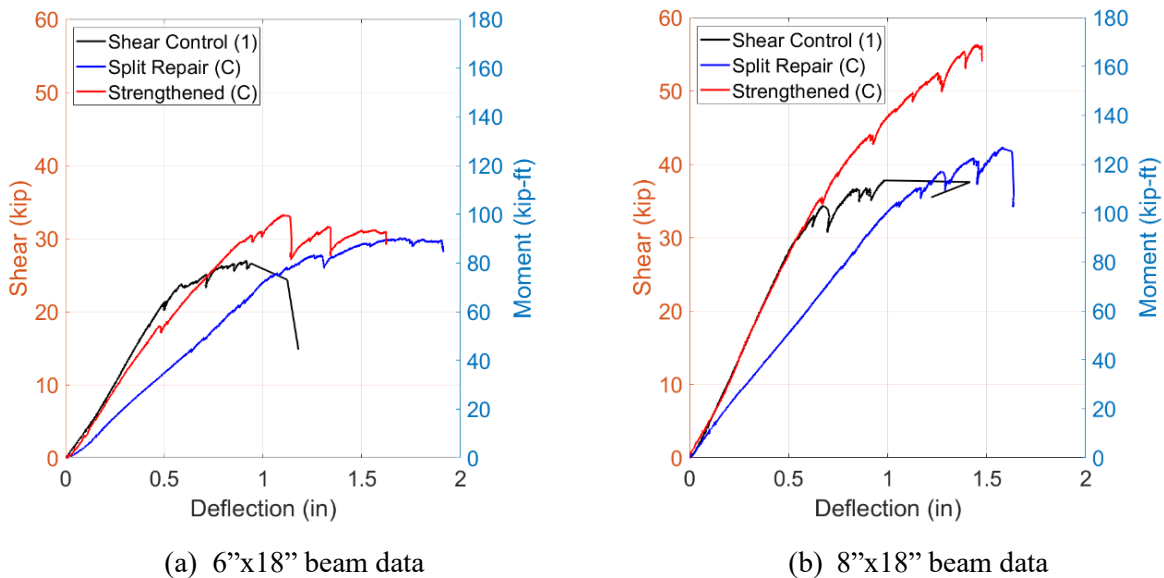
Figure 50: Comparison of control vs split repair and strengthened beams with channels in shear setup

Another observation from Figure 50 is the distinct differences in initial stiffnesses between the control beams and their repaired counterparts. The split-repair beams exhibited lower stiffnesses than their control counterparts, primarily due to bearing failures that occurred during the original control beam testing. This damage caused significant softening of the wood at the load and support points. Although FRP channels were attached on the sides to repair the splits, the bearing damage itself was not addressed, resulting in greater deflections when the repaired beams were reloaded. In contrast, the initial stiffness of the strengthened beams closely matched that of the control beams, as these beams had not experienced prior bearing damage.

Overall, for both beam sizes, the side-channel repairs restored and modestly increased the shear capacity relative to the control beams, but the repaired beams showed reduced initial stiffness due to the unrepaired bearing damage from the control-phase failures. The strengthened beams, on the other hand, achieved the highest ultimate shears and closely maintained the initial stiffness of the control beams. These results confirm the effectiveness of applying FRP channels on the sides of timber beams in both restoring and enhancing shear performance after shear-split damage.

6.3 Comparison of repair/strengthening techniques

This section compares the different repair/strengthening techniques for addressing cracks and splits in the 6"x18" and 8"x18" beams. The crack-repair beams are repaired either with the combination of FRP channels on the sides and an FRP strip on the bottom or FRP strips on the sides and bottom. For the 6"x18" beams, the crack-repair beam with channels on the sides and a strip on the bottom (Figure 51-a, red line) demonstrated superior performance compared to the beam repaired with only strips (Figure 51-a, blue line). The combination of channels and strip provided enhanced reinforcement and better moment capacity than the strips alone. Specifically, the channel-strip repair increased capacity by 29.9% over its corresponding control (145.6 to 189.2 kip-ft), while the strip-only repair showed 8.3% improvement (126.1 to 136.5 kip-ft). The added channels contributed additional support, particularly for beams with more severe damage.

Similarly, in the 8"x18" beam set, the repair using channels and a strip (Figure 51-b, red line) outperformed the repair with strips alone (Figure 51-b, blue line). The channel-strip repair led to a 50.5% increase in capacity compared to its control (176.0 to 264.8 kip-ft), whereas the strip-only repair doubled the capacity, showing a 96.7% increase over its respective control (96.0 to 188.8 kip-ft). The 8"x18" beams, with four FRP strips on the sides and one on the bottom, showed that while strips provided substantial improvement compared to the control, particularly because the corresponding control beam underperformed. Overall, the combination of channels and strips offered more significant enhancement, reinforcing the beam more effectively and improving overall structural performance. Control beam capacities are shown as dashed lines in Figure 51 for direct comparison.

(a) 6"x18" beam data   (b) 8"x18" beam data
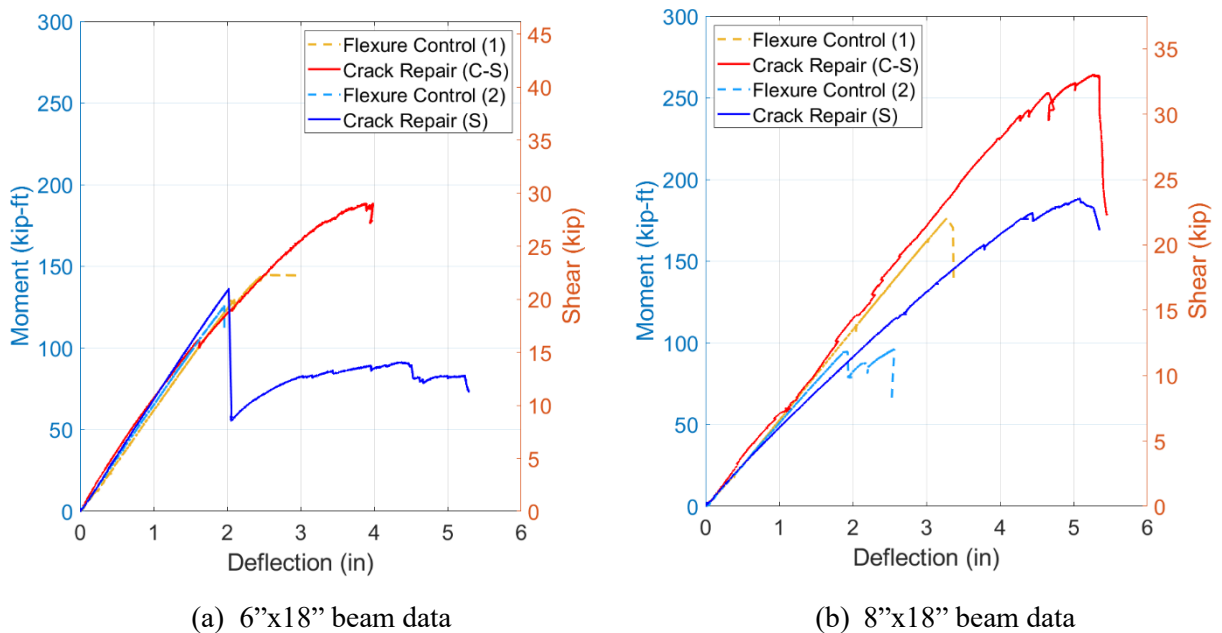
Figure 51: Comparison of different techniques of crack repair

The comparison between beams strengthened with a channel-strip combination and those strengthened with only strips shows that both techniques performed well, with the channel-strip configuration demonstrating a slight improvement in structural performance for both the 6"x18" and 8"x18" beams. For the 6"x18" beam, the configuration with two channels on the sides and a strip at the bottom (Figure 52-a, red line)

achieved an ultimate moment capacity of 182.0 kip-ft, representing a 25% increase over its corresponding control (145.6 kip-ft). The beam strengthened with strips only (Figure 52-a, blue line) reached 165.1 kip-ft, showing a 30.9% increase over its respective control (126.1 kip-ft).

Similarly, for the 8"x18" beam set, the channel-strip strengthened beam (Figure 52-b, red line) achieved an ultimate moment of 255.2 kip-ft, a 45.0% improvement compared to the control (176.0 kip-ft), while the strip-only beam (Figure 52-b, blue line) reached 230.4 kip-ft, marking a 140.0% increase over the control beam (96.0 kip-ft). This higher gain is partly attributed to the relatively lower performance of the corresponding control beam. While the channel-strip combination offers slightly higher moment capacity and improved structural integrity, the strips-only configuration also provided substantial reinforcement, indicating that both strategies are effective in enhancing beam performance. Control beam capacities are shown as dashed lines in Figure 52 for direct comparison.

(a) 6"x18" beam data   (b) 8"x18" beam data
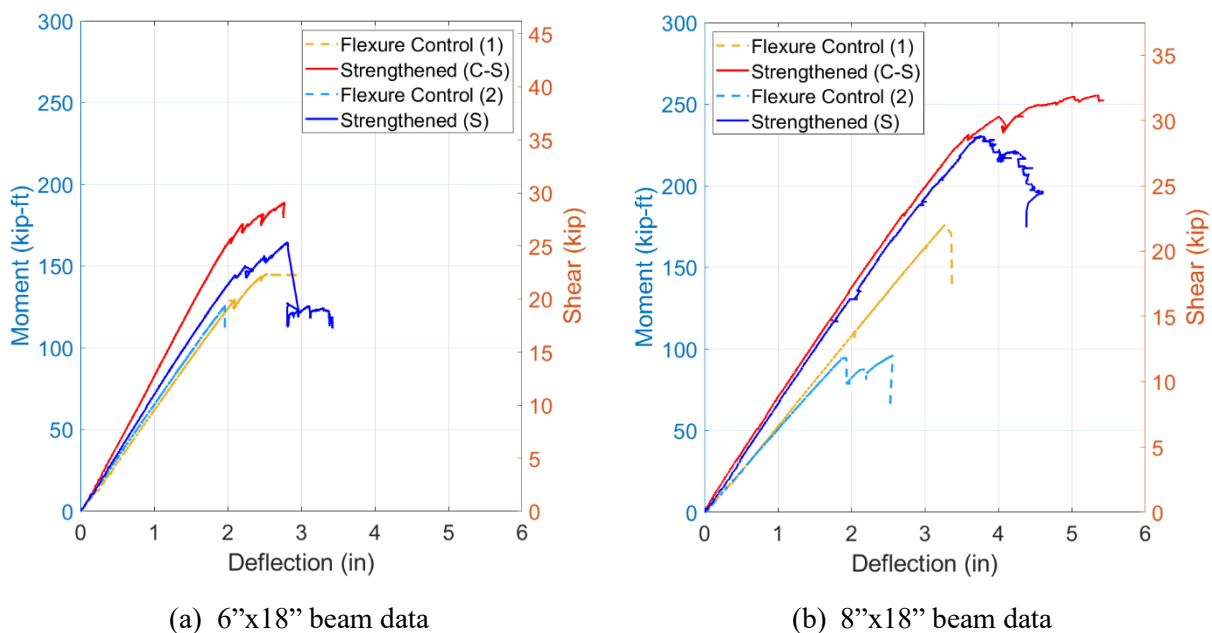
Figure 52: Comparison of different techniques of strengthening

The comparison of the three split-repair 6"x18" beams, presented in Figure 53, reveals notable differences in performance based on the repair techniques used. The beam repaired with FRP channels on the sides and an FRP strip on the bottom (red line) exhibited the most robust performance, with the highest moment capacity. In contrast, the beam with 6' channels on the ends of each side (blue line) demonstrated improved shear capacity but struggled with significant tension cracks and compression failures. The beam repaired with shorter 3' channels on the ends (green line) showed no improvement and underperformed compared to the controls (showed in dashed line Figure 53), as the limited channel length did not adequately support the beam and arrest the split growth, leading to premature failure. Thus, the combination of channels and strips proved to be the most effective repair method, offering superior reinforcement and performance compared to channel-only approaches.
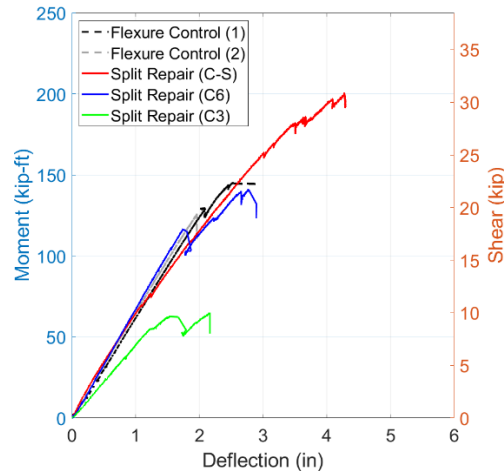
Figure 53: Comparison of different split repair techniques

Overall, the comparison of repair techniques for crack and split repair in both 6"x18" and 8"x18" beams shows that using a combination of FRP channels on the sides and an FRP strip on the bottom consistently outperformed the use of FRP strips alone. However, the strip only repair/strengthening beams still performed well and exceeded control capacities. The added channels significantly improved moment capacity, especially when repairing beams with more severe damage. In split-repair beams, the channels and strip combination proved to be the most effective, offering better structural performance and preventing premature failure, while shorter channel-only repairs were less successful.

6.4 <u>Summary of repaired beams</u>

This section does not present any new data but instead provides a detailed, side-by-side comparison of each beam that was tested, repaired, and retested (6 beams total). Because the same beam was used in both the initial control test and the repaired test, the comparisons directly reflect the effects of the repair methods.

As previously discussed, the 6"x18" and 8"x18" beam sets include three control beams each, one tested in the shear test setup and two in flexure test setups. After the control beams were tested for failure, they were subsequently repaired and retested. The shear setup beams (6–Sh(1) and 8–Sh(1)) failed due to splitting at the ends and were repaired with FRP channels attached to the sides (6–Sh(1)–SR(C) and 8–Sh(1)–SR(C)). The flexure setup beams (6–Fl(1), 8–Fl(1) and 6–Fl(2), 8–Fl(2)) failed due to tension cracking at the bottom mid-span. For the flexure beams, one set (6–Fl(1) and 8–Fl(1)) was repaired with FRP channels on the sides and an FRP strip on the bottom (6–Fl(1)–CR(C-S) and 8–Fl(1)–CR(C-S)). The other set (6–Fl(2) and 8–Fl(2)) was repaired with FRP strips attached on both the sides and bottom (6–Fl(2)–CR(S) and 8–Fl(2)–CR(S)).

For all 6"x18" beams, the repaired beams showed improvements in capacity compared to their respective control beams, highlighting the effectiveness of the repair techniques. The split-repair beam (Figure 54-a, blue line) which had channels attached on the sides, restored and enhanced the shear capacity by approximately 11% compared to the control beam (Figure 54-a, black line), demonstrating that the side channels effectively mitigated the damage and provided additional shear resistance. In the flexure setup, the crack-repair beam (Figure 54-b, blue line), reinforced with channels on the sides and a strip on the

bottom, exhibited a substantial 30% increase in ultimate moment capacity compared to the control beam (Figure 54-b, black line). The crack-repair beam, strengthened with strips on the sides and bottom (Figure 54-c, blue line), showed a 9% increase in moment capacity compared to the control beam (Figure 54-c, black line). Although this was slightly less optimal than the performance of the beam reinforced with both channels and strips, it still demonstrates an effective repair.
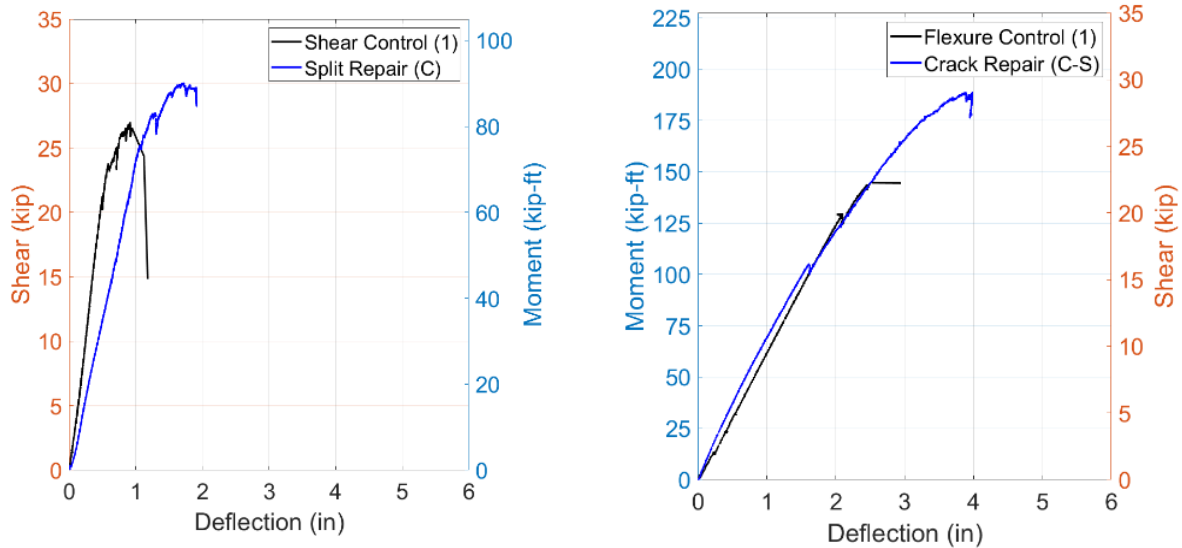
(a) Shear control vs split repaired with channels   (b) Flexure control vs crack repaired with channels and strip
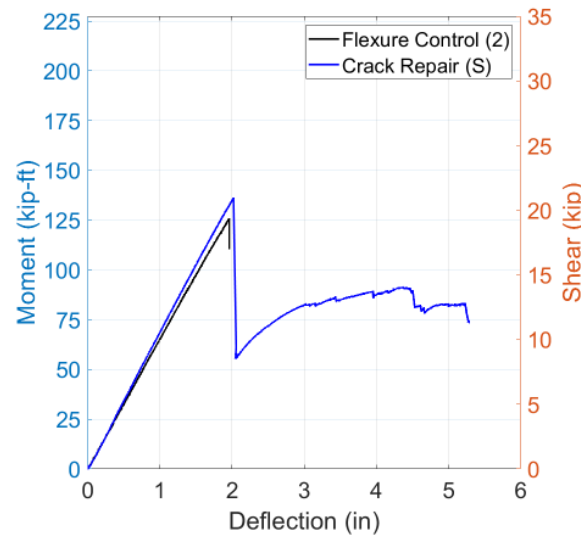
(c) Flexure control vs crack repaired with strip

Figure 54: 6"x18" control vs. repair beam results

The comparison of the control beams and their repaired versions in the 8"x18" beam set reveals significant improvements in capacity due to the repair techniques employed. In the shear setup, the control beam (Figure 55-a, black line) was repaired with channels on the sides (Figure 55-a, blue line), resulting in an

11.5% increase in shear capacity. This enhancement indicates that the side channels effectively repaired the split and strengthened the beam's shear resistance. For the flexure setup, the first control beam (Figure 55-b, black line) was repaired with channels on the sides and a strip on the bottom (Figure 55-b, blue line), which led to a substantial 50.1% increase in moment capacity. This approach significantly reinforced the beam against tension cracking and remarkably improved its performance. Similarly, the second flexure control beam (Figure 55-c, black line) was repaired with strips on the sides and bottom (Figure 55-c, blue line) resulting in an impressive 96.1% increase in moment capacity. The strips effectively confined cracking and greatly enhanced the flexural strength of the beam. However, it is important to note that the 96.1% increase may be artificially high as a result of the repaired capacity being compared with the lower capacity of the second control beam due to the pre-existing checking and wane defects.
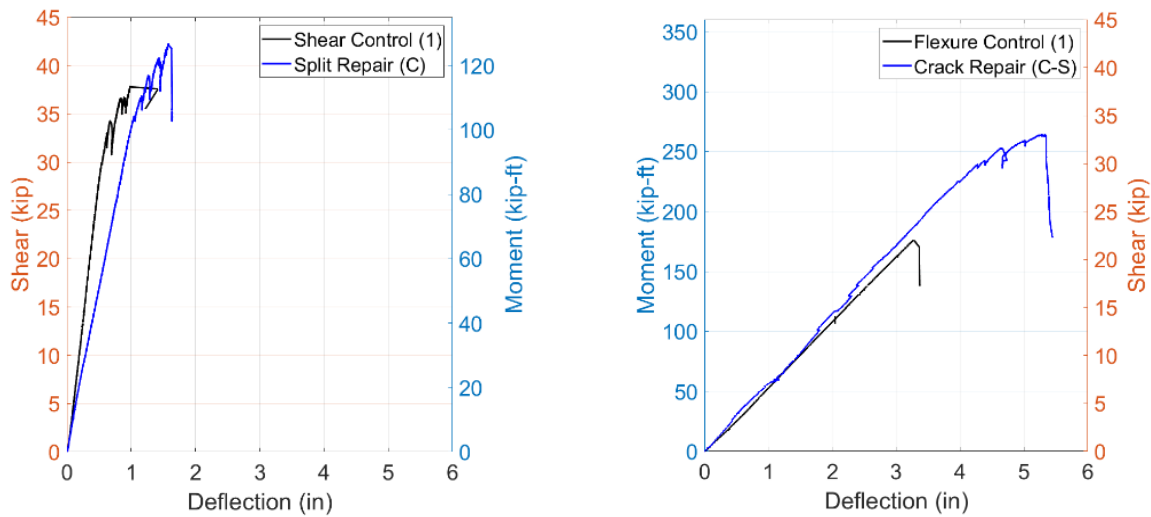
(a) Shear control vs split repaired with channels

(b) Flexure control vs crack repaired with channels and strip
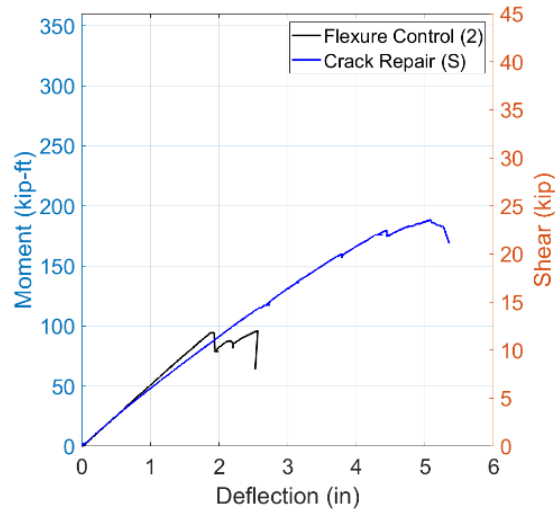
(c) Flexure control vs crack repaired with strip

Figure 55: 8"x18" control vs. repair beam results

Overall, the repair techniques applied to both the 6"x18" and 8"x18" beams restored the original capacities of the control beams, often increasing their capacities by significant amounts, and enhanced their performances. The combination of channels and strips was particularly effective in providing comprehensive reinforcement and resulting in the largest increases in capacity.

6.5 Consistency of Channel-Strip combination technique

The control beams (Figure 56), both 6" and 8", exhibited variability in their capacities due to the inherent inconsistencies, including grain orientation, and initial internal/external defects, typical for timber members. For the 6" beams, the difference between control beams (145.6 kip-ft and 126.1 kip-ft, respectively) resulted in a variation of approximately 13.4%. The 8" control beams showed even greater variability, with a substantial 45.45% difference between the control beams (176.0 kip-ft and 96.0 kip-ft, respectively), again keeping in mind the lowered capacity of the second control beam likely due to existing initial defects.

In contrast, the beams repaired and strengthened with the FRP channel and strip combination demonstrated notably consistent performance. For the 6" beams (Figure 57-a), the C-S combination resulted in a maximum variation of only 6.19%. The split repair beam (200.9 kip-ft) showed minimal deviation from the crack repair and strengthened beams, both of which achieved an ultimate moment capacity of 189.2 kip-ft. Similarly, the 8" beams (Figure 57-b) exhibited almost identical performance, with the crack repair and strengthened beams reaching ultimate moment capacities of 264.8 kip-ft and 271.2 kip-ft, respectively, showing a minimal variation of 3.63%. While the split repair beam exhibited slightly more variability, with a lower moment of 198.4 kip-ft and a 25.15% difference from the crack repair beam. This consistent performance underscores the effectiveness of applying FRP to timber beams in reducing the inherent variability, providing more reliable structural performance.

(a) 6"x18" beam data   (b) 8"x18" beam data
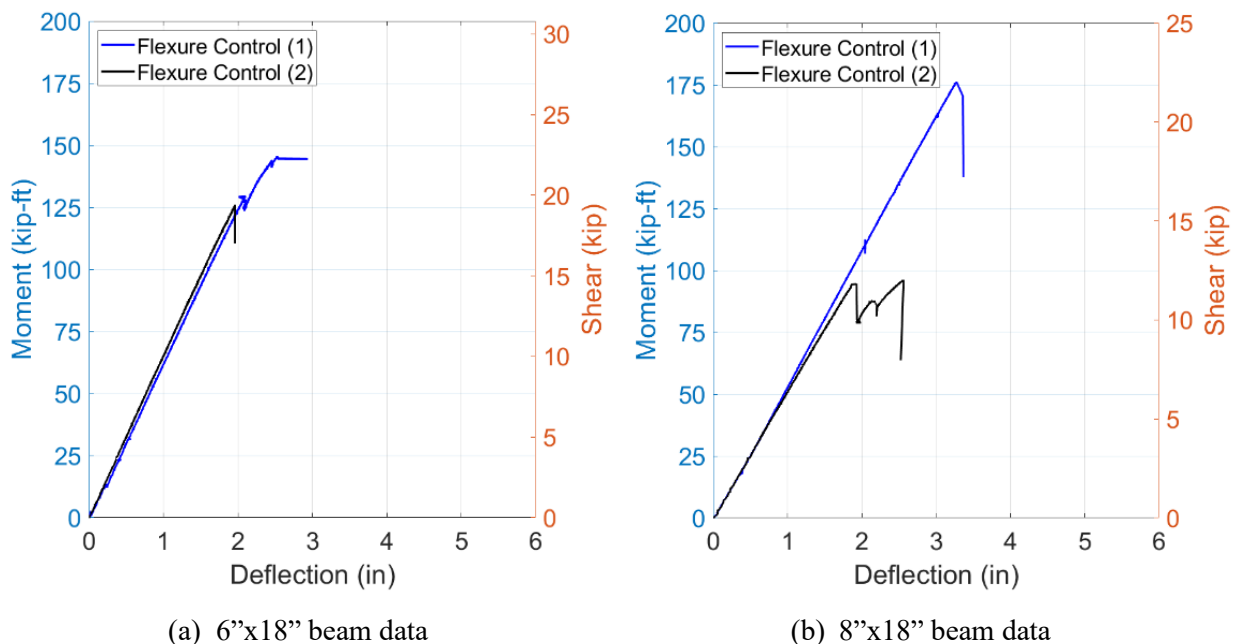
Figure 56: Moment vs deflection graph of control beams, tested in flexure setup

(a) 6"x18" beam data (b) 8"x18" beam data
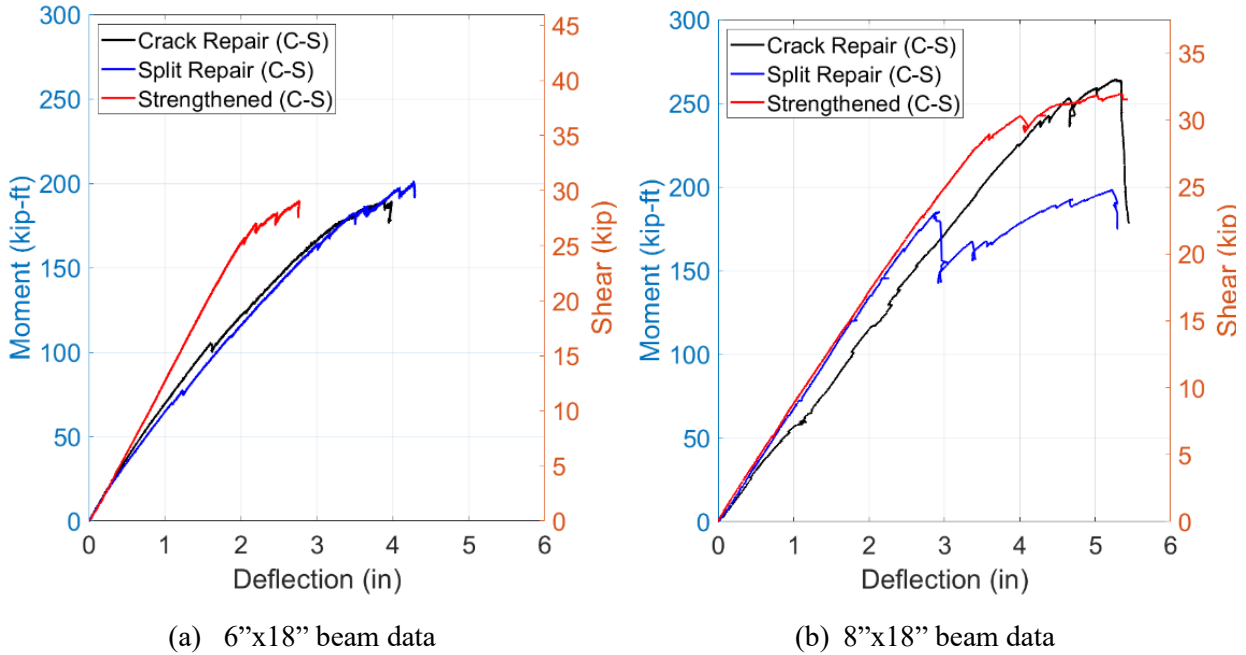
Figure 57: Moment vs. deflection graph of beams with C-S combination, tested in flexure setup

6.6 Comparison between measured and AASHTO predicted capacities

A comparison between the measured ultimate moments obtained from the experimental test and the calculated moment capacities based on standard design equations is presented in Table 4. The calculations follow procedures outlined in AASHTO Standard Specifications for Highway Bridges (2002), Chapter 13 [6]. This method includes factors that account for load duration, moisture content, lateral support conditions, and other variables influencing timber behavior. For the control timber beams, the baseline allowable bending and shear stresses were adjusted considering the effects of wet service conditions, load duration, member size, volume of stressed wood, lateral stability, non-uniform stress distribution, and repetitive member use. These adjustments produced the design values for bending and shear capacity used in the comparison.

For the FRP-strengthened beams, a transformed-section method was applied to account for the composite action between the timber and FRP components. The transformed section assumed a perfect bond and linear-elastic behavior between materials. Separate modular ratios were calculated for the FRP channels and strips based on their elastic moduli and the adjusted modulus of elasticity of the timber. The composite section was analyzed by transforming FRP widths into equivalent timber, calculating the transformed centroid and moment of inertia, and determining capacity based on the material that governed failure. In both control and strengthened cases, failure was assumed to occur when the stress in timber reached its adjusted allowable limit. More specific details on the calculations can be found in Appendix C.

As shown in the table, the calculated moment capacities are consistently lower than the experimentally measured values, highlighting the conservative nature of standard code predictions. This conservatism is expected: design codes include safety factors and use cautious assumptions to account for uncertainties in material properties, construction quality, and loading conditions. Consequently, all of the tested beams exceeded their calculated capacities, in many cases by a substantial margin.

On average, the 6"x18" beams exhibited a measured-to-calculated moment ratio of 3.1, indicating that the tested beams performed more than three times better than what the design equations predicted. The 8"x18" beams had a slightly lower average ratio of 2.8, which was influenced by one underperforming specimen. Even with this variation, the measured capacities significantly exceeded the calculated ones.

The consistency of the experimental results is also reflected in the coefficient of variation (CoV) values. For the 6"x18" beam group, the CoV is 0.07, indicating highly repeatable performance. In the 8"x18" group, the CoV was 0.31, primarily due to a single underperforming beam. When that outlier is excluded, the CoV drops to 0.10. This supports the reliability of the testing procedure and the overall effectiveness of the strengthening technique.

Table 4: Comparison of Measured and Calculated Moment Capacities

Beam	Measured Capacity (kip-ft)	Calculated Capacity (kip-ft)	Measured/calculated	Average measured/calculated	CoV
6-Fl(1)	145.6	46.0	3.2	3.1	0.07
6-Fl(2)	126.1		2.7		
6-Fl-St(C-S)	189.2	59.4	3.2		
6-Fl-St(S)	165.1	51.0	3.2		
8-Fl(1)	176.0	61.3	2.9	2.8	0.31
8-Fl(2)	96.0		1.6		
8-Fl-St(C-S)	255.2	75.1	3.4		
8-Fl-St(S)	230.4	66.5	3.5		

7. CONCLUSIONS

This section details the conclusions of the work completed as part of Task 2, Close Minor Research Gaps, of the research project titled "Use of Fiber-Reinforced Polymer Composites for Bridge Repairs in Montana." This study evaluated the use of FRP repairs on timber bridge girders through full-scale testing of salvaged Douglas-fir/Larch beams. Two groups of beams, sized 6"x18" and 8"x18", were tested in both flexure and shear. These groups included undamaged control beams, pre-damaged (cracks or splits) repair beams, and undamaged beams strengthened with FRP. Material tests were also conducted on the FRP components to confirm their mechanical properties. The capacity comparisons demonstrated that the FRP repair and strengthening techniques provided notable improvements in material performance, flexural and shear capacity, consistency in structural response, and design reliability. The key findings are summarized below:

- *FRP material performance*

Tensile tests on FRP coupons confirmed excellent strength and stiffness retention after undergoing full scale testing on the beams. Virgin GFRP channel coupons exceeded manufacturer values, achieving 177% of the reference tensile strength and 164% of the reference modulus. Channel coupons extracted from mid-span and end-regions of tested beams still retained over 150% of expected strength and over 120% of stiffness. Hybrid FRP strips also remained within ±10% of the tabulated values, confirming their durability and consistent mechanical performance.

- *Flexural capacity gains*

The application of FRP channels and strips significantly improved the flexural performance of timber beams. For 6"x18" beams, crack-repair using the channel-strip method resulted in a 29.7% increase in moment capacity, while strengthening of undamaged beams with the same configuration yielded a 29.9% improvement. In the 8"x18" group, crack-repair beams showed a 45% gain, and strengthened beams achieved a 50% increase over the controls.

FRP strips used alone also proved effective, though to a lesser extent in the smaller beams. For 6"x18" beams, crack-repair with strips produced an 8.4 % improvement, and strip-only strengthening achieved a 30.9 % increase. For 8"x18" beams, crack-repair using strips resulted in a 96.1 % increase, while strip only strengthened beams exhibited a 139.9% gain. These results confirm that FRP significantly enhances flexural strength, particularly when applied to intact or lightly damaged beams.

- *Addressing shear splits*

FRP channels provided effective restoration and improvement in the shear capacity for beams with end splits. In 6"x18" beams tested in shear setup, split repair using full-length channels improved capacity by 11.3%, while channel strengthening of undamaged beams achieved a 23.1% increase. For 8"x18" beams tested in shear setup, split-repair beams gained 11.5 %, and strengthened beams demonstrated a 48.5% improvement in shear capacity compared to controls.

Additional testing on beams with existing splits reinforced the value of combining channels and strips. For 6"x18" beams tested in flexure setup, this approach resulted in moment capacity increases of 37.9% and 59.4%. For 8"x18" beams tested in flexure, gains of 12.5% and 106.2% were observed. In contrast, split repair with 6' channels restored capacity to 97.1% and 112.2% of the controls, while 3' channel repairs underperformed. These findings emphasize the importance of using full-length channels whenever feasible for reliable split repair and shear strengthening, and 6' minimum end channels when full length is not feasible.

- *Channel-strip combination provided more effectiveness than strip-only*

For crack repair, the channel-strip (C-S) configuration significantly outperformed the strip-only method, improving moment capacity by 29.9% (6"x18") and 50.5% (8"x18"), compared to 8.3% and 96.7% gains from strip-only repairs. For strengthening, both techniques enhanced capacity, with the C-S method achieving 25.0% (6"x18") and 45.0% (8"x18") improvements, while strip-only strengthening showed 30.9% and 140.0% gains, respectively. The higher gain in the 8"x18" strip-only case was influenced by an underperformed control, reaffirming the consistent advantage of the C-S method across conditions.

Despite the superior capacity and more consistent performance of the C-S configuration, the strip-only technique still offers notable advantages. Its lighter weight and ease of installation make it a practical and cost-effective option, particularly in scenarios where access, equipment limitations, or installation time are critical factors. As such, the strip-only method may still be the preferred choice in certain applications.

- *FRP repaired pre-tested beams effectively*

The capacities of the pretested 6"x18" and 8"x18" beams repaired with various FRP techniques were restored to their original capacities and often achieved significant improvements. For 6"x18" beams,

channel-strip crack repair increased capacity by 29.7%, while strip-only repair showed an 8.4% improvement, and split repairs with channels achieved an 11.3 % increase. In 8"x18" beams, channel-strip crack repair achieved a 50.0% increase, strip-only repair improved by 96.1%, and split repair with channels showed an 11.5% enhancement.

- *FRP enhanced consistency in structural performance*

Although the number of test specimens was limited, the beams repaired or strengthened with C-S combination demonstrated reduced variability and more consistent performance compared to the control beams. For the 6"x18" beams, the control group exhibited a of 13.4% variation, while the FRP channel-strip (C-S) repairs significantly improved consistency. Both the C-S crack repair and the strengthened beams reached the same capacities. For the 8"x18" beams, the control group showed a much higher variation of 45.45%. In contrast, the C-S beams displayed improved consistency, with only a 3.63% difference between the crack repair and strengthened beams.

The channel placement for the split repair beams differed slightly (at mid-height). Despite this difference, the results remained fairly comparable, showing 6.19% and 25.15% difference between the split repair and crack repair cases for the 6"x18", and the 8"x18" beam, respectively.

- *Measured vs. calculated capacities*

The comparison between measured and calculated moment capacities clearly demonstrated that the tested beams outperformed code-based predictions by a wide margin, with 6"x18" beams showing an average measured-to-calculated ratio of 3.1, and 8"x18" beams exhibiting a ratio of 2.8. This highlights the inherent conservatism of standard design codes, which intentionally include safety factors to ensure structural reliability.

- *Summary*

This research successfully achieved its objectives by evaluating the feasibility and benefits of fiber-reinforced polymer (FRP) repair and strengthening techniques for timber bridges through full-scale testing of Douglas-fir/Larch beams. Although the sample size was relatively limited, the experimental program was extensive and conducted under realistic loading conditions, providing valuable insights into the structural performance improvements attainable through various FRP applications.

A key takeaway is that FRP retrofitting restores the original capacity of damaged timber beams and significantly enhances their strength and stiffness, especially when applied before severe deterioration occurs. This highlights the importance of proactive rehabilitation, as reinforcing intact or lightly damaged members enables more effective composite action and greater performance gains.

From an implementation perspective, these findings provide MDT engineers and bridge maintenance professionals (as well as other state DOTs) with clear, actionable guidance for applying FRP repair techniques in the field. The FRP channel and strip combination proved especially effective for both crack and split repairs, offering consistent improvements in load capacity, stiffness, and overall structural reliability. Full-length FRP channels are recommended for end-split repairs to ensure robust shear capacity restoration, while the use of both channels and strips provides optimal results in flexural strengthening and crack repair.

Additionally, the comparison between measured and design-predicted capacities revealed that even control beams outperformed standard code estimates, and FRP-strengthened beams exceeded them by an even greater margin. This confirms the conservative nature of current design codes and indicates that retrofitted members are likely to provide significant reserve capacity, contributing to increased safety and durability.

In summary, this task delivered comprehensive results and validated the effectiveness of several FRP-based repair and strengthening methods. The findings equip engineers and practitioners with practical knowledge to select appropriate repair strategies, improve the performance of aging timber infrastructure, and confidently implement FRP solutions in real-world applications.

8. REFERENCES

[1] F. C. McCormick, "Why not Plastic Bridges," *J. of Structural Division,* vol. 98, pp. 1757-1767, 1972.

[2] L. C. Bank, "Application of FRP Composites to Bridges in the USA.," *Proceedings of the International Colloquium on Application of FRP to Bridges,* vol. 1, pp. 9-16, 2006.

[3] "OKTA," Montana Departement of Transportaion, 2023.

[4] M. Chajes, T. Rollins, H. Dai *et al.*, *Report on Techniques for Bridge Strengthening: Main Report*, 2019.

[5] W. Frankhauser, K. Jamal Elkaissi, S., , S. McMillan *et al.*, "Advances in fiber-reinforced polymer composites in transportation infrastructure.," 2015.

[6] AASHTO, "Standard specifications for highway bridges (17th ed.)," American Association of State Highway and Transportation Officials, 2002.

[7] "Strongwell Corporation," https://www.strongwell.com/.

[8] ASTM, "D198 − 22a: Standard Test Methods of Static Tests of Lumber in Structural Sizes," American Society for Testing and Materials, 2023.

[9] ACI, "440.2R-17, Guide for the Design and Construction of Externally Bonded FRP Systems for Strengthening Concrete Structures," American Concrete Institute, 2017.

[10] ASTM, "D638 − 14: Standard Test Method for Tensile Properties of Plastics," American Society for Testing and Materials, 2015.

9. APPENDIX A: INDIVIDUAL BEAM RESULTS

A.1 <u>6–Sh(1)</u>

The beam had some minor checks and wane-type defects and some other minor handling impact damage on the top. Its actual dimensions were 5.75" x 17" and 10' 1" long. The beam was cut in half for the shear test setup. The span length of the test beam was 9 ft, with a 6.48" overhang on each side. The shear vs. deflection graph is shown in Figure 58. The bearing failure at the load-bearing blocks started at around 22.0 kips. A split started forming at the end of the beam (which was originally the middle of the beam) as the load progressed. The beam failed by splitting on the end of the beam (Figure 59-b) through a knot. The ultimate shear carried by the beam was 27.0 kips when the midspan deflection was 0.89".
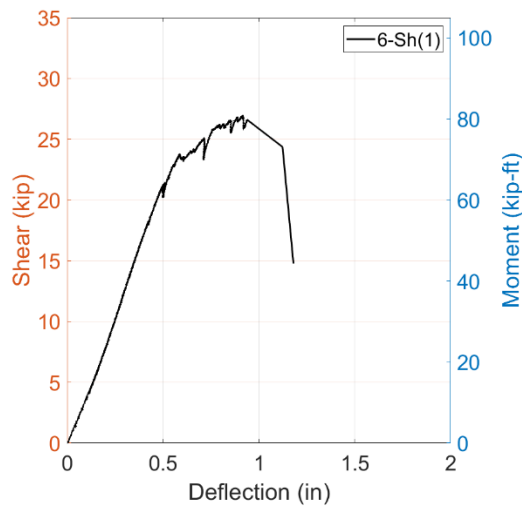
Figure 58: Shear vs deflection graph of 6-Sh(1)

(a) Bearing failure   (b) Split at the end
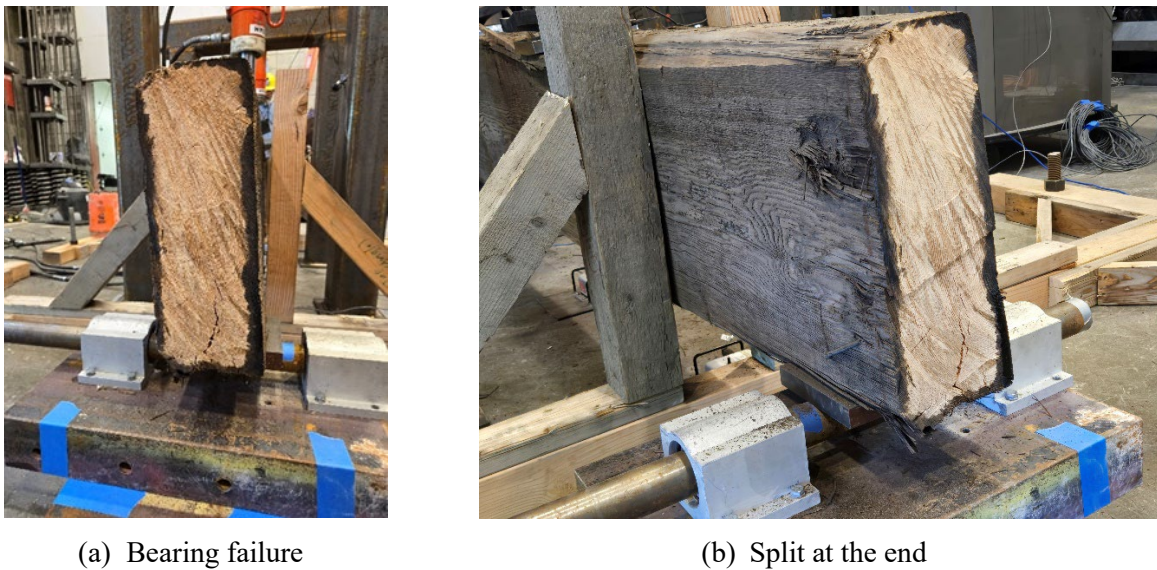
Figure 59: Failure propagation of 6-Sh(1)

A.2 <u>6-Fl(1)</u>

The beam was shorter, with an 18.5' span (19' 6" beam), and the supports needed to be adjusted to be 3" closer. The actual cross-section of the beam was 5.75" x 17". There were holes and bolts on the ends. Some holes were found near D2 and D3. Upon inspection, it was confirmed that this was an exterior beam, and core drilling confirmed no rot. The moment vs. deflection graph is shown in Figure 60. Creaking started at around 110.5 kip-ft. A flexural crack (Figure 61) formed near D1 at around 130.0 kip-ft. The ultimate moment carried by the beam was 145.6 kip-ft when the deflection was 2.53". The beam failed with a large pop as a flexural crack formed laterally with a diagonal run across the beam.
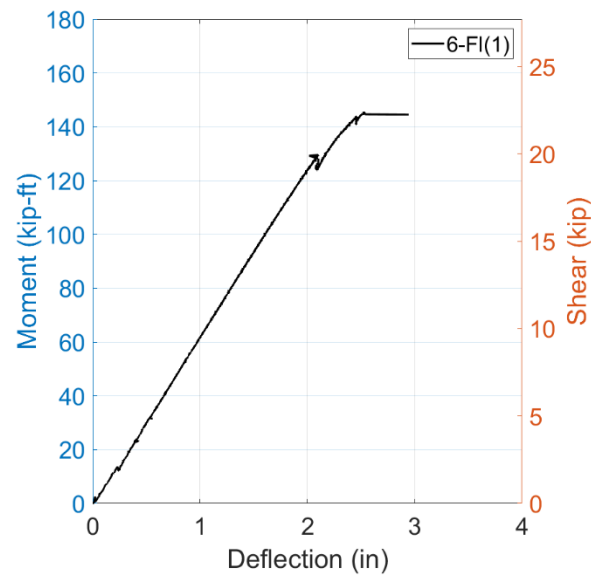
Figure 60: Moment vs deflection graph of 6-Fl(1)
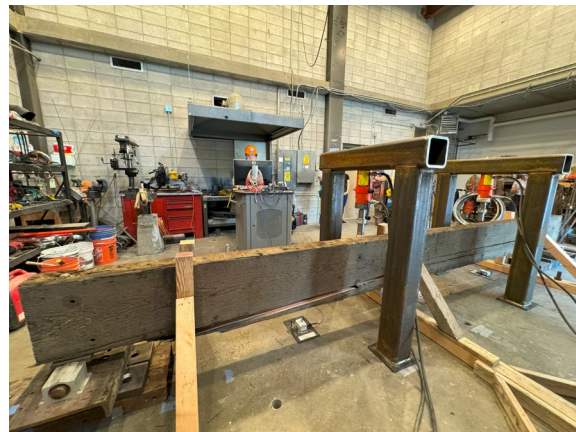
(a) Crack near D1   (b) Flexure crack across the beam

Figure 61: Failure propagation of 6-Fl(1)

A.3 <u>6–Fl(2)</u>

The beam's dimensions were 5.75" x 17" and 20' 0.75" in length. The beam had some minor checking. Figure 62 presents the moment vs deflection graph of the beam. The first creaking started at around 107.3 kip-ft. The beam failed due to a sudden flexure crack (Figure 63). The ultimate moment carried by the beam was 126.1 kip-ft at a deflection of 1.96".
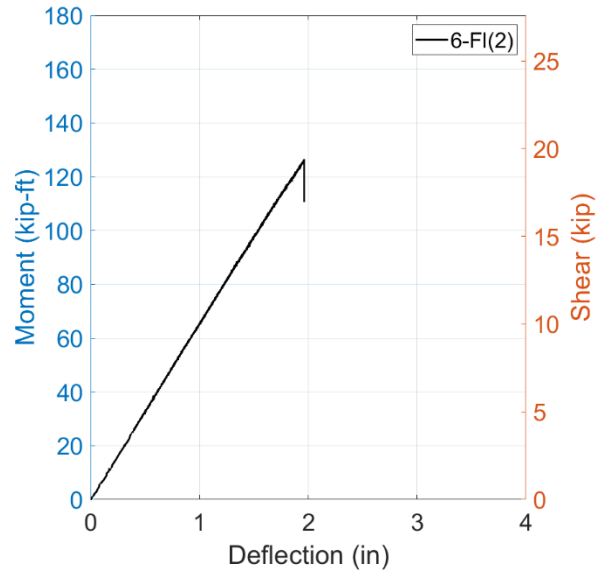
Figure 62: Moment vs deflection graph of 6-Fl(2)

Figure 63: Failure propagation of 6-Fl(2)

A.4 6–Fl(1)-CR(C-S)

This was the crack-repair beam of flexure control 1 (6-Fl(1)). The beam was repaired following the steps discussed in section 4. The string potentiometers were attached to the bottom flange of the side channel. The moment vs deflection curve is presented in Figure 64. The first creaking started at 89.7 kip-ft. The first crack occurred at 105.3 kip-ft when the mid-span deflection was 1.6". Crushing occurred under load block (Figure 65-a) at around 185.3 kip-ft. The ultimate moment carried by the beam was 189.2 kip-ft when the deflection was 3.98". The test was stopped after noticing that the reaction blocks weren't centered.
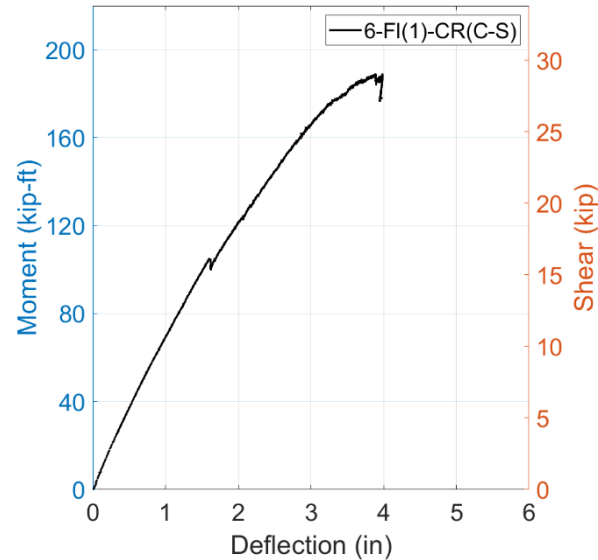
Figure 64: Moment vs deflection of 6-Fl(1)-CR(C-S)
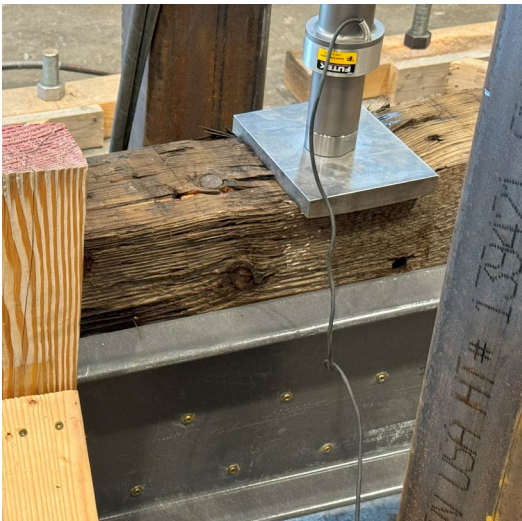
(a) Crushing under load block   (b) Fully loaded beam before release
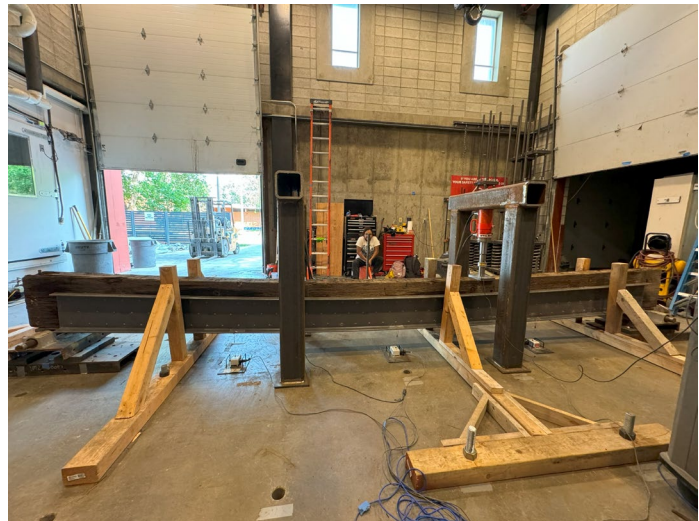
Figure 65: Failure propagation of 6-Fl(1)-CR(C-S)

A.5 6-Fl(2)-CR(S)

This was the crack-repair beam of flexure control 2 (6-Fl(2)), following the repair steps discussed in section 3.3. The repair included attaching two strips on the sides and one at the bottom. The string potentiometers were anchored about 0.5" above the side strip. The moment vs deflection graph is depicted in Figure 66. The beam started making creaking sounds around the middle at around 97.5 kip-ft. When the moment reached 136.5 kip-ft at a 2.02" deflection, there was a loud pop, and the beam split (Figure 67) almost immediately at the end. The split rapidly propagated towards the center, causing the moment to drop sharply to 55.3 kip-ft, indicating that the beam had not been properly confined by the strip. When the moment was increased to 91.0 kip-ft, the split opened further. The test needs to be stopped because the stroke limit was reached, necessitating the removal of the load.
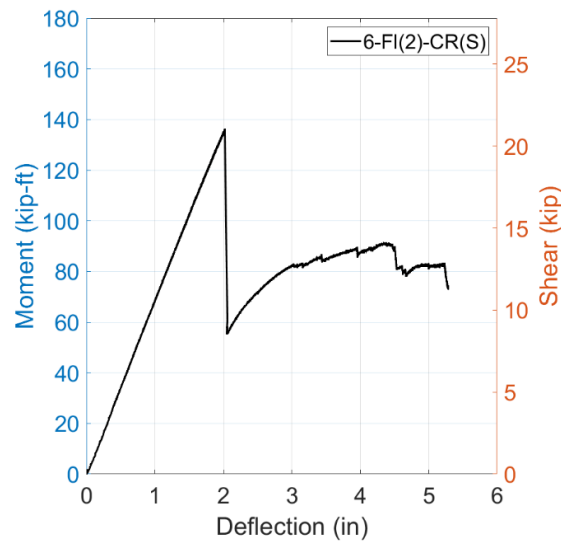
Figure 66: Moment vs deflection of 6-Fl(2)-CR(S)

(a) Split started on the end   (b) Propagating to the middle

Figure 67: Failure propagation of 6-Fl(2)-CR(S)

A.6 <u>6–Sh(1)-SR(C)</u>

The beam was the split-repair beam shear control 1 (6-Sh(a)). The repair was carried out following the steps discussed in section 4. There was an indentation at the bearing plates and a split on one end of the beam from the control beam testing. Figure 68 shows the shear vs deflection graph. The beam instantly settled into bearing dents at load points, and the split (Figure 69-a) instantly shifted with the load. There was a load pop at 21.0 kips. The beam started touching the garage side lateral bracing at around 26.0 kips. At around 29.0 kips, the beam started touching the lateral bracing. At around 30.0 kips, the beam leaned due to bearing failure (Figure 69-b), and the graph started to plateau, leading to the decision to end the test. The ultimate shear carried by the beam was 30.1 kips when the mid-span deflection was 1.69".
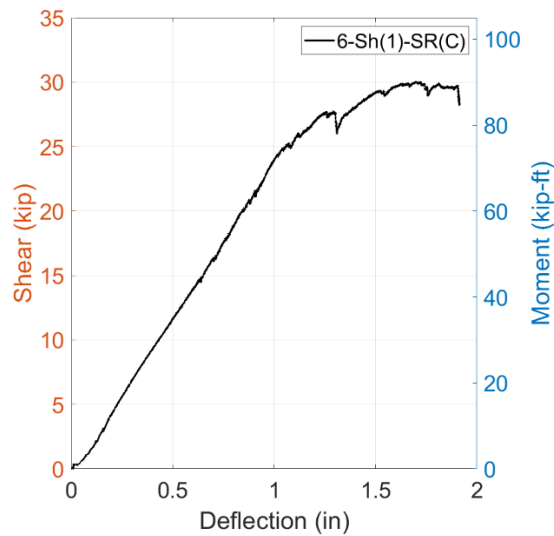
Figure 68: Shear vs deflection graph of 6-Sh(1)-SR(C)


(a) Split shifting on the end
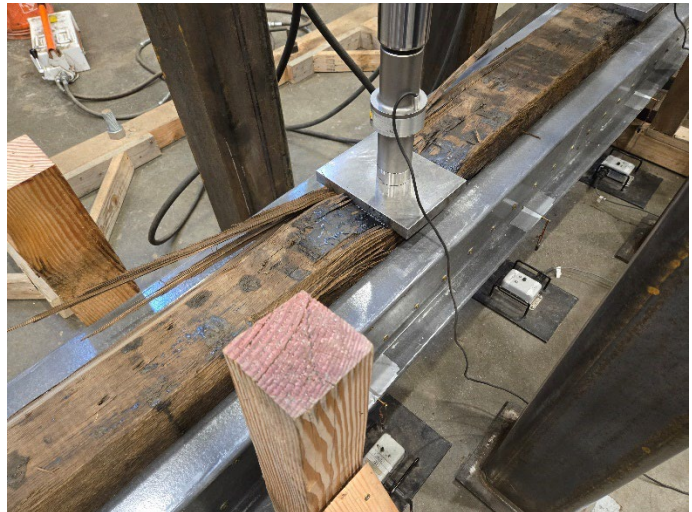
(b) Bearing failure under load block

Figure 69: Failure propagation of 6-Sh(1)-SR(C)

A.7 <u>6-Fl-SR(C-S)</u>

The actual dimensions of the beam were 5.75" x 17" with a length of 20' 2". There was a small split on one end. The beam was repaired following the steps previously discussed in section 4. There was a missing screw on the east channel. The moment-deflection graph (Figure 70) showed a linear slope until 39 kip-ft, slightly stiffer than the two control beams (6-Fl(1) and 6-Fl(2)), with no lateral supports making contact. By 58.5 kip-ft, creaking noises were noted at the ends, and at 68.3 kip-ft, a 1" deflection occurred as the split on the end began to shift. A loud pop was heard at 74.8 kip-ft. At 107.3 kip-ft, slight noise emerged from the support. At 123.5 kip-ft, the beam started touching the middle top lateral support. When the moment reached 162.5 kip-ft, a screw sheared off from the channel, though no drop in load was observed. At 182.0 kip-ft and 3.51" deflection, there appeared to be some compression crack at the top, with creosote pushing out at the load cells, and loud popping was heard from mid-span as the moment held steady around 185.3 kip-ft. At 196.9 kip-ft and a 4.1" deflection, another pop was noted as the split shifted further, and a crack appeared on the east side string potentiometer (D3). With increased load, all east lateral supports were in contact with the beam, and slight eccentricity was observed on the load cells, leading to the decision to end the test. The failure propagation of the beam is shown in Figure 71. The ultimate moment carried by the beam was 200.9 kip-ft at a mid-span deflection of 4.27".
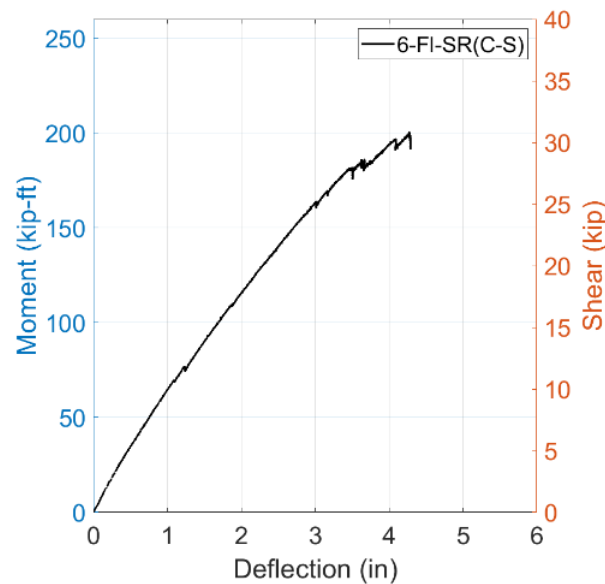
Figure 70: Moment vs deflection graph of 6-Fl-SR(C-S)

(a) Split shifting   (b) Creosote coming out   (c) Split shifting further

Figure 71: Failure propagation of 6-Fl-SR(C-S)

A.8 6-Fl-SR(C3)

The beam's actual dimensions were 5.75" x 17" with a length of 20' 2". It had an 18" long split at one end. The beam was split-repair with 3' long channels on the ends of each side. The detail of the repair technique is outlined in section 4. Figure 72 presents the moment vs deflection graph. Creaking started immediately when loading began. The first crack appeared in the mid-span at around 26.0 kip-ft. A distinct pop was heard as the moment increased to 32.5 kip-ft. The midspan crack noticeably widened at around 52.0 kip-ft, causing a 1.2" midspan deflection. At 55.3 kip-ft, the existing split shifted further and propagated beyond the channel. When the moment reached 62.4 kip-ft, the crack extended to the middle string potentiometer (D1) nail, leading to a sudden drop in the moment to 48.8 kip-ft. Shortly after, the D1 shot off the beam as the midspan crack expanded. Figure 73 shows the failure propagation of the beam. The ultimate moment carried by the beam was 64.35 kip-ft when the mid-span deflection was 2.16".
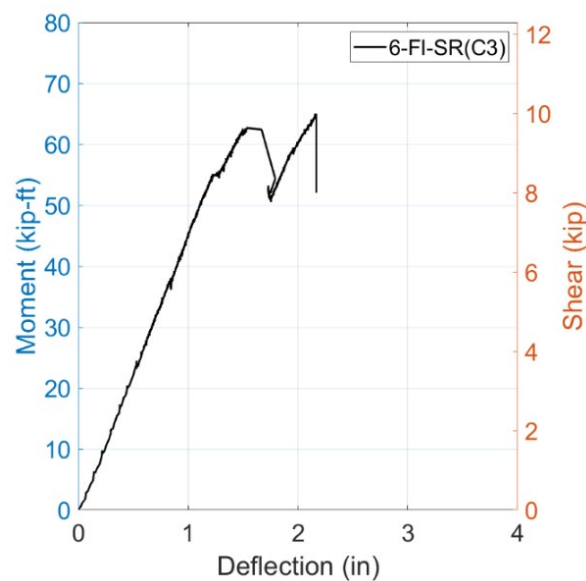
Figure 72: Moment vs deflection graph of 6-Fl-SR(C3)

(a) Crack started at mid-span	(b) Split shifting	(c) Mid-span cracked

Figure 73: Crack propagation of 6-Fl-SR(C3)

A.9 6-Fl-SR(C6)

The beam had a 12" long split at one end, which was repaired with 6' long channels attached at the ends of each side of the beam. The actual dimensions of the beam were 5.75" x 17" with a length of 20' 2" and the beam had notched ends. The moment vs deflection graph is presented in Figure 74. Creaking began at approximately 81.3 kip-ft, with compression failure initiating near the top, at around 84.5 kip-ft. At approximately 91 kip-ft, the entire load frame shifted. A compression crack (Figure 75-a) appeared near the load cell by the lateral support at 105.3 kip-ft. At a moment of 116.4 kip-ft, a mid-span crack occurred on both sides, accompanied by a loud pop, causing the moment to drop to 103.4 kip-ft. At 123.5 kip-ft, a flexure crack (Figure 75-b) developed with another loud pop, resulting in a 1.3 kip-ft moment drop. As the moment increased to 136.5 kip-ft, creaking noises were heard throughout the structure. At 139.8 kip-ft, a puff of dust emerged from the bottom near the load cell, leading to a sudden drop to 131.9 kip-ft. When the moment was increased again, the final crack at the bottom split open, indicating complete failure. The beam ultimately carried a moment of 141.1 kip-ft, at a mid-span deflection of 2.77".
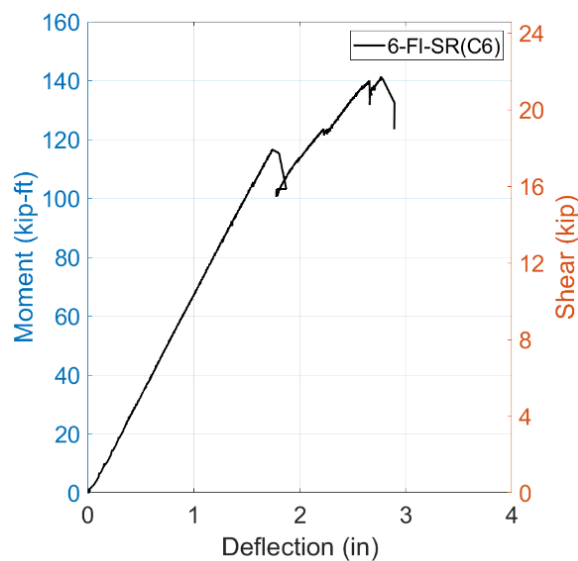
Figure 74: Moment vs deflection graph of 6-Fl-SR(C6)

| (a) Compression crack at top | (b) Flexure crack mid-span |

Figure 75: Failure propagation of 6-Fl-SR(C6)

A.10 6-Sh-St(C)

The beam's actual dimensions were 5.75" x 17" and 10' 0.5" long. It was cut in half for the shear test setup and strengthened by attaching channels in the middle of each side. Due to the uneven top surface, the beam was tested upside down. The shear vs deflection graph is shown in Figure 76. At 17.9 kip, a loud pop was heard followed by a sudden drop of shear to 17.1 kips. As the shear increased to 30.4 kips, a split was noticed at the end with a lot of creaking noise. When the shear hit 33.1 kips, another loud pop occurred, and a crack was observed at the bottom near the end, causing a drop to 27.2 kips. The loading continued and a split (Figure 77) also developed at the end. The beam's ultimate shear was 33.2 kips, at a mid-span deflection of 1.1". Eccentricity began to develop on the load cell due to bearing failure, prompting the decision to unload. No bearing issues were noted at the supports.
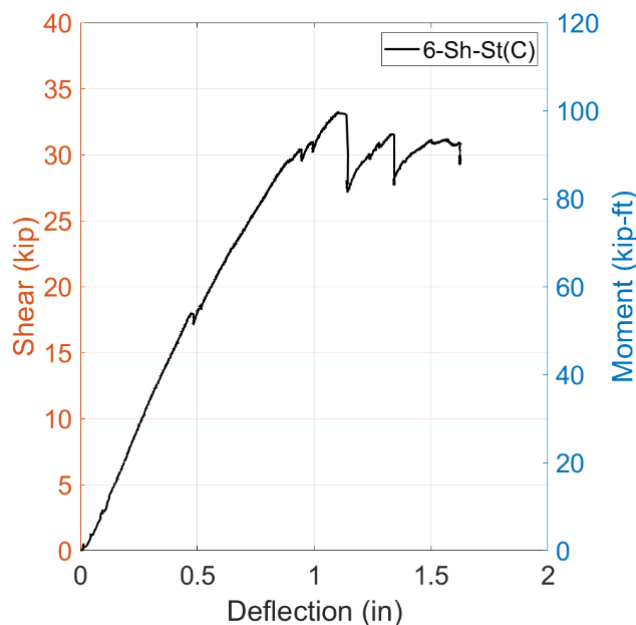
Figure 76: Shear vs deflection graph of 6-Sh-St(C)

Figure 77: Failure propagation of 6-Sh-St(C)

A.11 <u>6-Fl-St(C-S)</u>

This was a strengthened beam tested in a flexure setup. The strengthening was done by attaching two channels on the side and a strip at the bottom. It had dimensions of 5.75" x 17" and a length of 19' 10". There was an inclined cut on one end of the beam that added 3" to the total length of one side (Figure 78); however, the overall span length remained unaffected. A different size screw was mistakenly attached to the strip. The moment vs deflection graph is shown in Figure 79. During the load test, the first creaking was heard at around 58.5 kip-ft. At around 113.8 kip-ft, a small pop occurred on the end. At 136.5 kip-ft, a load pop occurred with no visible crack. When the moment was increased to 167.7 kip-ft, a crack emerged at the mid-span, accompanied by a distinct loud pop. At 176.2 kip-ft, creaking noises and a loud pop were heard as the crack in the mid-span expanded. The moment was then dropped to 170.9 kip-ft. At this point, one load cell was slightly eccentric, and creosote was oozing at the load cells (Figure 80-a). The crack propagated in the lower mid-span at around 182.0 kip-ft. The test was ultimately stopped at 189.2 kip-ft when the mid-span deflection was 2.77", due to bearing failure at the load cell.

Figure 78: inclined cut on one end
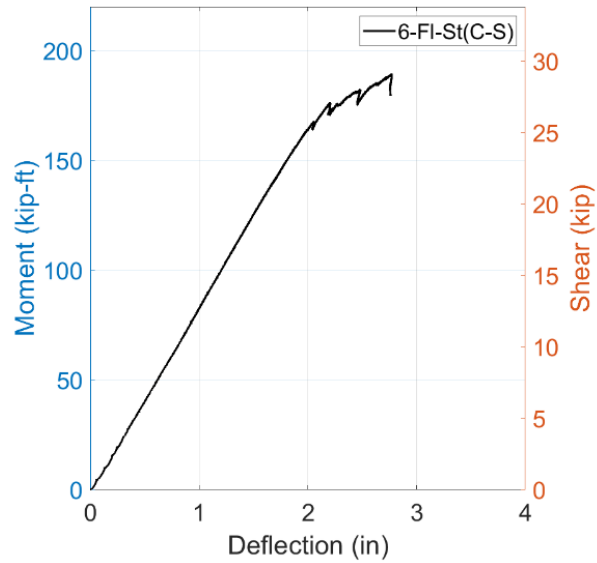
Figure 79: Moment vs deflection graph of 6-Fl-St(C-S)

| (a) Creosote under load-bearing block | (b) Fully loaded beam |
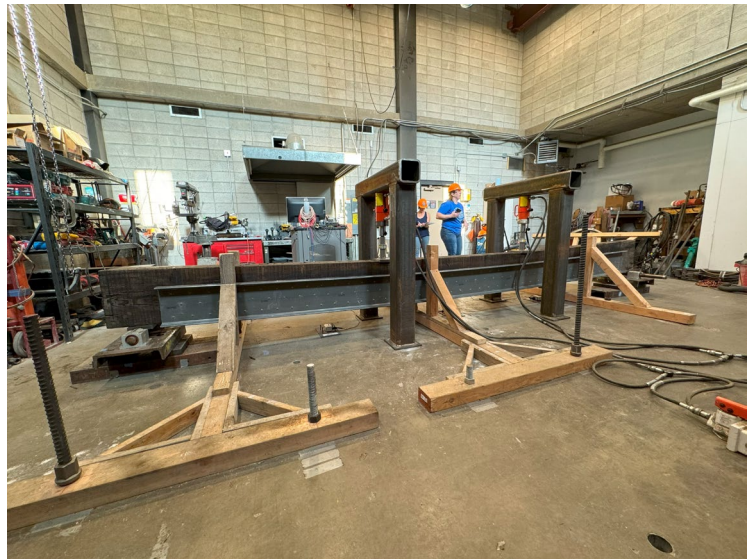
Figure 80: Failure propagation of 6-Fl-St(C-S)

A.12 <u>6-Fl-St(S)</u>

This was a strip-strengthened beam with three strips on the beam's sides and bottom. The beam's dimensions were 5.75" x 17" with a length of 19' 0.75". Like the 6-Fl-St(C-S) beam, there was an inclined cut on one end of the beam that added 3" to the total length of one side. The bottom of the beam was slightly uneven, so it was adjusted when loading, and then the deflection was re-zeroed after the beam was steady. The moment vs deflection is shown in Figure 81. Initially, a small pop occurred at approximately 65.0 kip-ft,

followed by a slight creaking at midspan around 84.5 kip-ft. A distinct pop was heard when the moment reached 136.5 kip-ft, yet no visible damage was seen. At 144.3 kip-ft, a loud pop was heard, shaking the strip on the east side of the beam, and the first signs of cracking appeared under it. As the moment increased to 146.3 kip-ft, the beam experienced a 2.4" deflection, another loud pop occurred, and flexure cracking continued without a dramatic drop in moment. By 156.0 kip-ft, midspan cracking was observed in the beam, with a noticeable compression failure under one load cell, causing the moment to drop slightly to 152.1 kip-ft. At 165.1 kip-ft, the beam split with a loud popping sound from a knot at the end, leading to a 53" long visible opening on the east side and causing the moment to drop to 113.1 kip-ft. A slight recovery followed, with the moment rising back up to 126.8 kip-ft, but another loud pop was accompanied by a puff of dust from the top due to compression, further opening the split and causing shifts. Ultimately, the beam failed in shear at the end. The failure propagation of the beam is shown in Figure 82. The ultimate moment carried by the beam was 165.1 kip-ft, at a mid-span deflection of 2.81".
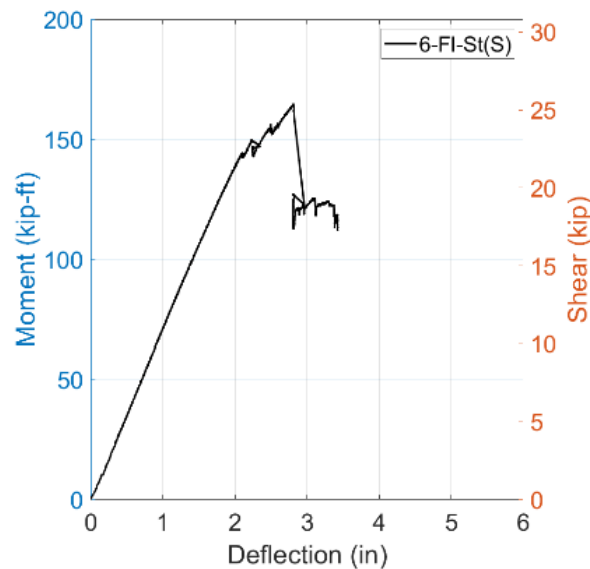
Figure 81: Moment vs deflection graph of 6-Fl-St(S)

(a) Crack at the middle   (b) Compression failure under load cell   (c) Split at the end

Figure 82: Failure propagation of 6-Fl-St(S)

A.13 <u>8-Sh(1)</u>

The actual dimensions of the beam were 7.75" x 17.5" and 26' long with no noticeable damage. The beam was cut in 10' 1' for having a span length of 9' with a 6.5" overhang on each side. Figure 83 shows the shear vs deflection of the beam. Bearing failure started forming at around 25.0 kips at the load-bearing blocks. The flexural crack started at the middle of the beam at around 34.0 kips when the mid-span deflection was 0.67". The crack was opening up with increased loading. The beam failed by splitting at the end. The failure propagation of the beam is presented in Figure 84. The ultimate shear carried by the beam was 37.9 kips at a mid-span deflection of 0.98".

Figure 83: Shear vs deflection graph of 8-Sh(1)

(a) Bearing failure started   (b) Flexure crack at the mid-span   (c) Split at the end

Figure 84: Failure propagation of 8-Sh(1)

A.14 8-Fl(1)

The beam's actual dimensions were 7.5" x 17" and 25' 9" long. Its span length was 25', with a 4.5" overhang on each side. The beam had no significant damage. Figure 85 presents the moment vs deflection of the beam. A flexural crack (Figure 86) started at around 132.0 kip-ft at the midspan of the beam and continued to open with higher load. The ultimate moment carried by the beam was 176.0 kip-ft at a midspan deflection of 3.28". The beam failed due to flexure, with the crack initiating 66" from the right end and extending to 84" from the left end. The crack was located approximately 4" from the bottom of the beam.
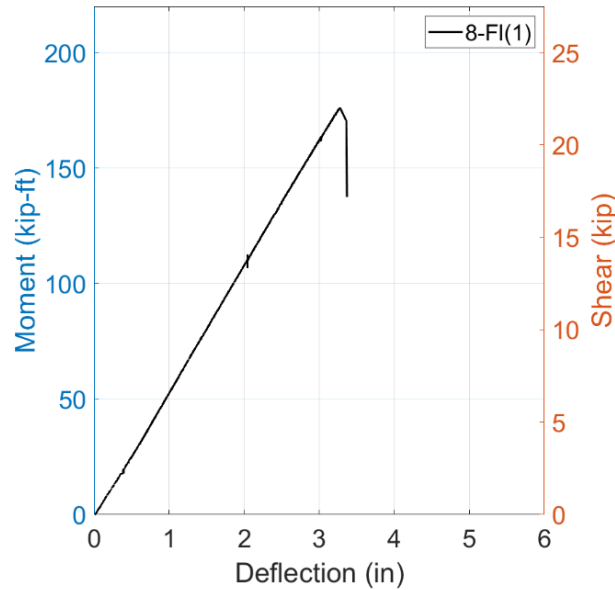
Figure 85: Moment vs deflection graph of 8-Fl(1)

(a) Flexure crack starting at mid-span   (b) Cracked beam

Figure 86: Failure propagation of 8-Fl(1)

A.15 8-Fl(2)

The beam had some minor checks and wane defects. Its actual dimensions were 7.75" x 17", and it was 26'
long. The moment vs deflection graph is shown in Figure 87. The creaking sound at mid-span started at
around 84.0 kip-ft. At 94.4 kip-ft, a split propagated, and compression failure (Figure 88-a) occurred,
resulting in a moment drop to 78.4 kip-ft. The beam failed at cracking in mid-span (Figure 88-b). The
ultimate moment carried by the beam was 96.0 kip-ft when the deflection was 2.56". Two holes were drilled
to see the beam's core, and it was confirmed that there was no rot.
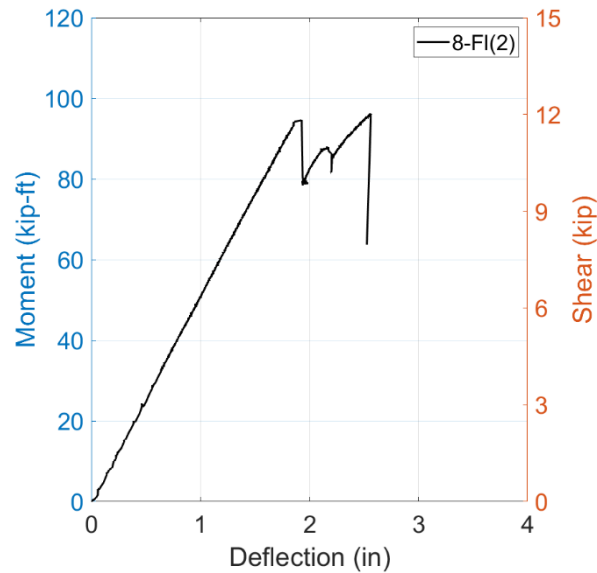
Figure 87: Moment vs deflection graph of 8-Fl(2)
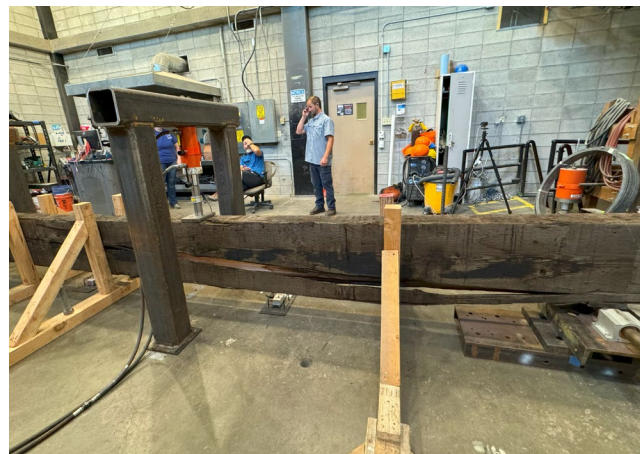
(a) Compression failure at top   (b) Cracking in the mid-span

Figure 88: Failure propagation of 8-Fl(2)

A.16 <u>8-Fl(1)-CR(C-S)</u>

This was the crack-repair beam for flexural control 1 (8-Fl(1)). The repair process involved attaching channels on the sides and a strip on the bottom, and the detailed repairing processes are discussed in section 4. The moment-deflection graph (Figure 89) showed a plateau at around 60 kip-ft, likely due to the screws engaging. There was a loud pop at around 242.4 kip-ft and a compression crack (Figure 90-a) near the load cell at 253.6 kip-ft. The test was stopped because the stroke limit was reached. The beam ultimately carried a moment of 264.8 kip-ft when the mid-span deflection was 5.28".
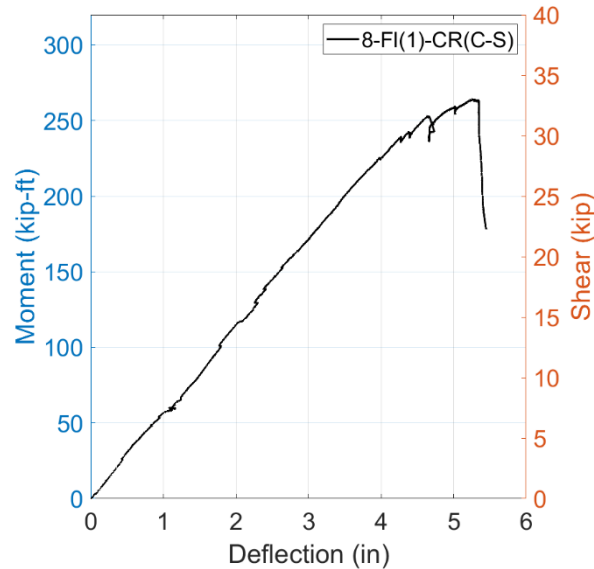
Figure 89: Moment vs deflection graph of 8-Fl(1)-CR(C-S)

(a) Compression failure at top
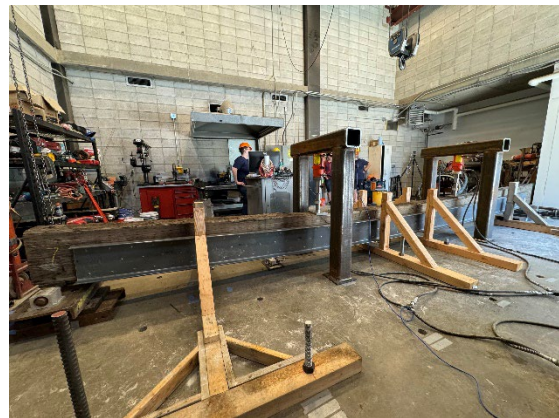
(b) Fully loaded beam

Figure 90: Failure propagation of 8-Fl(1)-CR(C-S)

A.17 <u>8-Fl(2)-CR(S)</u>

This was the Flexure Control 2 (8-Fl(2)) beam with crack repairs. Four strips were attached to the sides, and one was attached to the bottom. The detailed repair method is discussed in section 4. The string potentiometers were anchored in the middle of two strips on the side. The moment vs deflection graph is shown in Figure 91. Creaking started in the midspan at around 104.0 kip-ft and continued with higher moment. At 160.0 kip-ft, a crack was opening up at the top middle through a knot (Figure 92-a), leading to a drop in the moment to 156.8 kip-ft. At 183.2 kip-ft, a poof of dust emerged from the top middle of the beam. When the moment reached 184.0 kip-ft, the beam started contacting the two lateral bracings. The loading was paused to take pictures at around 188 kip-ft. The beam cracked a lot while holding the load and eventually failed compression through a knot at the top face middle (Figure 92-b). The ultimate moment carried by the beam was 188.8 kip-ft when the mid-span deflection was 5.08".
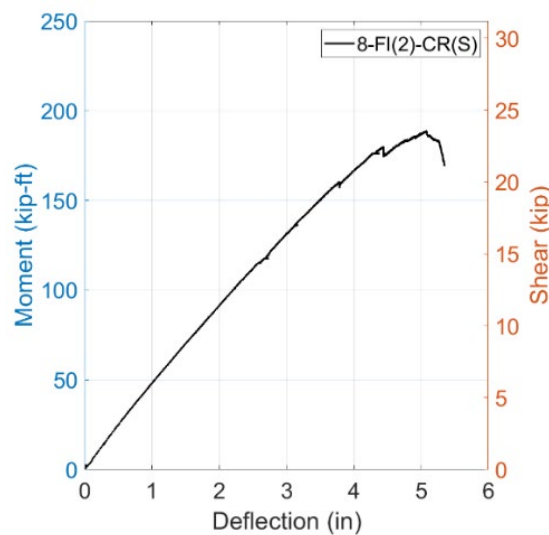
Figure 91: Load vs deflection graph of 8-Fl(2)-CR(S)

(a) Crack at mid-span through a knot   (b) Failure in compression

Figure 92: Failure propagation of 8-Fl(2)-CR(S)

A.18 <u>8–Sh(1)-SR(C)</u>

This was the split-repair beam of shear control 1 (8-Sh(1)), which was repaired following the steps outlined in section 4, including attaching channels on the sides. There is an existing split on the end from the control test. The shear vs deflection graph is presented in Figure 93. Bearing failure began under the load block and support at approximately 26.0 kips. The beam started making contact with lateral bracings at around 36.0 kips. The existing split shifted at 36.8 kips. At 38.9 kips, a crack at the bottom midspan occurred, causing the shear to drop to 36.4 kips, with a screw on the channel shearing off. The load continued to increase, and shear failure was controlled on the end. The failure propagation of the beam is presented in Figure 94. The ultimate shear carried by the beam was 42.3 kips when the deflection was 1.58".
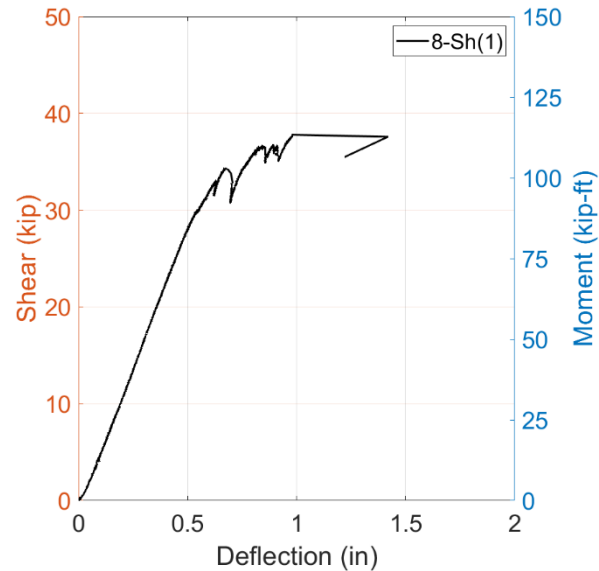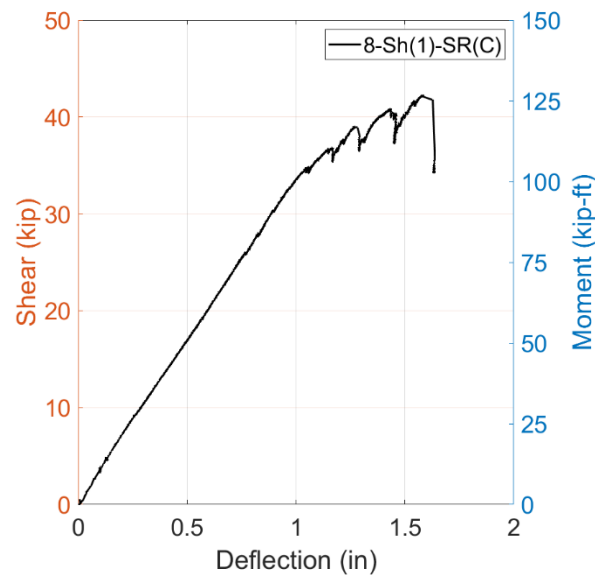

Figure 93: Moment vs deflection graph of 8-Sh(1)-SR(C)

(a) Bearing failure   (b) Screw sheared off   (c) Split at the end

Figure 94: Failure propagation of 8-Sh(1)-SR(C)

A.19 <u>8-Fl-SR(C-S)</u>

The beam's actual dimensions were 7.5" x 17" with a length of 26' 0.75". It had moderate checking along its length and was a split repaired beam with channels on the sides and a strip on the bottom. The beam had tapered ends and a through bolt was removed from one end. Figure 95 presents the moment vs deflection graphs. The first creaking occurred at around 94.4 kip-ft, and a small pop happened at around 112.0 kip-ft. A crack started forming in the bottom middle at around 133.6 kip-ft. Creaking continued with higher loading, and at a moment of 163.2 kip-ft, a crack formed under the channel, approximately 2" from the bottom on the east side, with a loud pop. As the moment increased to 175.2 kip-ft, a compression crack began to form near the top in the center of the beam. At 184.8 kip-ft, another loud pop was heard as the top middle of the beam buckled at the compression crack, causing the moment to drop to 143.2 kip-ft and then rebuild. At 167.2 kip-ft, a crack formation started near the D2 string potentiometer, about 12" from the load frame, followed by another crack at the bottom-mid, causing a slight load drop. As the moment reached 184.8 kip-ft, the beginning of a compression crack was observed near the center. At 187.2 kip-ft with 4.4" of deflection, a crack near the center began to open up. Finally, at 188.8 kip-ft with 4.7" of deflection, the bottom crack between the D1 and D2 string potentiometers started to widen, and a large crack formed near the D3 string potentiometer with a loud pop. The test was stopped after reaching the maximum stroke of the load cell. Figure 96 shows the failure propagation of the beam. The ultimate moment carried by the beam was 198.4 kip-ft at a mid-span deflection of 5.22".
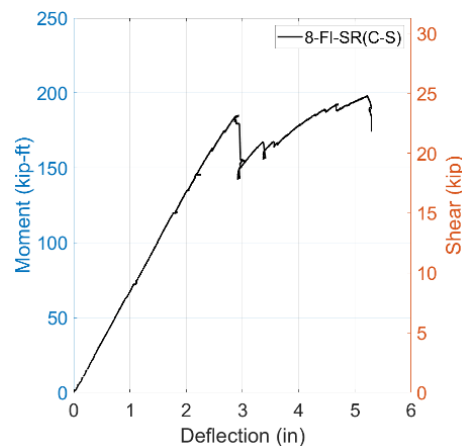
Figure 95: Moment vs deflection graph of 8-Fl-SR(S-C)
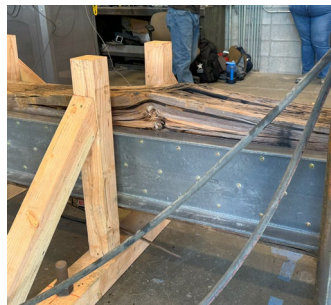
(a) Compression crack at top   (b) Beam buckled at top middle   (c) Flexure crack at bottom middle

Figure 96: Failure propagation of 8-Fl-SR(C-S)

A.20 <u>8-Sh-St(C)</u>

The actual dimensions of the beam were 7.5" x 17.5" with a length of 10'. It was a shear-strengthened beam cut into 10' section for the shear test setup. The strengthening process involved attaching channels on the sides, and more detailed information on the strengthening can be found in section 4. String potentiometers were attached to the bottom flange of the channel. The bottom surface of the beam was not flat, so it was necessary to hold the beam in place before starting the loading. Figure 97 shows the shear vs deflection graph of the beam. The first creaking noise was heard at around 35.0 kips, and bearing failure occurred at both supports at around 43.0 kips (Figure 98-a). Creaking continued with higher loading, and a tension crack occurred at the bottom midspan at 52.5 kips, causing a slight load drop. The beam was continuously loaded and ultimately failed due to shear at one end, which caused split propagation and a shift (Figure 98-b). The ultimate shear carried by the beam was 56.3 kips at a mid-span deflection of 1.45".
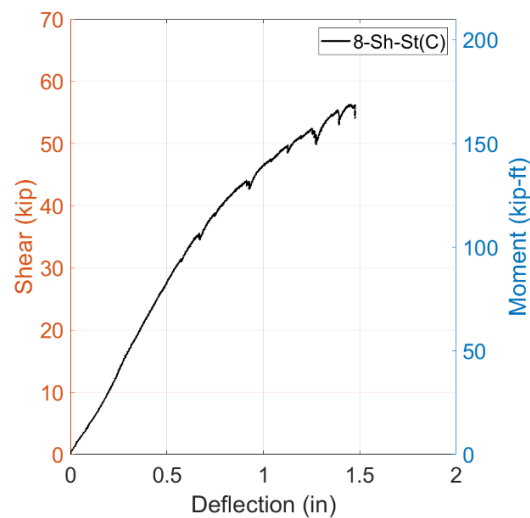
Figure 97: Load vs deflection graph of 8-Sh-St(C)

(a) Bearing failure at load block   (b) Split at the end

Figure 98: Failure propagation of 8-Sh-St(C)

A.21 <u>8-Fl-St(C-S)</u>

The beam was a strengthened beam with channels on the sides and a strip on the bottom. Its dimensions were 7.5" x 17" with a length of 26' 1.5". The moment vs deflection graph is shown in Figure 99. The first creaking noise was heard at around 128.0 kip-ft. At 144.0 kip-ft, there was a creak and a small pop from one end. As the moment increased to 172 kip-ft, crackling sounds accompanied by a small pop were heard from the end. When the moment reached 228.0 kip-ft, a loud pop was heard as a large compression crack began to form, causing a change in slope. At around 232.0 kip-ft, with a 4" mid-span deflection, the beam cracked just below the D2 string potentiometer with a loud pop (Figure 100-a), although the strip remained intact. At 252 kip-ft, with 5" of deflection, flange buckling was observed. Finally, at 255.2 kip-ft and 5.36" of deflection, a loud pop was heard as a small fragment flew off. The beam ultimately carried a moment of 255.2 kip-ft at a mid-span deflection of 5.32".
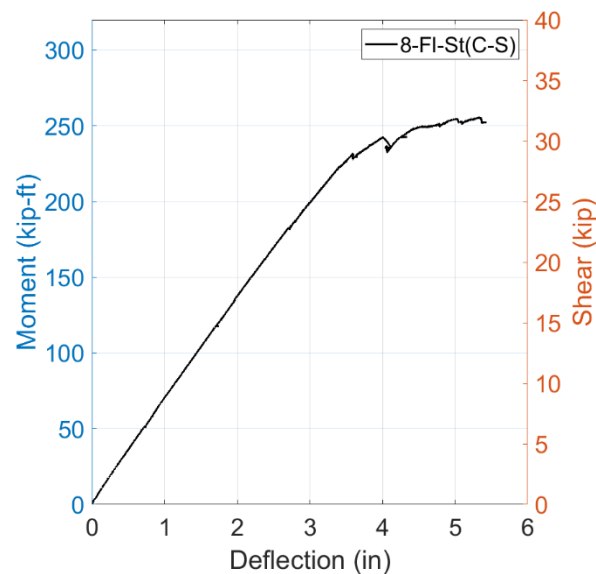
Figure 99: Moment vs deflection graph of 8-Fl-St(S-C)

(a) Crack at the bottom (b) Fully loaded beam

Figure 100: Failure propagation of 8-Fl-St(C-S)

A.22 <u>8-Fl-St(S)</u>

This was a beam reinforced with strips, with three strips attached to the sides and bottom. The beam's actual dimensions were 7.75" x 17.5" with a length of 26' 6.75". There was some significant checking and a large notch on one end, causing the strips to hang over. The string potentiometers were anchored above the strip on the side. The moment vs deflection is shown in Figure 101. Creaking began at around 112.0 kip-ft throughout the beam and continued with higher loading. Loud pops were heard at 168.0 kip-ft and 181.6 kip-ft with no significant drop in load. A crack (Figure 102-a) began propagating at 230.4 kip-ft on the bottom through a knot with a loud pop, causing the moment to drop to 214.4 kip-ft. The beam started touching the middle lateral bracing. Ultimately, the beam failed with a crack propagating to the midspan and compression failure under the load block (Figure 102-b) at around 200.0 kip-ft with a loud pop. The ultimate moment carried by the beam was 230.4 kip-ft when the deflection was 3.76".
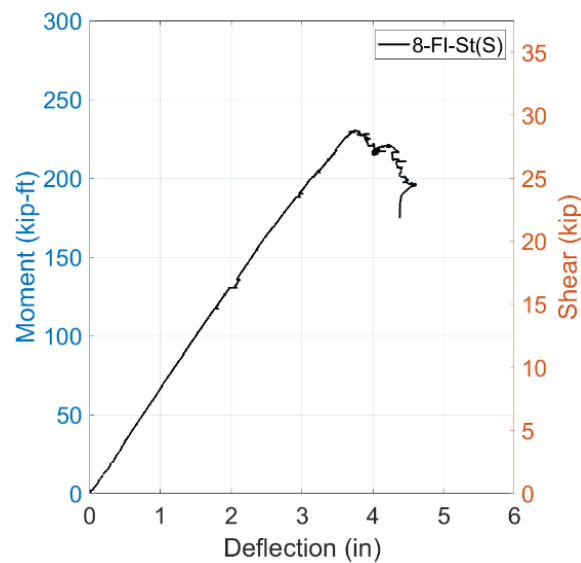
Figure 101: Moment vs deflection graph of 8-Fl-St(S)

(a) Crack starting

(b) Compression at top

Figure 102: Failure propagation of 8-Fl-St(S)

APPENDIX B: TIMBER BEAM INVENTORY

Acronym	Actual cross-section	Actual length	Pre-existing crack/split	Misc. Notes
6-Sh(1)	5.5" x 17"	10.08'	Minor checks and wane-type defects from handling.	Beam cut in half for shear setup.
6-Fl(1)	5.75" x 17"	19.50'	Clean.	Exterior beam. Some holes and bolts on both ends. Shorter beam, supports need to be moved 3" closer.
6-Fl(2)	5.75" x 17"	20.06'	Minor checking.	**
6-Fl(1)-CR(C-S)	5.75" x 17"	19.50'	Crack from control beam test.	Shorter beam, supports need to be moved 3" closer.
6-Fl(2)-CR(S)	5.75" x 17"	20.06'	Crack from control beam test.	**
6-Sh(1)-SR(C)	5.75" x 17"	10.08'	Split from control beam test. Indentation at the bearing plates. Split on the left end of the beam through a knot.	Beam cut in half for shear setup.
6-Fl-SR(C-S)	5.75" x 17"	20.17'	Small splits on one end.	Missing screw on the east channel.
6-Fl-SR(C3)	5.75" x 17"	20.21'	18" long split on end.	**
6-Fl-SR(C6)	5.75" x 17.25"	20.17'	12" long split on one end.	Notched end.
6-Sh-St(C)	5.75" x 17"	10.04'	The top surface was uneven. Tested upside down.	Beam cut in half for shear setup.
6-Fl-St(C-S)	5.75" x 17"	19.83' + 3"	Clean.	Inclined cut in one end.
6-Fl-St(S)	5.75" x 17"	19.06' + 3	Pre-existing damage on top. Uneven bottom.	Inclined cut in one end.
8-Sh(1)	7.75" x 17.25"	10.08'	Clean.	Cut in 10.08' for the shear setup.
8-Fl(1)	7.5" x 17"	25.75'	Clean.	**
8-Fl(2)	7.75" x 17"	26.00'	Minor checking. Wane-type defect.	**
8-Fl(1)-CR(C-S)	7.75" x 17.25"	25.75'	Crack from control beam test.	**
8-Fl(2)-CR(S)	7.5" x 17"	26.00'	Crack from control beam test.	5-strips were attached.
8-Sh(1)-SR(C)	7.75" x 17"	10.08'	Split from control beam test. Existing split on the end.	Beam cut in half for shear setup.
8-Fl-SR(C-S)	7.5" x 17"	26.06'	Moderate checking along the length.	Tapered ends. Through bolt removal from the end.
8-Sh-St(C)	7.5" x 17.5"	10.00'	Heavy checking on the other half.	Beam cut in half for shear setup.
8-Fl-St(C-S)	7.5" x 17"	26.13'	Clean.	**
8-Fl-St(S)	7.75" x 17.5"	26.56'	Moderate checking.	Large notch on one end, causing the strips to hang over.

APPENDIX C: CALCULATIONS

This section provides a detailed discussion of the hand calculations for the capacities of both control and strengthened beams. It also includes the calculations for determining the required number of fasteners and the screw placement pattern for different lengths of FRP channels and strips.

C.1 Capacity calculations

The following calculations evaluate both the control timber beam and the FRP-strengthened timber beam to determine their flexural and shear strengths, incorporating adjustments for material properties and design specifications.

Control beam

For the control timber beam, section dimensions b_t (beam width) and h_t (beam height) and material properties F_b (allowable bending stress), F_v (allowable shear stress), and E_t (modulus of elasticity) establish the base parameters. Adjustment factors from the AASHTO Standard Specification for Highway Design - 2002 edition, chapter 13 [6], including C_M, C_D, C_F, C_V, C_L, C_f, C_{fu}, and C_r account for criteria such as loading conditions, moisture content, lateral support, and beam geometry. The assumptions for this calculation are as follows: the beam is subjected to vehicle live load (2 months) and is in a dry service environment with a moisture content below 19%. It also assumes adequate lateral support to prevent buckling, a standard depth-to-width ratio, and no incising or repetitive member use.

The adjusted bending capacity (F_b') and shear capacity (F_v') are calculated using eqn. 1 and 2, respectively.

$$F_b' = F_b \, C_M \, C_D \, C_F \, C_V \, C_L \, C_f \, C_{fu} \, C_r \qquad \text{(Eqn. 1)}$$

$$F_v' = F_v \, C_M \, C_D \qquad \text{(Eqn. 2)}$$

These adjustments yield conservative design values for bending and shear capacities. The centroid (y_c) and moment of inertia (I_b) for the timber beam are calculated. Using these properties, the moment capacity (M) and shear capacity (V) are then determined by eqn. 3 and 4, respectively.

$$M = \frac{F_b' \times I_b}{y_c} \qquad \text{(Eqn. 3)}$$

$$V = \frac{F_v' \times a}{1.5} \qquad \text{(Eqn. 4)}$$

Where, a is the support to load distance. The load required for failure, P, is calculated based on both moment capacity (eqn. 5) and shear capacity (eqn. 6), with the smaller load value controlling. This load represents the predicted maximum load the timber beam can support before failure under these design conditions.

$$P = \frac{M}{a} \qquad \text{(Eqn. 5)}$$

$$P = V \qquad \text{(Eqn. 6)}$$

Strengthened beams

The transformed section method is applied to analyze the FRP-strengthened composite beam consisting of a timber section reinforced with GFRP channels and hybrid FRP strip. This method simplifies the analysis by allowing the composite beam to be treated as a single homogeneous section, making it easier to calculate properties like centroid, moment of inertia, and load capacities under bending and shear. The following assumptions are made in calculating the strength:

1) The composite beam has a perfect bond between the timber and FRP materials, ensuring that the strain is consistent across the interface.

2) The composite section is assumed to remain within the elastic range, meaning that both timber and FRP exhibit linear elastic behavior under the applied loads.

The implementation of the transformed section method is started by calculating the modular ratio (n), defined as the ratio between the modulus of elasticity of the FRP (E_{fc} and E_{fs} for channel and strip, respectively) and timber (E_t'). The adjusted modulus of elasticity of timber (E_t') is calculated by eqn. 7 considering adjustment factors.

$$E_t' = E_t \, C_M \, C_t \, C_i \tag{Eqn. 7}$$

Where, E_t is the tabulated modulus of elasticity for timber. Separate modular ratios are calculated for channels (n_c) and strip (n_s) using eqn. 8 and 9, respectively.

$$n_c = \frac{E_{fc}}{E_t'} \tag{Eqn. 8}$$

$$n_s = \frac{E_{fs}}{E_t'} \tag{Eqn. 9}$$

The widths of the FRP components are then transformed to equivalent timber widths using the modular ratios. The centroid (y_{tr}) and moment of inertia (I_{tr}) for the transformed section are calculated. The moment capacity (M, at either the top or bottom edge) and shear capacity (V, at the centroid) of the timber beam are then determined by eqn. 10 and 11, respectively.

$$M = min \; of \begin{array}{l} M_c = \frac{F_c \times I_{tr}}{y_{tr} \, (bottom)} \\[6pt] M_s = \frac{F_s \times I_{tr}}{y_{tr} \, (bottom)} \\[6pt] M_t = \frac{F_b' \times I_{tr}}{y_{tr} \, (top)} \end{array} \tag{Eqn. 10}$$

$$V = \frac{F_v' \times I_{tr} \times t}{Q} \tag{Eqn. 11}$$

Where, F_c and F_s are tensile strength of FRP channel and strip, respectively, and Q is the first moment of the area. The load required for failure, P, is calculated based on both moment capacity (eqn. 12) and shear capacity (eqn. 13), with the smaller load value controlled. This load represents the maximum allowable load the composite beam can support under these design conditions.

$$P = \frac{M}{a} \tag{Eqn. 12}$$

$$P = V \tag{Eqn. 13}$$

C.2 <u>Screw pattern</u>

The following calculations determine the number of fasteners required to securely attach FRP strips to the timber beam, ensuring that the strips can achieve their intended tensile capacity. 1/4"x3-1/2" RSS-GRK screws were selected for the strips (detailed in section 3.4). The calculation steps start by considering the properties of the FRP strip, including tensile strength (f_f), adjusted for exterior exposure conditions using the coefficient C_e, from ACI 440.2 [9]. The FRP geometric properties, such as the thickness (t_f) and width (b_f) are used to calculate the strip's area (A_f). The area of the fastener hole (A_h) is also calculated from the hole diameter (d_h) and thickness of the FRP (t_f).

Fastener spacing in both horizontal (S_h) and vertical (S_v) directions are considered when calculating two configurations: fasteners in straight and staggered lines. The spacing requirements outlined in GRK specification (Appendix D.4) were satisfied. The area for each configuration is calculated with eqn. 14 and 15, where A_{st} and A_{diag} represent the areas along the straight line and diagonal line, respectively.

$$A_{st} = A_f - (N_{st} \times A_h) \qquad \text{(Eqn. 14)}$$

$$A_{diag} = A_f - (N_s \times A_h) + \left(N_{stagg} \times \frac{t_f \times S_h{}^2}{4 \times S_v}\right) \qquad \text{(Eqn. 15)}$$

Where, the N_{st}, N_s, and N_{stagg} are number of holes in a straight line, staggered line, and number of staggers, respectively. The smaller of these two areas is chosen as the effective area (A_e) to calculate the tensile capacity of the FRP (T_f) shown in eqn. 16.

$$T_f = A_e \times f_f \qquad \text{(Eqn. 16)}$$

The tensile capacity (T_f) and shear capacity (V_b) of the selected fasteners are then used to calculate the total number of fasteners (n) using eqn. 17.

$$n = 2 \times \frac{T_f}{V_b} \qquad \text{(Eqn. 17)}$$

Considering practical aspects such as potential load distribution along the length of the strip, the initially calculated total number of fasteners (n) is conservative. It is assumed that 50% of the fasteners, particularly those located near the strip ends, are effectively engaged in bearing. Accordingly, the final number of fasteners required (n_T) is determined using eqn. 18.

$$n_T = \frac{1}{2} \times n \qquad \text{(Eqn. 18)}$$

The schematic diagrams of the fastener patterns of the 17.5' strip for the 19' span beam and 23.5' strip for the 25' span beam are shown in Figure 103 and Figure 104, respectively.
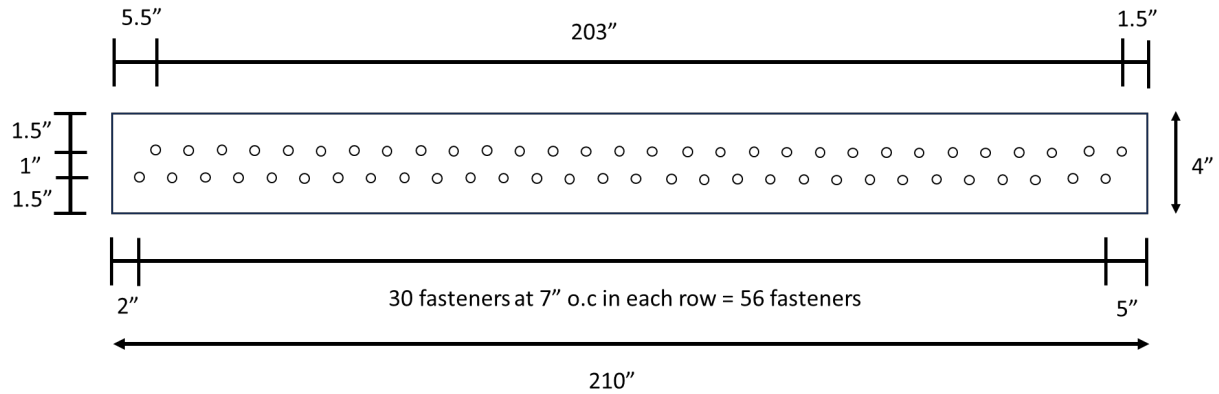
Figure 103: Fastener pattern of the 17.5' strip
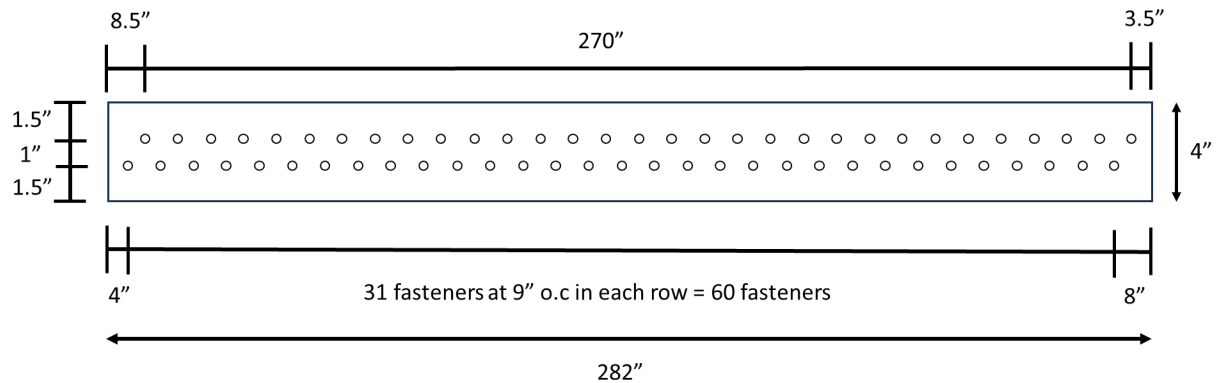
Figure 104: Fastener pattern of the 23.5' strip

The calculations for determining the number of fasteners required to attach FRP strips to the timber beam securely are similar to the fastener calculation for the FRP strips. However, 5/16" x 3-1/8" RSS-GRK screws were selected for the channels (detailed in Section 3.4). Two spacing requirements are outlined in the GRK specification (Appendix D.4) and the Strongwell Extern brochure (Appendix D.3), both of which were satisfied when determining the number of fasteners and their pattern for the channels. There are a total of five different channel lengths: 24' channels for a 25' span beam (Figure 105), 18' channels for a 19' span beam (Figure 106), 8' channels for a 9' span beam (Figure 107), and 6' (Figure 108) and 3' (Figure 109) channels for the existing split repair beams. However, the required number of fasteners for the 8', 6', and 3' channels could not be provided due to the constraints of the minimum spacing requirement.
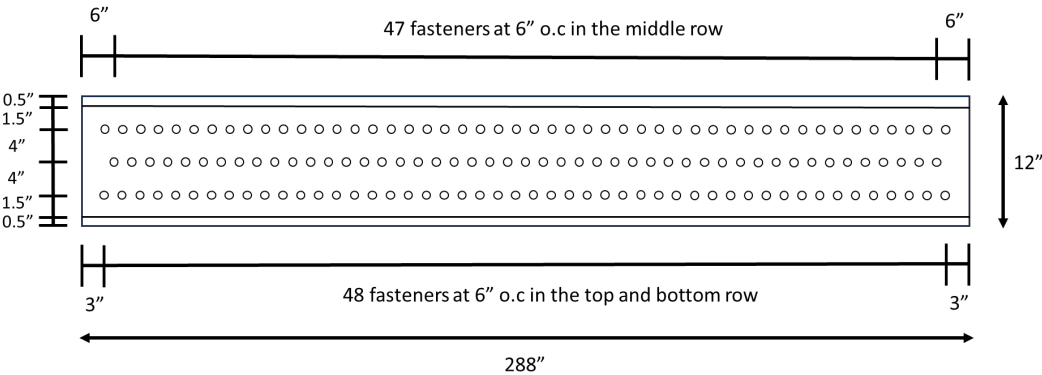
Figure 105: Fastener pattern of the 24' channel
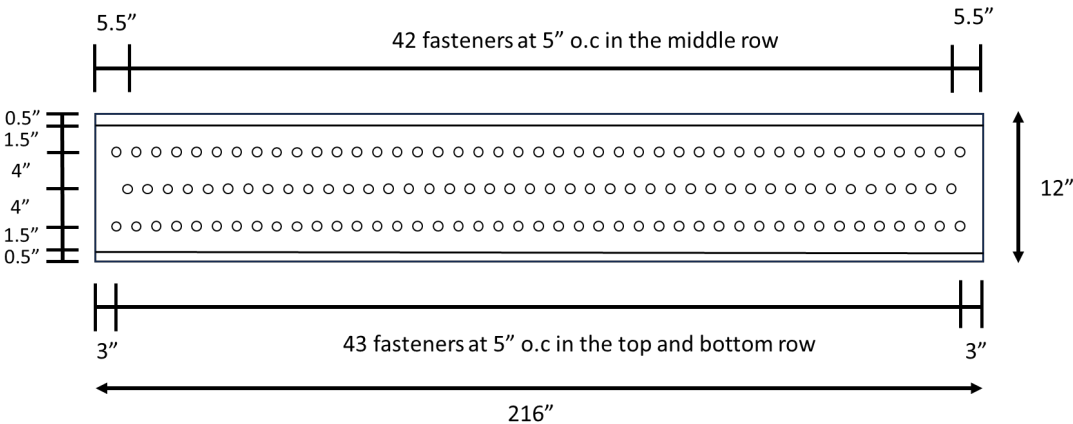
Figure 106: Fastener pattern of the 18' channel
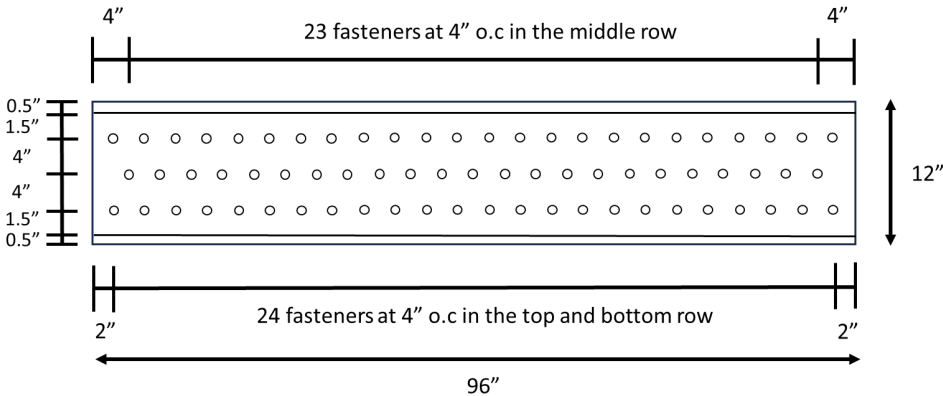
Figure 107: Fastener pattern of the 8' channel
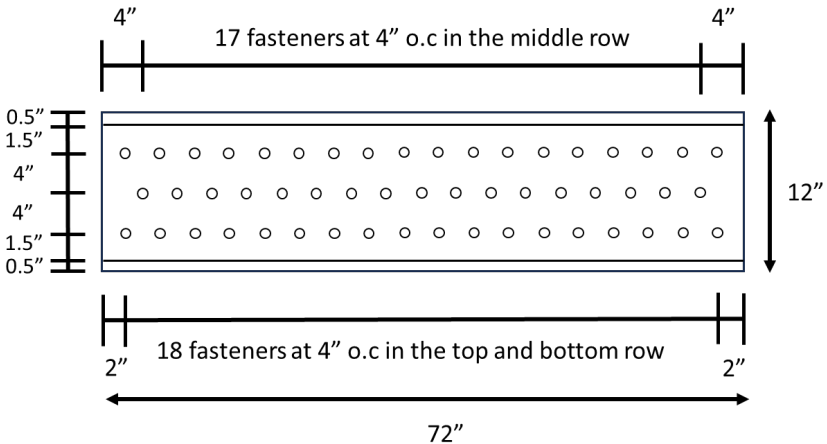
Figure 108: Fastener pattern of the 6' channel
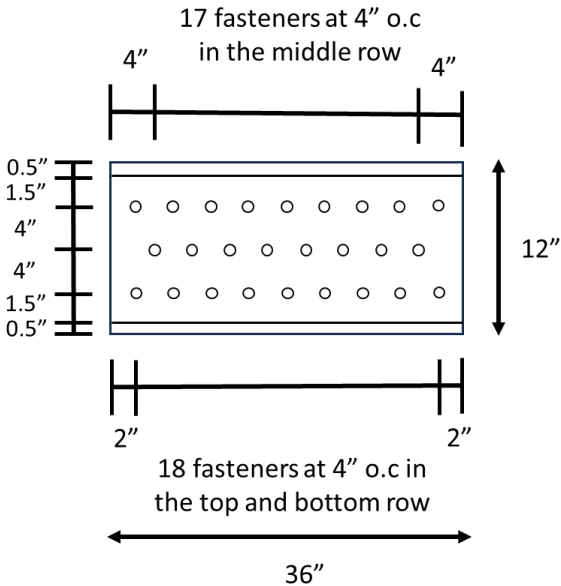
Figure 109: Fastener pattern of the 3' channel

APPENDIX D: MANUFACTURER INFORMATION

This section presents manufacturer brochures for the FRP strip, FRP channel, and GRK screws.

D.1 <u>FRP strip</u>

STRONGWELL

EXCLUSIVELY MADE IN THE USA

SAFSTRIP®

FIBER REINFORCED STRENGTHENING STRIP

SAFSTRIP® is a pultruded composite strip that improves the strength of an existing structural member when mechanically fastened to the structure. SAFSTRIP® has high bearing and longitudinal properties and is designed to strengthen the flexural capacity on the tension face of concrete girders, slabs, and decks. Installation on bridges can occur without any interruption of service.

SAFSTRIP® is supplied in rolls and may be pre-drilled with holes at the required fastener spacing to receive fasteners. SAFSTRIP® measures 4" wide x 1/8" thick and is shipped in rolls up to 100 ft. long. SAFSTRIP® is designed to be easily field cut by the customer into shorter lengths using standard carpenter tools.

SAFSTRIP® provides these features:

- Easy to install, no skilled labor necessary
- Minimal surface preparation is needed for installation
- Structure is usable immediately after installation
- Cost effective system for increasing load capacity of bridges
- Will not split or delaminate when drilled

FIBER REINFORCED STRENGTHENING STRIP

Workers installed SAFSTRIP® on this bridge in Edgerton, Wisconsin, using the MF-FRP system. The load rating for the bridge increased from HS-17 to HS-25 as a result.

The posted load for this bridge that spans the Meramec River in Missouri was increased from 10 tons to 18 tons by installing SAFSTRIP® using the MF-FRP system.

The abutment and deck of this bridge in Phelps County, Missouri, was strengthened using SAFSTRIP®. As a result, the existing 12-ton load posting was removed.

Materials of Construction

SAFSTRIP® is composed of carbon tows sandwiched between layers of fiberglass mats and rovings. The materials are bonded together by a highly corrosion resistant vinyl ester resin. Carbon fibers increase the stiffness of the strip while glass mat provides the proper bearing strength. These combined properties allow SAFSTRIP® to be mechanically attached to a structural member. A synthetic surfacing veil is also incorporated into the composite to improve resistance to corrosion and UV degradation.

What is MF-FRP?

SAFSTRIP® is designed to be installed using an attachment method known as mechanically-fastened fiber reinforced polymer (MF-FRP). Using this method, SAFSTRIP® is attached to an existing concrete girder, slab, or deck using closely spaced powder actuated fastening pins or steel expansion anchors. The pins are applied by using a powder actuated fastener gun or other portable fastener gun. Expansion anchors are installed with a pneumatic powered torque wrench. If desired, rubber or neoprene washers may be used between the fasteners and the strip prior to inserting the fastener through the strip.

MF-FRP is an alternative to externally bonded fiber reinforced polymer (EB-FRP). As opposed to the MF-FRP system, in which the load is transferred to the composite strip through a fastener, the EB-FRP system uses an adhesive.

Research and Development

Research and development for SAFSTRIP® was funded by the U.S. Army Engineer Research and Development Center (ERDC). Laboratory research was conducted at the University of Wisconsin Structures and Materials Testing Laboratory and at ERDC's test laboratories. Bridge demonstration projects were conducted in Wisconsin and Missouri.

Engineering Design

The repair of concrete structures using SAFSTRIP® is dependent upon the concrete's condition. The local engineer must determine the strength of the existing concrete. It must then be determined how much SAFSTRIP® is required and the spacing of fasteners.

Design of MF-FRP systems follows the methodology of *ACI PRC-440.2: Design and Construction of Externally Bonded Fiber-Reinforced Polymer (FRP) Systems for Strengthening Concrete Structures*. Design assistance can be obtained by contacting Strongwell – Chatfield Location.

MECHANICAL PROPERTIES

CONTINUOUS STRAND GLASS MAT
TOP & BOTTOM

4"

1/8"

POLYESTER SURFACING
VEIL - PERIMETER

CARBON TOWS & FIBERGLASS ROVINGS
VINYL ESTER RESIN
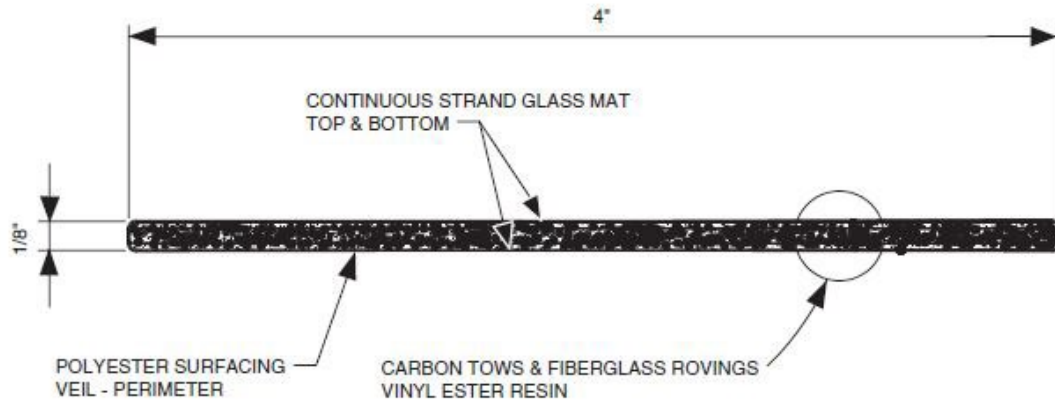
Property	ASTM Test Method	Average Value[1] psi (MPa)	Design Value[2] psi (MPa)
Tensile Strength*	D-638	123,613 (852)	92,902 (640)
Tensile Modulus*[3]	D-638	9.02 x 10⁶ (62,190)	9.02 x 10⁶ (62,190)
Clamped Bearing Strength*	D-5961	50,955 (351)	40,540 (279)
Unclamped Bearing Strength**	D-5961	31,044 (214)	26,046 (180)
Open Hole Strength*	D-5766	94,641 (652)	78,846 (543)

* 20 Sample coupons per test series
** 17 Sample coupons per test series
[1] Average value of test series
[2] Average value minus three standard deviations
[3] Modulus design values are not reduced in accordance with ACI 440.2R-17

This underground parking garage for an apartment complex in Ontario, Canada, recently underwent a concrete support renovation. To provide the necessary improvements, SAFSTRIP® was installed with a small team and minimal onsite equipment.

This bridge, located in St. James, Missouri, was load posted at the time of strengthening. After mechanically attaching SAFSTRIP® with concrete wedge bolts and anchors, the bridge load limit was raised to 20 tons.

Severe deterioration prevented the application of a bonded strengthening system to this bridge in Pulaski County, Missouri, but MF-FRP applied SAFSTRIP® was able to repair the bridge.

	MF-FRP INSTALLATION VS.	**EB-FRP INSTALLATION**
FASTENING SYSTEM	Mechanical - concrete wedge bolts and anchors or powder actuated fasteners.	Adhesive - usually epoxy.
SURFACE PREPARATION	Minimal	Requires the time consuming process of sandblasting, cleaning, and application of epoxy putty that must be ground down for a smooth surface.
WEATHER CONDITIONS FOR APPLICATION	No restrictions. Can be installed even during inclement weather.	Application surface must be moisture-free. Cannot be properly installed in extreme temperatures.
INSTALLATION TIME	Minimal - generally a few hours	Extensive due to the surface preparation, mixing of adhesives, and care required to properly apply the adhesive.
LABOR COSTS	Unskilled labor using standard carpenter tools for cutting and installing strips reduces labor costs.	Skilled labor required to properly prepare the surface and mix the adhesives, which results in higher labor costs.
BOND STRENGTH	Not highly affected by poor condition of the existing outer/superficial concrete substrate.	Dependent on the quality of the concrete substrate.
AVAILABILITY OF STRUCTURE	Available for immediate use upon application.	May require up to seven days to achieve full adhesive strength.
DURABILITY	Tests show excellent retention strength for anchor bolts. Very good fatigue strength.	Research suggests high strain gradient is found in adhesive layer where strips terminate or in proximity of substrate discontinuity (such as cracks). Debonding can be problematic.

STRONGWELL.

ISO 9001 Quality Certified Manufacturing Plants

CHATFIELD LOCATION*
1610 Highway 52 South
Chatfield, MN 55923 USA
(507) 867-3479
www.strongwell.com

ST0324
© 2024 Strongwell

D.2 <u>FRP channel</u>

EXTREN® FIBERGLASS STRUCTURAL SHAPES AND PLATE

This entire rooftop structure was built using EXTREN®, to take advantage of its transparency to RF and cellular signals.

EXTREN® structural shapes have become an ideal alternative for traditional wood in cooling tower construction.

What is EXTREN®?

EXTREN® replaces steel, aluminum, and wood in a wide variety of structural applications. EXTREN® is a durable, lightweight, cost saving structural material. This brochure provides basic information about the EXTREN® product line and shows many examples of how EXTREN® provides solutions for end users in a variety of markets and applications.

EXTREN® is:

- Corrosion Resistant
- Structurally Strong
- Impact Resistant
- Lightweight
- Easy to Field Fabricate
- Low in Thermal and Electrical Conductivity

EXTREN® is manufactured by the pultrusion process. In its simplest terms, pultrusion is the process of pulling fiberglass (or other) reinforcements through a "bath" of thermosetting resin and into a heated forming-and-curing die to produce composite structural shapes. Reinforcement placement, resin formulation, catalyst levels, die temperature and pull speed are critical process parameters. Strongwell is world leader of the pultrusion process with more than 60 pultrusion machines in four plant locations across North America.

Why Use EXTREN®?

EXTREN® is the result of decades of experience in manufacture, design, and fabrication. EXTREN® offers the following advantages:

- **Corrosion Resistance** - Superior resistance to a broad range of chemicals. Unaffected by moisture or immersion in water when sealed. Will not rust like metal and will not rot like wood.

- **High Strength-to-Weight** - Pound-for-pound, EXTREN® pultruded fiberglass structural shapes are stronger than steel in lengthwise direction. Strongwell FRP weighs up to 75% less than steel and 30% less than aluminum - ideal when maximum performance is required but every pound counts.

- **Easy Installation** - Can be field fabricated using simple carpenter tools and is easily lifted into place during installation with less equipment or specialized labor vs. steel.

- **Cost Effective** - Because installation of Strongwell FRP is much simpler and quicker than steel, structures built using Strongwell's pultruded products can cost as much as 15% less than carbon steel, 30% less than galvanized steel, and as much as 50% less than stainless steel.

- **Virtually Maintenance Free** - Will not permanently deform under impact. Corrosion resistance eliminates need for constant painting and upkeep. Provides long-term, cost effective solutions with lower life cycle costs.

- **Durability & Weatherability** - Resists impact, non-denting and hard to break. Pigmented resin, surfacing veil, and UV-Inhibitors prevent moisture absorption, warping, fiber bloom, and delays fading.

Materials of Construction

EXTREN® is an engineered composite consisting of:

- Fiberglass rovings for increased strength
- Continuous strand mat for crosswise strength and imact resistance
- Synthetic surfacing veil for corrosion and UV protection
- Resin (specified by Series)
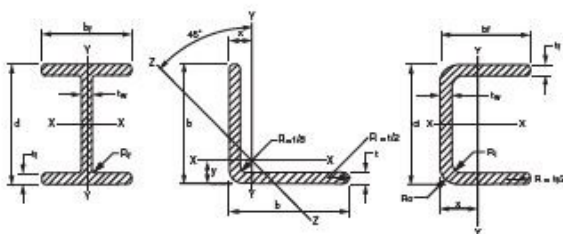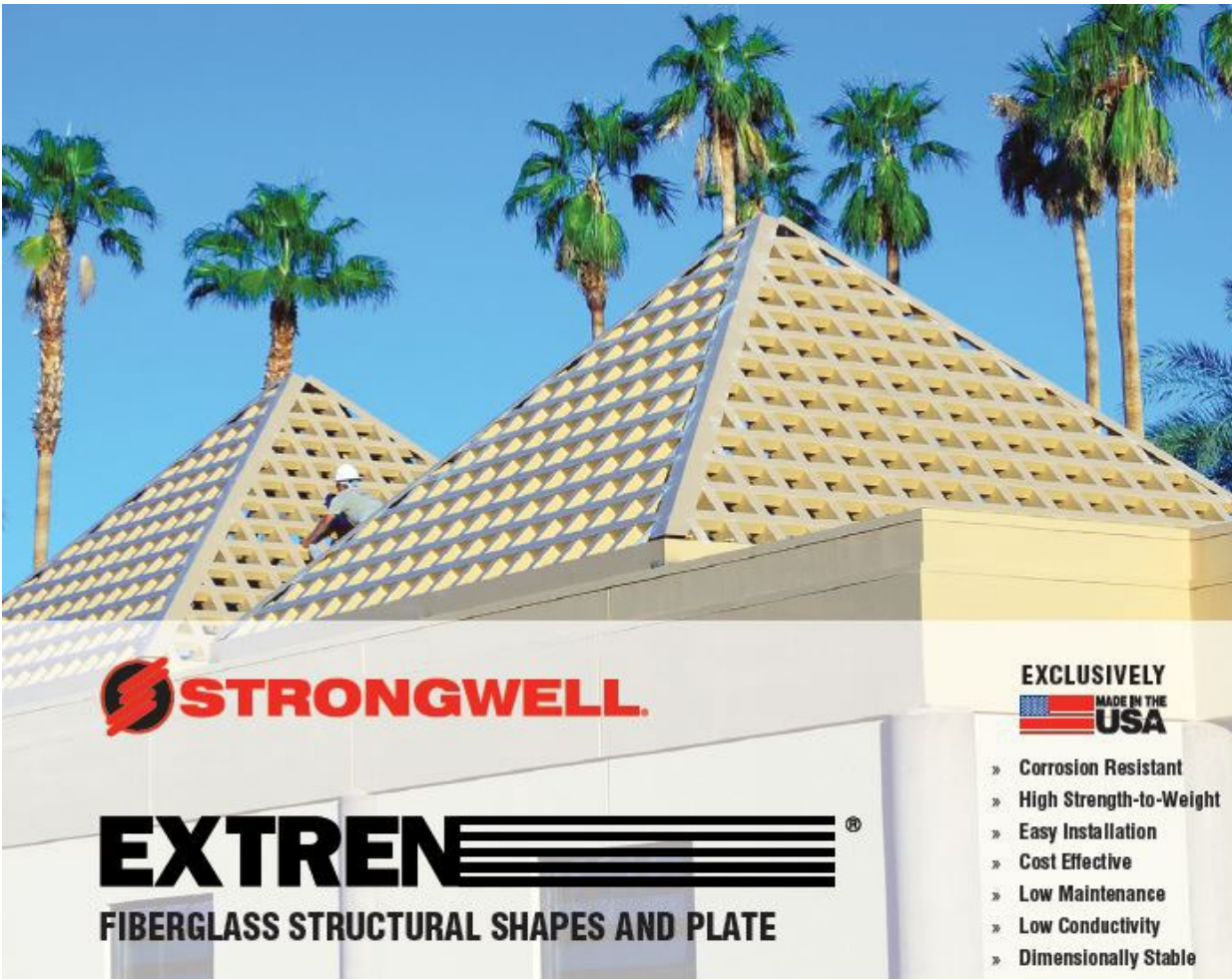
THE EXTREN® SERIES

EXTREN® is pultruded structural composite profiles and plate produced exclusively by Strongwell with the EXTREN® logo embedded in the surfacing veil. It meets or exceeds the minimum published mechanical, physical, electrical, flammability, and corrosive properties of the respective Series published in the *Strongwell Design Manual*.

EXTREN® Series 500

Premium Polyester Resin, UV inhibitor added
Standard Color: olive green
A general purpose resin with excellent corrosion properties

EXTREN® Series 525

Premium Polyester Resin, UV inhibitor added, Flame retardant additives
Standard Color: slate gray
A general purpose resin with excellent corrosion properties and improved fire performance

EXTREN® Series 600

Premium Vinyl Ester Resin, UV inhibitor added
Standard Color: light gray
For harsher corrosive environments and higher temperature applications

EXTREN® Series 625

Premium Vinyl Ester Resin, UV inhibitor added, Flame retardant additives
Standard Color: beige
For harsher corrosive environments, higher temperature applications, with improved fire performance

EXTREN® Series 900

In addition to the above EXTREN® products, Strongwell manufactures custom pultrusions. These pultrusions vary from EXTREN® in either shape, resin type, or reinforcement (type, amount, location and/or orientation). Designers may choose to vary one or all of these parameters to improve strength, temperature resistance, corrosion resistance, machinability, or some other characteristic. Consult Strongwell with specific needs or questions.

E23

All standard EXTREN® products meet and/or exceed the structural requirements of E17 European standards. EXTREN® can be manufactured upon request to meet the mechanical and physical properties of BS EN 13706 (E23) European standards.

NSF International

Most Strongwell products can be manufactured to meet NSF-61 certification upon request. Contact Strongwell for details.

EXTREN® Series: (left to right) 500, 625, and 525.

EXTREN® structural shapes were used in a SXEW copper refinery because of the highly corrosive environment.

A 63' (19.2m) high freestanding fiberglass stair tower at Ft. Story Army Base, Virginia Beach, Virginia.

PROPERTIES

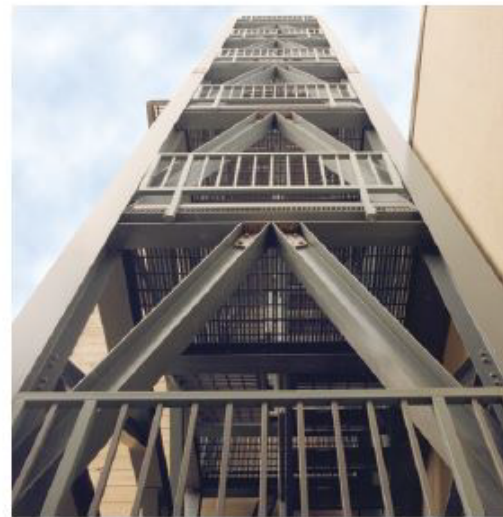|	ASTM TEST METHOD	UNITS/ VALUE	SERIES 500/525 SHAPES	SERIES 600/625 SHAPES	SERIES 500/525 PLATE ④			SERIES 600/625 PLATE ④		
					1/8" 3.175mm	3/16" - 3/8" 4.76-9.5mm	1/2" - 1" 9.5-25.4mm	1/8" 3.175mm	3/16" - 1/4" 4.76-6.35mm	3/8" - 1" 9.5-25.4mm
MECHANICAL										
Tensile Stress, LW	D638	psi	30,000	30,000	20,000	20,000	20,000	20,000	20,000	20,000
		N/mm²	207	207	138	138	138	138	138	138
Tensile Stress, CW	D638	psi	7,000	7,000	7,500	10,000	10,000	7,500	10,000	10,000
		N/mm²	48.3	48.3	51.7	68.9	68.9	51.7	68.9	68.9
Tensile Modulus, LW	D638	10⁶ psi	2.5	2.6	1.8	1.8	1.8	1.8	1.8	1.8
		10³N/mm²	17.2	17.9	12.4	12.4	12.4	12.4	12.4	12.4
Tensile Modulus, CW	D638	10⁶ psi	0.8	0.8	0.7	0.9	1.0	1.0	1.0	1.0
		10³N/mm²	5.52	5.52	4.83	6.21	6.89	6.89	6.89	6.89
Compressive Stress, LW	D695	psi	30,000	30,000	24,000	24,000	24,000	24,000	24,000	24,000
		N/mm²	207	207	165	165	165	165	165	165
Compressive Stress, CW	D695	psi	15,000	16,000	15,500	16,500	20,000	16,500	17,500	17,500
		N/mm²	103	110	107	114	138	114	121	121
Compressive Modulus, LW	D695	10⁶ psi	2.5	2.6	1.8	1.8	1.8	1.8	1.8	1.8
		10³N/mm²	17.2	17.9	12.4	12.4	12.4	12.4	12.4	12.4
Compressive Modulus, CW	D695	10⁶ psi	0.8	0.8	0.7	0.9	1.0	1.0	1.0	1.0
		N/mm²	5.52	5.52	4.83	6.21	6.89	6.89	6.89	6.89
Flexural Stress, LW	D790	psi	30,000	30,000	24,000	24,000	24,000	24,000	24,000	24,000
		N/mm²	207	207	165	165	165	165	165	165
Flexural Stress, CW	D790	psi	10,000	10,000	10,000	13,000	17,000	10,000	13,000	17,000
		N/mm²	68.9	68.9	68.9	89.6	117	68.9	89.6	117
Flexural Modulus, LW	D790	10⁶ psi	1.6	1.6	1.1	1.1	1.4	1.1	1.1	1.4
		10³N/mm²	11.0	11.0	7.58	7.58	9.65	7.58	7.58	9.65
Flexural Modulus, CW	D790	10⁶ psi	0.8	0.8	0.8	0.8	1.3	0.8	0.9	1.3
		10³N/mm²	5.52	5.52	5.51	5.51	8.96	5.51	6.21	8.96
Modulus of Elasticity ①	full section	10⁶ psi	2.6	2.8	LW: 2.0 / CW: 0.8	2.0 / 0.8	2.0 / 1.3	2.0 / 0.8	2.0 / 0.9	2.0 / 1.3
		10³N/mm²	17.9	19.3	LW: 13.7 / CW: 5.51	13.7 / 5.51	13.7 / 8.96	13.7 / 5.51	13.7 / 6.21	13.7 / 8.95
Modulus of Elasticity: W & I shapes > 4" / W & I shapes > 102mm	full section	10⁶ psi	2.5	2.5	-	-	-	-	-	-
		10³N/mm²	17.2	17.2	-	-	-	-	-	-
Shear Modulus, LW ②③	D5379	10⁶ psi	0.425	0.425	-	-	-	-	-	-
		10³N/mm²	2.93	2.93	-	-	-	-	-	-
Short Beam Shear, LW ②③	D2344	psi	4,500	4,500	-	-	-	-	-	-
		N/mm²	31.0	31.0	-	-	-	-	-	-
Ultimate Bearing Stress, LW	D953	psi	30,000	30,000	32,000	32,000	32,000	32,000	32,000	32,000
		N/mm²	207	207	221	221	221	221	221	221
Poisson's Ratio, LW ④	D3039	in/in	0.33	0.33	0.31	0.31	0.31	0.32	0.32	0.32
		mm/mm	0.33	0.33	0.31	0.31	0.31	0.32	0.32	0.32
Poisson's Ratio, CW ④	D3039	in/in	-	-	0.29	0.29	0.29	0.24	0.24	0.24
		mm/mm	-	-	0.29	0.29	0.29	0.24	0.24	0.24
Notched Izod Impact, LW	D256	ft-lbs/in	25	25	15	10	10	15	10	10
		J/mm	1.33	1.33	0.801	0.533	0.533	0.801	0.533	0.533
Notched Izod Impact, CW	D256	ft-lbs/in	4	4	5	5	5	5	5	5
		J/mm	0.214	0.214	0.267	0.267	0.267	0.267	0.267	0.267

	ASTM TEST METHOD	UNITS/ VALUE	SERIES 500/525 SHAPES	SERIES 600/625 SHAPES	SERIES 500/525 PLATE ④			SERIES 600/625 PLATE ④		
					1/8" 3.175mm	3/16" - 3/8" 4.76-9.5mm	1/2" - 1" 9.5-25.4mm	1/8" 3.175mm	3/16" - 1/4" 4.76-6.35mm	3/8" - 1" 9.5-25.4mm
PHYSICAL*										
Barcol Hardness	D2583	–	45	45	40	40	40	40	40	40
24 hr Water Absorption ⑥	D570	% Max	0.60	0.60	0.60	0.60	0.60	0.60	0.60	0.60
Density	D792	lbs/in³	0.062-0.070	0.062-0.070	0.060-0.068	0.060-0.068	0.060-0.068	0.060-0.068	0.060-0.068	0.060-0.068
		10^3 g/mm³	1.72-1.94	1.72-1.94	1.66-1.88	1.66-1.88	1.66-1.88	1.66-1.88	1.66-1.88	1.66-1.88
Coefficient of Thermal Expansion, LW ⑧	D696	10^6 in/in/°F	7	7	8	8	8	8	8	8
		10^6 mm/mm/°C	12	12	14.5	14.5	14.5	14.5	14.5	14.5
Coefficient of Thermal Expansion, CW ⑧	D696	10^6 in/in/°F	16	16	-	-	-	-	-	-
		10^6 mm/mm/°C	28.8	28.8	-	-	-	-	-	-
Thermal Conductivty ⑧	C177	BTU-in/ft²/hr/°F	4	4	-	-	-	-	-	-
		W(m * °K)	0.58	0.58	-	-	-	-	-	-

All values are minimum ultimate properties from coupon tests except as noted.

ELECTRICAL										
Arc Resistance, LW ⑧	D495	seconds	120	120	-	-	-	-	-	-
Dielectric Strength, LW ⑤	D149	KV/in	35	35	35	35	35	35	35	35
		KV/mm	1.38	1.38	1.38	1.38	1.38	1.38	1.38	1.38
Dielectric Strength, PF ⑤	D149	volts/mil	200	200	200	-	-	250	-	-

FLAMMABILITY ⑥			
Flammability Classification	UL 94	V-0	
Tunnel Test	E84	25 Max	
NBS Smoke Chamber	E662	650-700 (Typical)	
Flammability	D635	Self Extinguishing	
UL Thermal Index	Generic	266°F	
		130°C	
British Fire Test	BS 476-7	Class 1	

① This value is determined from full section simple beam bending of EXTREN® structural shapes.
② The Shear Modulus value has been determined from tests with full sections of EXTREN® structural shapes. (See Strongwell's *Design Manual* for further information.)
③ Value would be 50 if the surfacing veil were not there.
④ Plate compressive stress/modulus measured edgewise and flexural stress/modulus measured flatwise.
⑤ Values apply to Series 525 and 625 (≥ 1/8" thickness).
⑥ Measured as a percentage maximum by weight.
⑦ Span to depth ratio of 3:1; EXTREN® angles will have a minimum value of 4000 psi and the I/W shapes are tested in the web.
⑧ Typical values.

LW – Lengthwise
CW – Crosswise
PF – Perpendicular to laminate face

D.3 Fastener spacing recommendation by Strongwell

STRONGWELL.

THREADED FASTENERS

BEARING
ALLOWABLE LOADS IN POUNDS

FIBERGLASS THICKNESS	BOLT DIAMETER					
	1/4"	3/8"	1/2"	5/8"	3/4"	1"
1/8"	234	352	469	586	703	938
1/4"	469	703	938	1172	1406	1875
3/8"	703	1055	1406	1758	2109	2812
1/2"	938	1406	1875	2344	2812	3750
3/4"	1406	2109	2812	3516	4219	5625

Allowable load = Allowable bearing stress x bearing area.

EXAMPLE

1/4" thickness with 1/2" dia. bolt

Allowable load = $\dfrac{30,000 \text{ psi}}{4}$ x .25" x .50" = 938 lbs.

NOTE: The above table assumes the bearing stress on fiberglass controls. The designer should verify that no other element of the connection controls.

SHEAR
ALLOWABLE LOADS IN POUNDS

BOLT TYPE	BOLT DIAMETER					
	1/4"	3/8"	1/2"	5/8"	3/4"	1"
S.S. Single Shear	1473	3312	5889	9204	13254	23562
S. S. Double Shear	2964	6624	11778	18408	26508	47124
FIBREBOLT®, Single Shear	—	400	650	950	1550	3750
FIBREBOLT®, Double Shear	—	750	1250	1875	3000	5000

NOTE: The above table assumes the shear capacity of the fastener controls. The designer should verify that no other element of the connection controls.

RECOMMENDED MINIMUM FASTENER EDGE DISTANCES AND PITCH RATIO OF DISTANCE TO FASTENER DIAMETER

	RANGE	COMMON
Edge Distance - end	2.0 to 4.5	3.0
Edge Distance - side	1.5 to 3.5	2.0
Pitch	4.0 to 5.0	5.0

D.4 GRK screw

GRK FASTENERS™

ESR-2442

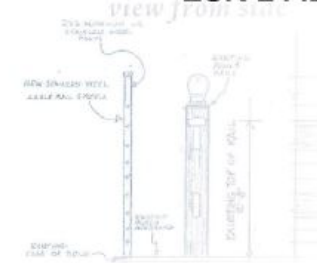**FASTENER TECHNICAL DATA**

ICC **ES**™

RSS™

TABLE 1—RSS™ FASTENER SPECIFICATIONS

FASTENER DESIGNATION		LENGTH[1] (inches)	THREAD LENGTH[2] (inches)	HEAD DIAMETER (inch)	DRIVE SIZE	HEAD HEIGHT (inch)	SHOULDER ø (inch)	MINOR THREAD DIAMETER (inch)	SHANK DIAMETER (inch)	OUTSIDE THREAD DIAMETER (inch)	SPECIFIED BENDING YIELD STRENGTH[3] F_yb (psi)	ALLOWABLE STEEL STRENGTH	
												TENSILE (lbf)	SHEAR (lbf)
RSS™	1/4 x 2 1/2"	2 1/2	1 1/2	0.533	T-25	0.110	0.244	0.152	0.169	0.236	153,400	1112	754
	1/4 x 2 3/4"	2 3/4	1 3/4										
	1/4 x 3 1/8"	3 1/8	2										
	1/4 x 3 1/2"	3 1/2	2 3/8										
	5/16 x 2 1/2"	2 1/2	1 1/2	0.620	T-30	0.157	0.301	0.167	0.195	0.276	171,800	1415	982
	5/16 x 2 3/4"	2 3/4	1 3/4										
	5/16 x 3 1/8"	3 1/8	2										
	5/16 x 3 1/2"	3 1/2	2 3/8										
	5/16 x 4"	3 7/8	2 1/2										
	5/16 x 5 1/8"	5	3 3/8										
	5/16 x 6"	5 7/8	3 7/8										
	3/8 x 3 1/8"	3 1/8	2	0.689	T-40	0.181	0.364	0.191	0.219	0.313	160,200	1941	1231
	3/8 x 4"	3 7/8	2 1/2										
	3/8 x 5 1/8"	5	3 3/8										
	3/8 x 6"	5 7/8	3 7/8										
	3/8 x 7 1/4"	7	4 3/8										
	3/8 x 8"	7 3/4	4 3/8										
	3/8 x 10"	9 3/4	5										
	3/8 x 12"	11 3/4	5 7/8										
	3/8 x 14 1/8"	14 1/8	5 7/8										
	3/8 x 16"	15 5/8	5 7/8										
RSS PHEInox™	1/4 x 2 1/2"	2 1/2	1 1/2	0.533	T-25	0.110	0.244	0.152	0.169	0.236	100,300	620	546
	1/4 x 3 1/8"	3 1/8	2										
	5/16 x 2 1/2"	2 1/2	1 1/2	0.620	T-30	0.157	0.301	.167	0.195	0.276	106,500	806	668
	5/16 x 3 1/8"	3 1/8	2										
	5/16 x 4"	3 7/8	2 1/2										
	5/16 x 5 1/8"	5	3 3/8										
	5/16 x 6"	5 7/8	3 7/8										
RSS JTS™	1/4 x 5"	5	1 3/8	0.534	T-25	0.090	0.244	0.152	0.171	0.240	203,700	1104	769
	1/4 x 6 3/4"	6 5/8	1 3/8										

For SI: 1 inch = 25.4 mm; 1 psi =6.9 kPa; 1 lbf = 4.4 N.

[1]The length of fasteners is measured from the underside of the head to bottom of the tip. See Figure 1.
[2]Length of thread includes tip. See Figure 1.
[3]Bending yield strength determined in accordance with ASTM F1575 using the minor thread diameter.
[4]See Figure 1 for additional dimensional information.

GRK FASTENERS

RSS™ FASTENER TECHNICAL DATA

ESR-2442

ICC ES

TABLE 4 - CONNECTION GEOMETRY

| CONNECTION GEOMETRY/ CRITERIA	DIAMETERS[1]	REQUIRED DIMENSION (inches)		
		RSS, RSS PHEinox & RSS JTS ¼" NOMINAL DIAMETER	RSS & RSS PHEinox ⁵/₁₆" NOMINAL DIAMETER	RSS ³/₈" NOMINAL DIAMETER
Minimum Edge Distance				
Loading Parallel to Grain	8	1½	1⅝	1⅞
Loading Perpendicular to Grain, Loaded Edge	8	1½	1⅝	1⅞
Loading Perpendicular to Grain, Unloaded Edge	8	1½	1⅝	1⅞
Minimum End Distance				
Tension Load Parallel to Grain	15	2⅝	3	3⅜
Compression Load Parallel to Grain	10	1¾	2	2¼
Load Perpendicular to Grain	10	1¾	2	2¼
Spacing (Pitch) Between Fasteners in a Row.				
Parallel to Grain	15	2⅝	3	3⅜
Perpendicular to Grain	10	1¾	2	2¼
Spacing (Gage) Between Rows of Fasteners				
In-Line	5	⅞	1	1⅛
Staggered	2½	½	½	⅝
Minimum Penetration into Main Member for Single Shear Connections	6	1⅛	1¼	1⅜

For SI: 1 inch = 25.4 mm.

[1]Diameter is the shank diameter as specified in Table 1.
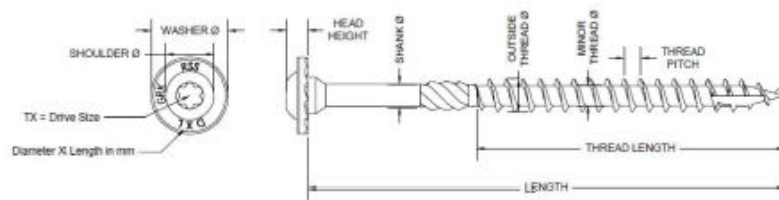
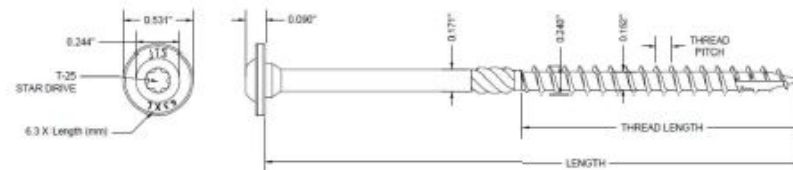

FIGURE 1—RSS™ AND RSS PHEINOX™ SCREWS

FIGURE 2—RSS JTS™ SCREWS

APPENDIX E: FRP COUPON TESTING

E.1 Specimen Preparation

Tensile test coupons were prepared from the two types of FRP materials used in this study: glass FRP channels and carbon-glass hybrid FRP strengthening strips. For clarity, these are referred to throughout the study as channel coupons and strip coupons, respectively.

Each material set consisted of the following three types of specimens:

1. Control: untested and undamaged raw materials
2. Tested coupon (mid): material cut from the middle region of a full-scale FRP material that was tested on a timber beam
3. Tested coupon (end): material cut from the end region of a full-scale FRP material that was tested on a timber beam

A total of three channel coupons and four strip coupons were tested. All coupons were cut to a standard tensile specimen shape using a water jet cutter to maintain dimensional accuracy. Testing followed the procedures outlined in ASTM D638-14 standard [10], where channel coupons were dimensioned as Type III specimens due to their thickness, and strip coupons were Type I. Figure 110 and Figure 111 show schematic diagrams of the channel and strip coupon geometries, respectively.
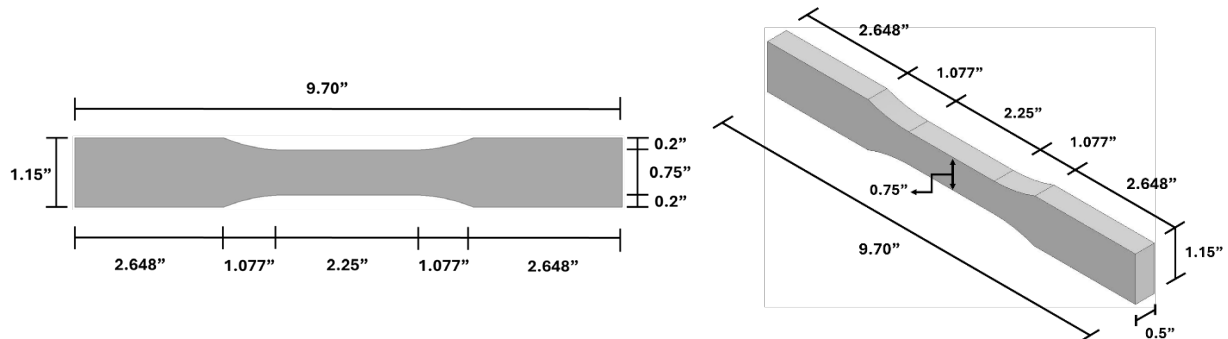

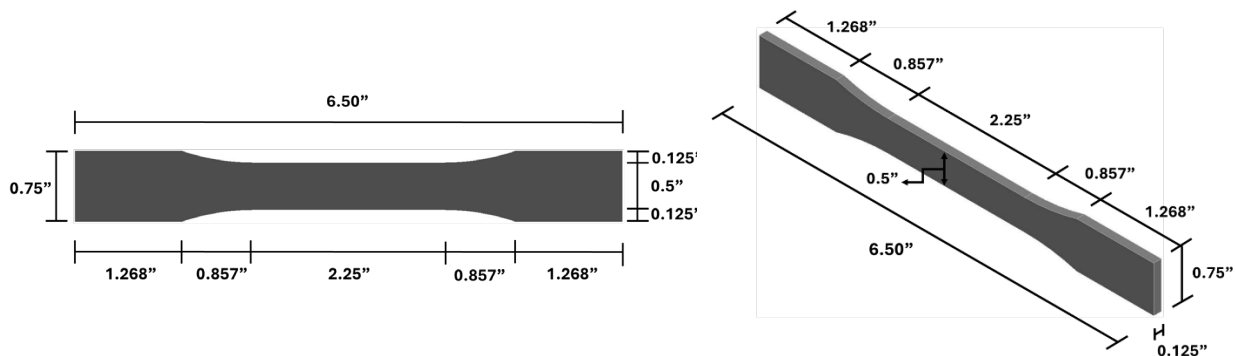Figure 110: Schematic of the GFRP channel coupon geometry

Figure 111: Schematic of the carbon-glass hybrid FRP strengthening strip coupon geometry

Coupon dimensions were measured prior to testing using slide calipers. The measured values were used to calculate the cross-sectional area for stress calculations. Dimensional data for the channel coupons are shown in Table 5, while Table 6 summarizes the data for the strip coupons.

Table 5: GFRP channel coupon dimensions

Coupon	Width (in)	Thickness (in)	Area (in^2)
Control	0.752	0.500	0.376
Tested (mid)	0.755	0.497	0.375
Tested (end)	0.754	0.498	0.375

Table 6: Hybrid FRP strip coupon dimensions

Coupon	Width (in)	Thickness (in)	Area (in^2)
Control 1	0.504	0.127	0.064
Control 2	0.504	0.125	0.063
Tested (mid)	0.505	0.126	0.063
Tested (end)	0.505	0.126	0.063

E.2 Test Setup and Instrumentation

All tensile tests were conducted at the Materials Testing Lab, Montana State University, using an MTS Testing Machine. The tests followed the guidelines of ASTM D638-14, and the loading rate was maintained at 0.0033 in/sec for all specimens. Proper alignment of the coupons in the grips was ensured to avoid eccentric loading. Specimens were instrumented with an MTS extensometer to capture accurate strain responses and stress was calculated using the measured loads and cross-sectional areas. Photographs of the test setup and mounted coupons are provided in Figure 112.
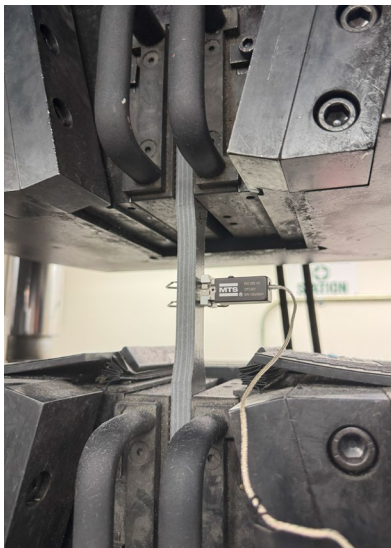
(a) Glass FRP channel coupon   (b) Hybrid FRP strip coupon

Figure 112: Tensile test setup for FRP coupons

E.3 Results

The primary goals of the coupon testing were to determine the tensile properties of the GFRP channels and carbon-glass hybrid FRP strips and to assess what level of damage (if any) occurred on the FRP during the timber beam testing. The experimental values measure here were used in the theoretical capacity calculations presented previously.

The measured tensile strength and modulus of elasticity values for each coupon are summarized in Table 7 and Table 8, along with their corresponding tabulated reference values. Ratios of measured to tabulated values are included to quantify performance retention.

Table 7: Tensile strength of FRP coupons

FRP		Tensile Strength (ksi)		Measured/tabulated (%)
		Tabulated	Measured	
Channel	Control	30	53.2	177
	Tested (mid)		47.1	157
	Tested (end)		45.7	152
Strip	Control 1	123	131.8	107
	Control 2		133.7	109
	Tested (mid)		125.1	102
	Tested (end)		121.8	99

Table 8: Modulus of elasticity of FRP coupons

FRP		Modulus (ksi)		Measured/tabulated (%)
		Tabulated	Measured	
Channel	Control	2500	4090	164
	Tested (mid)		3351	134
	Tested (end)		3076	123
Strip	Control 1	9020	9822	109
	Control 2		9413	104
	Tested (mid)		8817	98
	Tested (end)		9619	107

In the case of the GFRP channels, the control specimen exhibited a tensile strength 77% above the tabulated value and an elastic modulus 64% higher than tabulated. Although there was a reduction in strength and modulus from the raw material to the tested channel coupons, the tested specimens still demonstrated substantial mechanical performance, retaining over 150% of the expected tensile capacity and more than 120% of the expected modulus. The FRP strip coupons showed consistent behavior. All control and tested specimens had tensile strengths near or above the design values, and modulus values stayed within ±10% of the reference across all specimens.

Figure 113-a shows the stress–strain response of the strip coupons, while Figure 113-b presents the data for the channel coupons. To prevent damage while still capturing a substantial portion of the linear elastic zone, the extensometer was removed before the specimens reached ultimate failure. For the strip coupons, it was removed at approximately 55 ksi, and for channel coupons, at approximately 25 ksi. Enough of the linear elastic region was captured to calculate slope and the data was used to determine the modulus of elasticity for each coupon.

In both materials, the tested coupons (mid and end) exhibited slightly lower stiffness compared to the corresponding control coupons, indicating minor degradation after full-scale experimental testing. However, the stiffness of all tested specimens remained higher than the tabulated design values (with the exception of the strip coupon tested (mid) at 98%), confirming the retention of structural integrity and supporting the reuse potential of these FRP materials.
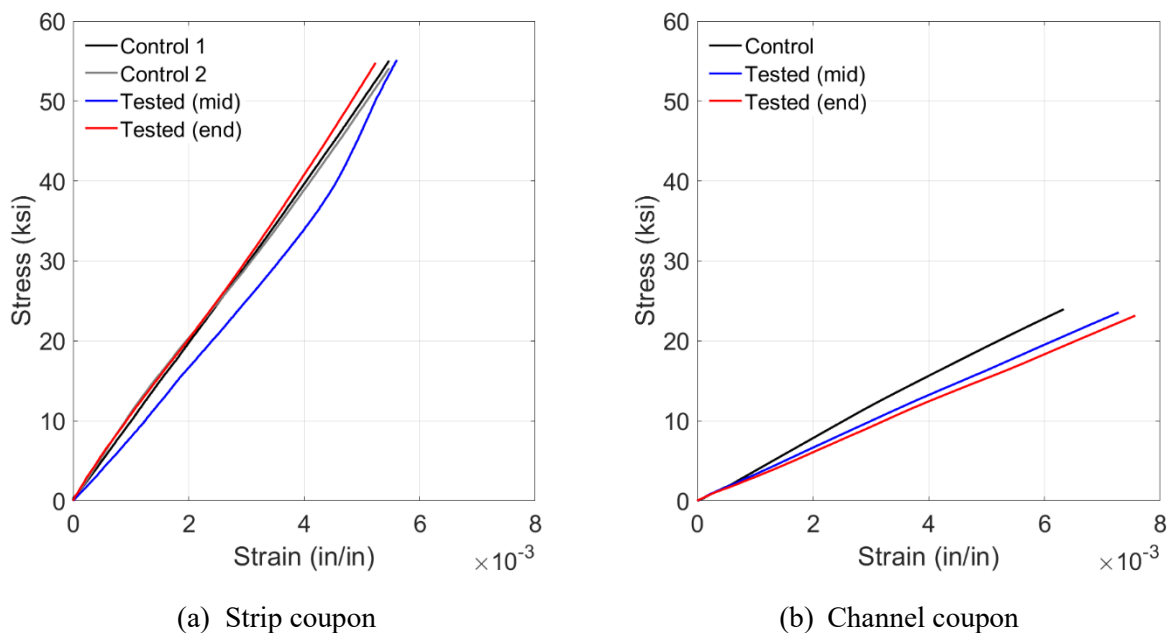

(a) Strip coupon   (b) Channel coupon

Figure 113: Stress–strain curves of FRP coupons